



**HAL**  
open science

## Recent developments in solid-state cold spraying of Al matrix composites: a critical review

Xinliang Xie, Shuo Yin, Rija-Nirina Raoelison, Chaoyue Chen, Christophe Verdy, Wenya Li, G Ji, Zhongming Ren, Hanlin Liao

### ► To cite this version:

Xinliang Xie, Shuo Yin, Rija-Nirina Raoelison, Chaoyue Chen, Christophe Verdy, et al.. Recent developments in solid-state cold spraying of Al matrix composites: a critical review. Journal of Materials Science and Technology, 2021, JOURNAL OF MATERIALS SCIENCE & TECHNOLOGY, 86, pp.20-55. 10.1016/j.jmst.2021.01.026 . hal-03323673

**HAL Id: hal-03323673**

**<https://hal.science/hal-03323673v1>**

Submitted on 23 Aug 2021

**HAL** is a multi-disciplinary open access archive for the deposit and dissemination of scientific research documents, whether they are published or not. The documents may come from teaching and research institutions in France or abroad, or from public or private research centers.

L'archive ouverte pluridisciplinaire **HAL**, est destinée au dépôt et à la diffusion de documents scientifiques de niveau recherche, publiés ou non, émanant des établissements d'enseignement et de recherche français ou étrangers, des laboratoires publics ou privés.

## **Al matrix composites fabricated by solid-state cold spray deposition: a critical review**

Xinliang Xie<sup>1,2,4\*</sup>, Shuo Yin<sup>3</sup>, Rija-nirina Raoelison<sup>1</sup>, Chaoyue Chen<sup>5</sup>, Christophe Verdy<sup>1</sup>, Wenya Li<sup>6</sup>, Gang Ji<sup>2\*</sup>,  
Zhongming Ren<sup>5</sup>, Hanlin Liao<sup>1</sup>

1. *ICB UMR 6303, CNRS, Univ. Bourgogne Franche-Comté, UTBM, F-90010 Belfort, France*
2. *Univ. Lille, CNRS, INRAE, Centrale Lille, UMR 8207 - UMET - Unité Matériaux et Transformations, F-59000 Lille, France*
3. *Department of Mechanical and Manufacturing Engineering, Trinity College Dublin, The University of Dublin, Parsons Building, Dublin 2, Ireland*
4. *Institute of Mechanics, Materials and Civil Engineering, UC Louvain, Louvain-la-Neuve, Belgium*
5. *State Key Laboratory of Advanced Special Steels, School of Materials Science and Engineering, Shanghai University, Shanghai 200444, P.R. China*
6. *State Key Laboratory of Solidification Processing, Shaanxi Key Laboratory of Friction Welding Technologies, Northwestern Polytechnical University, Xi'an 710072, P.R. China*

\*Corresponding authors: Dr. Xinliang Xie (xlxie1990@gmail.com); Dr. Gang Ji ([gang.ji@univ-lille.fr](mailto:gang.ji@univ-lille.fr))

**Abstract:** Cold spraying (CS), or cold gas dynamic spray (CGDS), is an emerging solid-state powder deposition process, allowing fast and mass production and restoration of metallic components. CS of metal matrix composites (MMCs) has attracted increasing attention from academia and industry over the last decades, especially in the area of Al matrix composites (AMCs), which have demonstrated a high potential for applications in aerospace, automotive, and electronics industries. This article aims to summarize the recent development of CS-processed AMCs in terms of composite powder preparation, deposition processing, microstructure evolution, mechanical and corrosion properties. Furthermore, this review also reports the relevant research progress with the focus on post-treatments of the AMCs for CS additive manufacturing applications including heat treatment, hot rolling, and friction stir processing. Finally, the challenges and perspectives on the fabrication of advanced AMCs by CS are addressed.

**Keywords:** Al matrix composites; solid-state cold spraying; additive manufacturing; post-treatments.

## Content

<b>1. Introduction to Al matrix composites and their manufacturing routes ..</b>	<b>3</b>
1.1 An overview on the development of Al matrix composites .....	3
1.2 Cold spraying as an innovative solid-state technique .....	5
<b>2 Composite powder preparation routes for cold spraying.....</b>	<b>8</b>
2.1 Mechanical mixing/blending .....	9
2.2 Satelliting/wet granulation.....	10
2.3 Mechanical ball milling.....	11
2.4 Spray drying .....	15
2.5 Gas atomization .....	16
<b>3 Cold spray processing of Al matrix composites: deposition behavior and features .....</b>	<b>24</b>
3.1 Deposition behavior.....	24
3.2 Reinforcement volume fraction and porosity evolution.....	26
3.3 Characterization of deposit microstructure and its formation mechanisms.....	29
<b>4 Properties of Al matrix composites manufactured by cold spraying .....</b>	<b>33</b>
4.1 Hardness and bonding strength .....	33
4.2 Wear resistance .....	35
4.3 Corrosion resistance.....	37
4.4 Tensile properties.....	39
<b>5 Strengthening strategies for cold sprayed Al matrix composites .....</b>	<b>42</b>
5.1 Post-heat treatment .....	42
5.2 Post hot rolling treatment .....	46
5.3 Post friction stir processing treatment.....	48
<b>6 Conclusions and future perspectives .....</b>	<b>53</b>
<b>Acknowledgments.....</b>	<b>56</b>

# 1. Introduction to Al matrix composites and their manufacturing routes

## 1.1 An overview on the development of Al matrix composites

Today, rapid technology innovation and economic development have resulted in an increasing demand for lightweight Al alloys with superior mechanical properties in critical industrial sectors such as automobile and aerospace. The production of metal matrix composites (MMCs) is an effective way to produce high-performance metallic materials [1-3], with the possibility to combine the properties of the matrix (e.g. ductility and toughness) and reinforcement phase (e.g. high strength and modulus, high thermal properties) for a designed performance [1, 4, 5]. After more than 40 years of development, Al matrix composites (AMCs) have been widely used in the aerospace and automotive industries due to their low specific density, high strength and stiffness, and good wear resistance [6-9]. Basically, there are three major categories of AMCs depending on the type of reinforcements [3]: i) continuous fiber strengthened AMCs, ii) whisker or short fiber strengthened AMCs, and iii) particulate-reinforced AMCs (P-AMCs) (see Fig. 1).

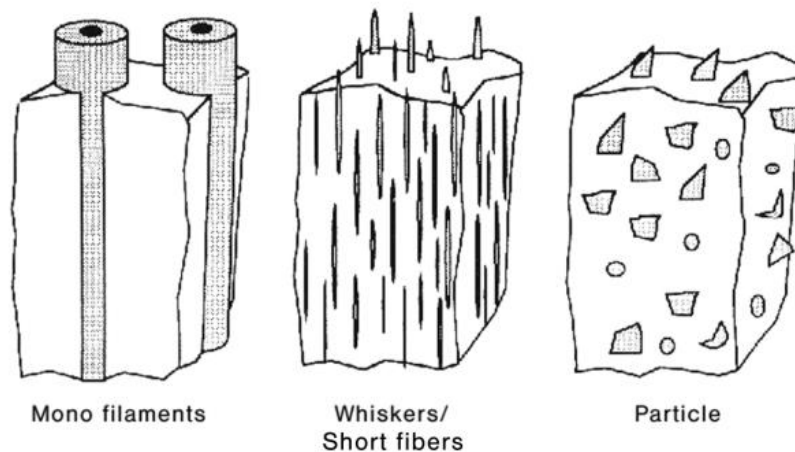


*Fig. 1 Schematic illustration of three types of shapes of reinforcements in AMCs [10].*

Recently, P-AMCs have attracted considerable attention due to their relatively low production cost and characteristic isotropic properties [3]. The commonly used reinforcement particles for the production of P-AMCs include ceramic particles ( $\text{SiC}$ ,  $\text{B}_4\text{C}$ ,  $\text{Al}_2\text{O}_3$ ,  $\text{TiB}_2$ ,  $\text{TiN}$ ), and carbon-based materials, such as carbon fibers, synthetic diamond particles, carbon nanotubes, and graphene [3, 11]. The properties of P-AMCs are predominantly determined by the type, size, and volume fraction of the reinforcements as well as their distribution in the Al matrix [12-14]. The formation of strong interface bonding between the reinforcements and the Al matrix is also substantial [14, 15]. Over the decades, various processing techniques have been developed to optimize the microstructures and properties of P-AMCs, and also to obtain a structure with a homogeneous distribution of reinforcement particles, free of defects, and strong interface bonding [3]. According to the material physical state during processing,

the techniques for fabricating P-AMCs can be generally classified into the following four major categories: solid-state processing, liquid-phase processing, deposition processing, and additive manufacturing (AM) (Fig. 2).

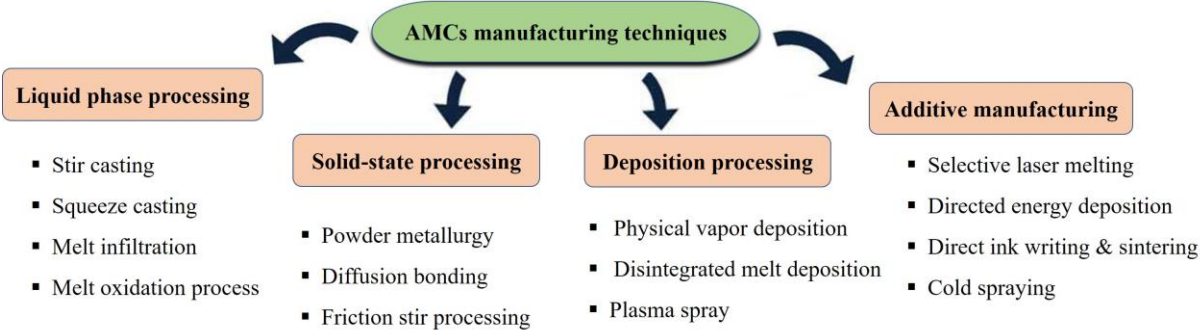


Fig. 2 Summary of the manufacturing techniques for AMCs.

Among these techniques, stir casting and powder metallurgy are widely used for producing P-AMCs in industries. In recent years, other advanced technologies such as in-situ synthesis [16, 17] and friction stir processing (FSP) [18, 19] have also been developed to fabricate P-AMCs. However, most of these techniques are often accompanied by problems of high porosity, large grain size, clustering of particles, poor interface bonding, and undesirable interfacial reactions, which can degrade their final mechanical performance. Moreover, these techniques show limitations in producing net-shape components.

AM, also called 3D printing, is a novel manufacturing method that undergoes rapid development during the last decade because it allows to producing complex or near-net-shape parts efficiently and rapidly using powders or wires as raw materials. Most AM methods use a high power energy source such as laser, arc, plasma, or electron beam to melt metal or composite feedstocks (powders or wires) through layer by layer deposition or powder bed fusion [20, 21].

Cold spray (CS) or cold gas dynamic spray (CGDS) is a kinetic spray additive method and has received increasing attention due to its solid-state deposition nature. Different from thermal spray or laser-based AM techniques, the interparticle bonding in CS is formed through severe plastic deformation of the particles upon high-velocity impact and the consequent interparticle metallurgical bonding and/or interlocking. CS is a low-temperature method, compared with the fusion-based AM technologies such as selective laser melting (SLM), which thereby can prevent the adverse effects of oxidation, phase transformation, excessive interface reaction, and grain growth involved in the CS parts. CS also exhibits other unique advantages including a high production rate (as high as 30 Kg/h), unlimited component size, and feasibility in repairing damaged parts. These advantages make CS an ideal technique for manufacturing coatings, repairing structures, forming free-standing components, particularly for producing thermally sensitive materials like AMCs.

## 1.2 Cold spraying as an innovative solid-state technique

CS technique was invented by Papyrin and his colleagues in Russian in the mid-1980s [22, 23]. They selected a range of metallic materials such as Al, Cu, Ni to understand the bonding mechanisms involved in the CS deposition process [24-28]. Since then, CS has drawn worldwide attention and underwent rapid development in academic laboratories and industries, especially during the last fifteen years [27, 29-31].

As the bonding in CS relies on the extent to which the feedstock particles can be plastically deformed, one must ensure that the velocity of flying particles exceeds the so-called critical velocity upon impact with the substrate [29, 32, 33]. The high velocity is achieved using a pressurized and preheated process gas (air, N<sub>2</sub>, and He) that expands through a converging/diverging nozzle known as De Laval nozzle which generates supersonic gas flow [29]. In this process, a fluidized powder feedstock is fed into the nozzle at high pressure so that the powder particles are accelerated within the gas stream to reach high velocities up to 1200 m/s or even higher (Fig. 3a). CS process is then featured by high particle impact velocity but low particle temperature compared with other conventional thermal spray processes (Fig. 3b).

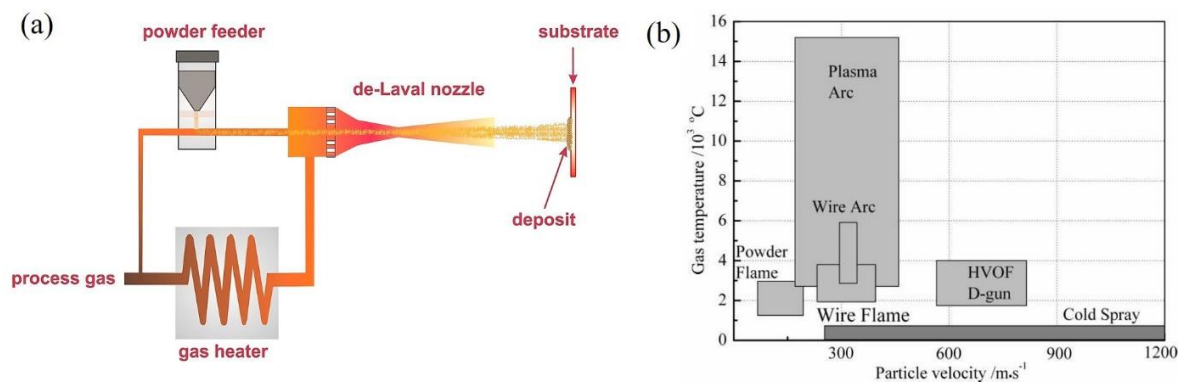
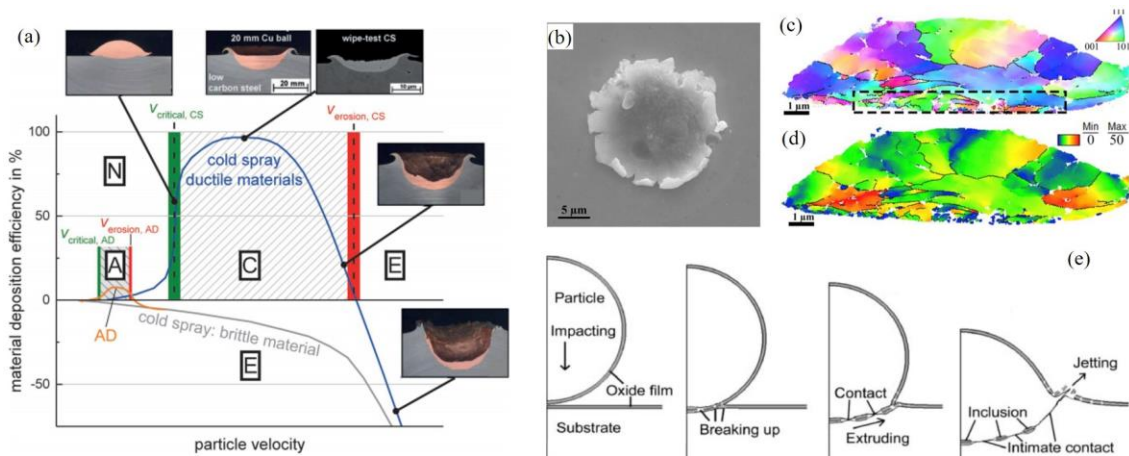


Fig. 3 Schematic diagram of (a) high-pressure CS system [29] and (b) comparison of CS with other thermal spray processes [34].

The most commonly accepted mechanisms related to coating deposition are mechanical interlocking and metallurgical bonding [29, 35-37]. Mechanical bonding is formed by interlocking of hard particles into the soft substrate without chemical reaction or atomic diffusion [38-41]. Metallurgical bonding takes place via a chemical reaction or atomic diffusion at the highly deformed interface (particle/particle or particle/substrate), where oxide-free and metal-to-metal contact are required [36, 41, 42]. Due to severe localized deformation after impacting upon a substrate, there is an adiabatic shear instability (ASI) and adiabatic temperature rise [35, 36] that lead to a thermal softening at the interface [35]. The material acts as a viscous fluid and protrudes radially from the edge of the particle to form an outward jet, as schematically shown in (Fig. 4b). In the ASI region (Fig. 4e), the outward jet can clean the oxide fragments from the interface. This cleaning effect is capable of promoting intimate contact

between fresh metal [42, 43], and thereby inducing metallurgical bonding. The adiabatic heating generated within this highly sheared zone causes a rapid local temperature rise and confined melting phenomena at the interface [44], where the grains are extensively deformed and refined through dynamic recrystallization [45, 46] (see Fig. 4c and d). According to Schmidt et al. [47], the particles need to reach a critical velocity for successful bonding, while the particles rebound below it. When the particle impact velocity is too high (much higher than the critical velocity), the surface of the substrate could be eroded by the particles. The velocity range between the critical velocity and erosion velocity defines the window for CS deposition (Fig. 4a) [48]. The particles having a velocity within this window can achieve a successful bonding. This theory has been further confirmed by a series of experimental results and simulation results [49-53].



*Fig. 4 Deposition characteristics of a single ductile particle impacting on metal substrate: (a) schematic deposition window for ductile material [48]; (b) typical morphology of a deformed Al alloy splat [54]; (c) and (d) microstructure evolution within the deformed particle [54]; (e) schematic diagram of the bonding process during particle impact [43].*

Recently, Hassani et al. successfully observed the real-time particle impact and deposition behaviors through an in-situ observation system [32, 33]. Based on a series of measurements, the critical velocities for the successful deposition of pure metals (Al, Ni, Cu, Zn) and Al alloys (2024Al, 6061Al, 7075Al) have been determined. The authors also developed a mechanistic framework to estimate the critical velocity for jetting based on a hydrodynamic spall process [33, 55]. Their numerical simulation results revealed that it is the hydrodynamic plasticity caused by the interaction of strong pressure waves during high-velocity impact, rather than the shear instability, inducing interface bonding. Furthermore, the authors found out the critical velocity is related to the bulk speed of sound. Based on these findings, the authors proposed a new mechanism to explain the jetting formation and the particle bonding related to the CS process. However, this theory remains a subject of debate [55, 56].

The researchers have been demonstrating great enthusiasm in exploring potential applications of this new technique while devoting themselves to an in-depth understanding of the deposition

mechanisms. CS has been extensively used for producing a variety of metallic materials for different applications including Al alloy [57-60], pure Cu and its alloy [61-63], Ti and its alloy [64-66], Ni-based superalloy [67, 68], stainless steel [69-71], and MMCs [72-77]. As a new member of the AM techniques, CS has been developed for the applications of surface functionalization, damage repair, and the fabrication of large scale components [61, 64, 78-80]. For instance, a thick Cu coating was deposited inside a pressure ring device for food processing machine applications (see Fig. 5a). Very rapid production of a Ti6Al4V axisymmetric bulk component and a cone structure was achieved by using CSAM (see Fig. 5b and c). CS is also capable of metallization of polymers or ceramics for producing electronic heat sinks (see Fig. 5) and damage repair due to its high feasibility, low thermal effects on the target, and low-cost. As shown in Fig. 6, some damaged transmission gearboxes and housings were successfully restored using CSAM. The repaired parts exhibited high adhesion strength, wear resistance, and corrosion resistance, which again extends their service life [78]. More specific applications of CS were reported in Refs [28, 78, 81].

Also, CS offers high feasibility in the fabrication of MMCs by using composite powders prepared by different technologies. Various MMCs including Al-based, Cu-based, Ni-based, and Fe-based composites have been developed using CS for different purposes [77, 82-86]. Among these, CS AMCs have received the most attention due to their large potential applications in damage repair, especially for aircraft and marine components. Up to now, various AMCs have been deposited by CS. Typical CS AMCs that can be found in literature include SiC/Al-12Si [87], Al<sub>2</sub>O<sub>3</sub>/Al [88, 89], TiN/Al [90], SiC/Al5056 [91, 92], TiB<sub>2</sub>/Al [93], SiC/7075Al [94], TiB<sub>2</sub>/7075Al [76, 94], CNT/Al [95, 96], diamond/Al [97-99]. In the following sections, we will provide a detailed review of CS AMCs from the aspects of composite powder preparation, processing, microstructure evolution, and properties.

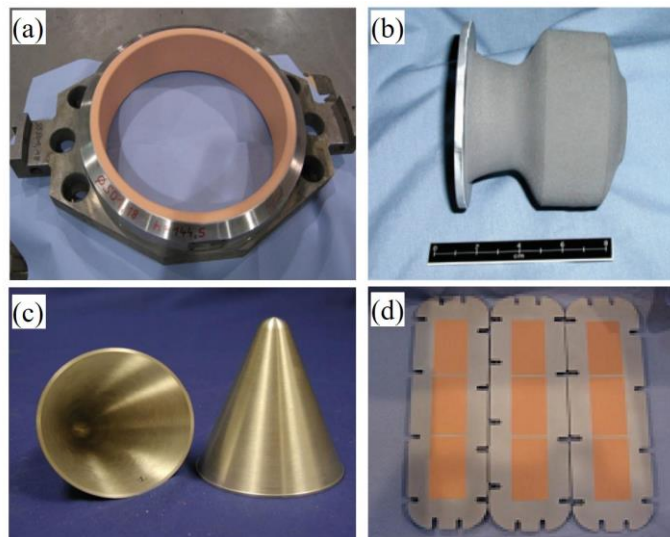


*Fig. 5 Photos of CS components with complex structures and thin coatings: (a) a thick Cu coating was deposited inside a pressure ring for food processing machine; (b) an axisymmetric bulk (Ti6Al4V); (c) a cone structure; (d) Cu coating for power electronic heat sink [28, 100].*

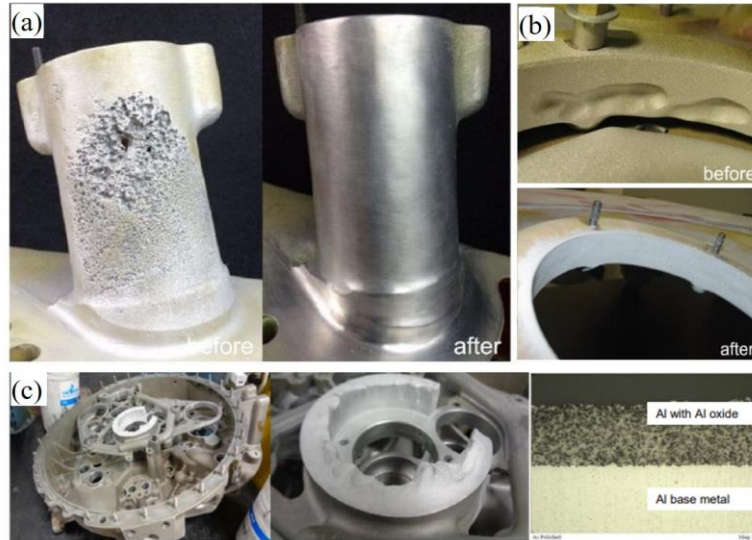


Fig. 6 Photos of damaged parts before and after CS repair: (a) S-92 helicopter gearbox sump; (b) UH-60 helicopter gearbox sump; (c) gearbox housing repairation using blended Al and Al<sub>2</sub>O<sub>3</sub> powders [101, 102].

## 2 Composite powder preparation routes for cold spraying

It has been widely accepted that the nature of feedstock powders directly affects the microstructure and properties of CS-processed deposits or components. In general, there are five different methods for composite powders preparation: (i) simple mechanical mixing/blending, (ii) satellite/wet granulation, (iii) mechanical ball milling, (iv) dry spraying, and (v) gas atomization. The advantages and limitations of these methods are summarized in Table 1.

Table 1 Summary of the different composite powder production approaches [103].

Methods	Advantages	Shortcomings
Mechanical blending	<ul style="list-style-type: none"> <li>The content of reinforcement particles can be adjusted over a wide range.</li> <li>No interface reaction.</li> <li>Simple operation and low cost.</li> </ul>	<ul style="list-style-type: none"> <li>Particle size limitation.</li> <li>Loss of reinforcements during deposition.</li> <li>Uneven distribution of reinforcements.</li> <li>Poor interface bonding between the reinforcement particles and the matrix.</li> </ul>
Satellite/wet granulation	<ul style="list-style-type: none"> <li>Controlled adherence of small reinforcement particles.</li> <li>Increased level of ceramic attachment in the CS deposits.</li> </ul>	<ul style="list-style-type: none"> <li>A little complicated compared to mechanical blending.</li> <li>A small amount of remaining binder.</li> <li>Poor interface bonding between the reinforcement particles and the matrix.</li> </ul>
Mechanical ball-milling	<ul style="list-style-type: none"> <li>Capable of producing a fine and homogeneous structure within the composite powder.</li> <li>Good control of the volume fraction, size, and distribution of</li> </ul>	<ul style="list-style-type: none"> <li>Particle morphology change and possible interface reaction.</li> <li>More complex than mechanical blending.</li> <li>Very low deposition efficiency (DE).</li> </ul>

	<ul style="list-style-type: none"> <li>reinforcement particles.</li> <li>Produce a relatively strong interface bonding.</li> <li>Available for producing nanostructured composite powder.</li> </ul>	<ul style="list-style-type: none"> <li>Introduction of impurities during ball milling.</li> </ul>
Spray drying	<ul style="list-style-type: none"> <li>Obtaining homogeneous agglomerated composite powders.</li> <li>Powder with controllable particle size and low oxygen.</li> <li>A relatively simple operation process.</li> </ul>	<ul style="list-style-type: none"> <li>Poor cohesion strength.</li> <li>Low production efficiency and high production cost.</li> <li>Presence of ultrafine particles</li> </ul>
Gas-atomization	<ul style="list-style-type: none"> <li>Introduction of uniformly distributed (nanosized) reinforcements.</li> <li>Uniformly distributed reinforcements.</li> <li>Strong interface bonding between the reinforcement and the matrix.</li> <li>Relative high DE</li> </ul>	<ul style="list-style-type: none"> <li>Limited reinforcement content</li> <li>High production cost</li> </ul>

## 2.1 Mechanical mixing/blending

As summarized in [Table 2](#), mechanical mixing/blending has been widely applied for preparing composite feedstocks due to its simple operation and low cost. The most prominent benefit of this approach is that it is very easy to control the composition of the composite by varying the volume fraction of reinforcement particles in the mixture feedstocks. As shown in [Table 2](#), the ceramic particle fraction varies in the range from 5 to 75 vol.%. Besides, the morphology of the ceramics could be near-spherical or irregular (see [Fig. 7](#)). Generally, irregularly shaped particles are beneficial for embedding into the deposit and for obtaining high content of reinforcements in the composite deposit. In contrast, spherical particles could result in a lower content of reinforcement but enhanced the in-situ hammering effect due to unsuccessful deposition, which contributes to a denser structure and improved grain refinement effect.

However, this method also brings some shortcomings in CS AMCs. Generally, to achieve a successful deposition of the reinforcement particles into composite deposits, the size of ceramic reinforcement particles needs to be larger than 5  $\mu\text{m}$  as smaller particles penetrate through the bow shock in front of the substrate [103]. This means that it is technically difficult to obtain an AMC reinforced with ultrafine or even nanosized particles by CS. Secondly, the brittle ceramic particles possess lower DE than the ductile metal particles, which results in low retention of reinforcements in the deposits, especially when a high content of ceramic particles is added to the powder feedstock. Furthermore, the reinforcement ceramic particles are mainly dispersed at the Al splat boundaries and have a very poor interface bonding with each other, which can dramatically weaken the mechanical performance of the CS AMCs.

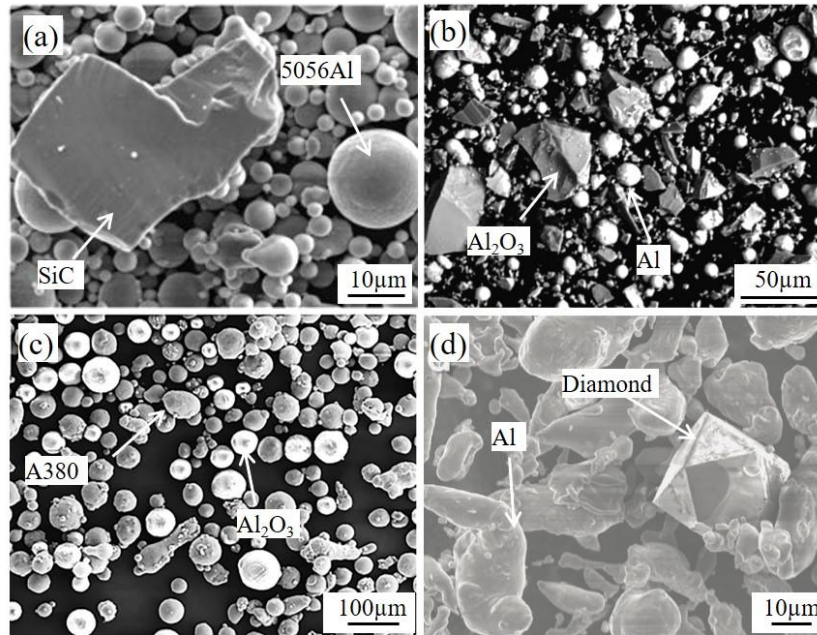
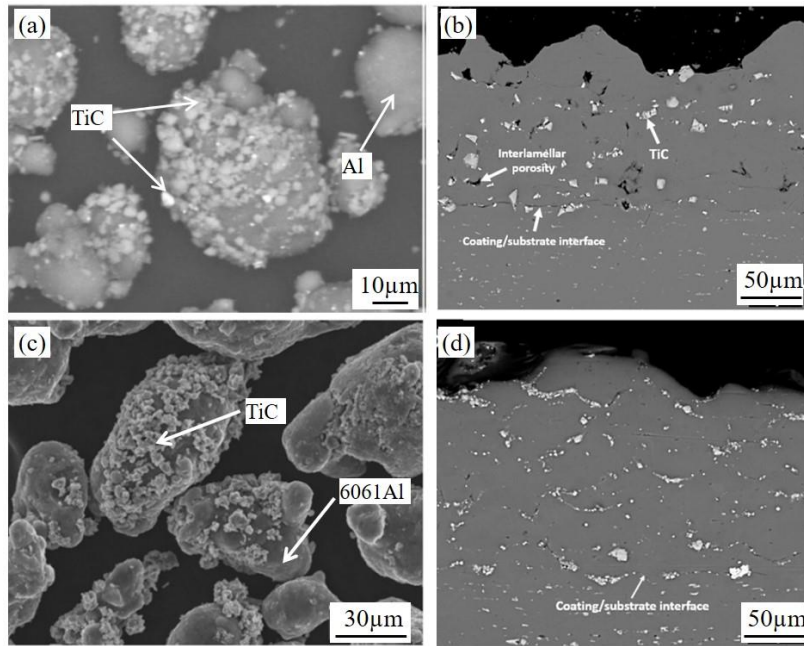


Fig. 7 The blending mixed powders with different particle morphologies: (a) irregular SiC/5056Al [91]; (b) irregular Al<sub>2</sub>O<sub>3</sub>/Al [104]; (c) dodecahedral diamond/Al [105]; (d) near-spherical Al<sub>2</sub>O<sub>3</sub>/A380 [106].

## 2.2 Satelliting/wet granulation

To improve the dispersion of the reinforced particles, satelliting, also named wet granulation, was employed for producing composite feedstocks with a liquid binder (for example polyvinyl alcohol) to attach small (satellite) ceramic particles onto relatively large Al particles [107]. By using this method, it is capable of synthesizing the composites reinforced with very fine particles (<5 µm), which is quite different from the mechanical blending method. Examples of TiC/Al and TiC/6061Al composite feedstocks produced by satelliting method are given in Fig. 8. A high level of small TiC particles was attached to the surface of the large Al particles using a binder [108, 109]. However, some reinforcement particles could also rebound away and be lost during deposition due to the poor adhesive strength of the binder. The reinforcement particles were mainly distributed along the inter-splat boundaries within the deposit. This method has not been widely used for CS AMCs preparation so far.



*Fig. 8 Scanning electron microscope (SEM) images showing the surface morphologies of the (a, c) satellited composite feedstocks with attached fine TiC particles and (b, d) the cross-sectional microstructures of the corresponding CS deposits: (a) and (b) TiC/Al; (c) and (d) TiC/6061Al [108, 109].*

### 2.3 Mechanical ball milling

Mechanical ball milling of a powder mixture is another effective way to improve the distribution of reinforcement phases and to enhance reinforcement/matrix interfacial bonding. Ball milling has high feasibility in the synthesis of composite powders feedstock as it enables the control of content, size, and distribution of the two phases in an acceptable way [103]. As summarized in Table 3, many studies have reported the fabrication of Al nanocrystalline composites via high-energy ball milling. It was reported that a homogeneous structure with ultrafine grains as well as the work hardening effect produced during the ball-milling effectively increased the microhardness of the composite deposit. Meanwhile, the increased microhardness of the composite powder resulted in very low particle DE [93]. Therefore, higher processing parameters (high gas temperature and pressure) or expensive He is required to achieve higher particle impact velocities for successful deposition, which significantly increases the cost and reduces the attractiveness of the ball-milled powders for industrial applications [103]. Furthermore, the ball milling process may bring some impurities such as oxides into the composite powder, which, in turn, can hinder the metallic bonding of the deformed particles and thereby decrease the mechanical properties of the CS AMCs.

The composite particle morphology, size distribution, microstructure, and phase composition could be changed during the ball milling process and can affect the deposition behavior of the particle, the microstructure, and the properties of the CS composite deposit. The influence of various ball-milling

conditions on the microstructure and properties of the obtained AMC powder was systematically studied [97, 98, 110]. For instance, according to the study of Gojon et al [110], increasing the ball milling time from 2 h to 8 h further refined and homogenized the distribution of SiC particles in the 5056Al matrix, but made the powder shape more irregular at the same time (see Fig. 9). Fig. 10 shows another example of nanodiamond-reinforced AMC (ND/AMC) powders synthesized utilizing high energy ball milling for CS deposition. A total of 27 different ND/Al composites were produced by varying ND content and ball-milling parameters (i.e., milling time and ball-to-powder ratio). It was found that the ball-to-powder ratio and milling time had a significant effect on the crystal size and hardness of the composite powder. The high-energy ball milling created a uniform distribution of ND within the Al composite particle and simultaneously induced a thin  $Al_4C_3$  layer at the ND/Al interface which enhanced the interfacial bonding between the reinforcement particle and Al matrix. Two other examples of CS AMCs using ball-milled powders are given in Fig. 11. In the former case,  $TiB_2$  particles were distributed inside the Al matrix through a high energy ball milling process (Fig. 11a-c). The composite powder fabricated with this method always has a very low DE due to the enhanced work hardening effect. In contrast, when the relatively low processing energy was applied during ball milling, a core-shell structure could be obtained (Fig. 11d-f). The out layer was composed of the composite structure with uniformly distributed ceramic particles in the Al matrix, while the inner core remained the initial structure of Al particle with the little embedment of reinforcements.

Besides, the ball milling process is commonly used for dispersing CNTs or graphene into an Al matrix to produce CNTs reinforced AMC for CS deposition [111, 112]. The dispersion of CNTs into metal particles is more difficult than that for ceramic particles because the CNTs have a much higher specific surface area. Therefore, before milling, the blended mixtures are commonly ultrasonicated within ethanol for homogeneous dispersion of the CNTs. As revealed in Fig. 12, the ball-milling process is effective in the dispersion of CNTs into the Al matrix. Meanwhile, it causes some damages to the integrity structure of CNTs due to the high energy input. Recently, a new shift-speed ball milling process was applied to fabricate the CNT/Al composite powder for CS deposition [96]. As illustrated in Fig. 13, CNTs were first mixed with the pure Al powders using a blender followed by ball milling in a planetary ball mill at a relatively low speed, during which the CNTs could uniformly disperse into the Al matrix. Afterward, the powder mixture was milled again at a higher velocity for a short time to acquire the final CNT/Al composite powder. Compared to the commonly used high energy ball milling process, the shift-speed ball milling dispersion method demonstrated uniform distribution of CNTs, strong interfacial bonding, but less structural damage of CNTs because of the relatively low energy input.

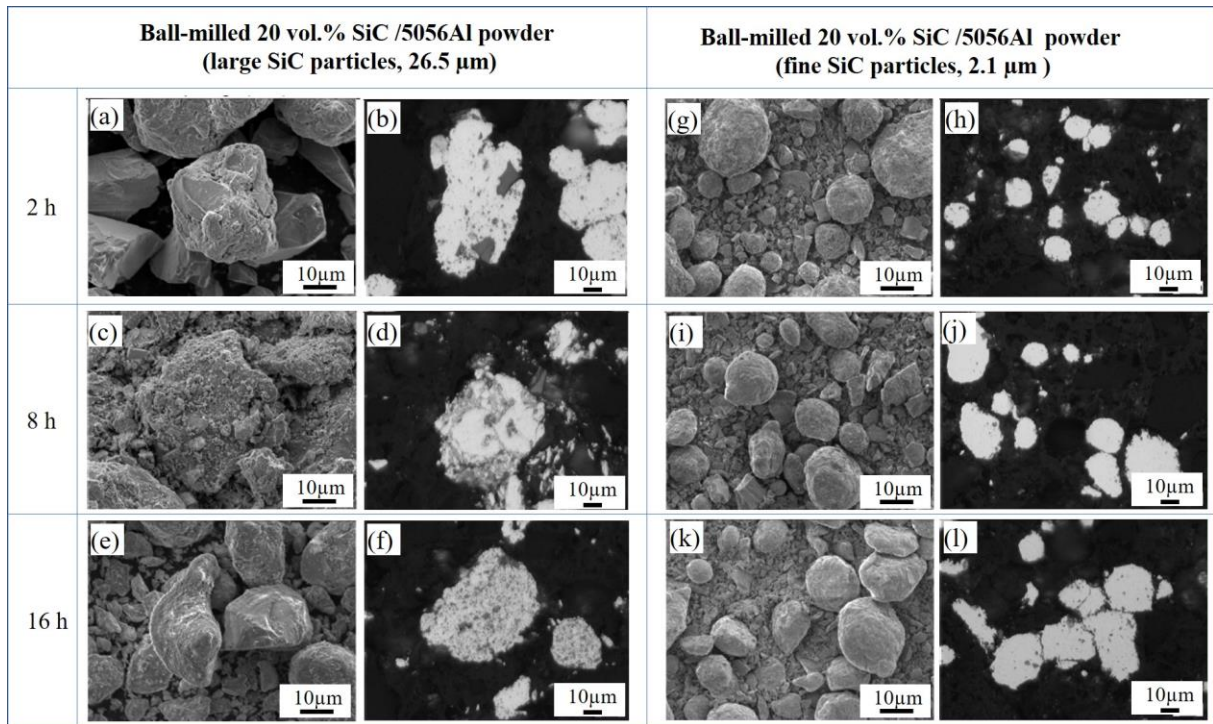


Fig. 9 Particle morphology evolution as a function of ball-milling time (2h, 8h, and 16h) for the 20 wt.% SiC/5056Al composite powders with large and fine SiC particles [110].

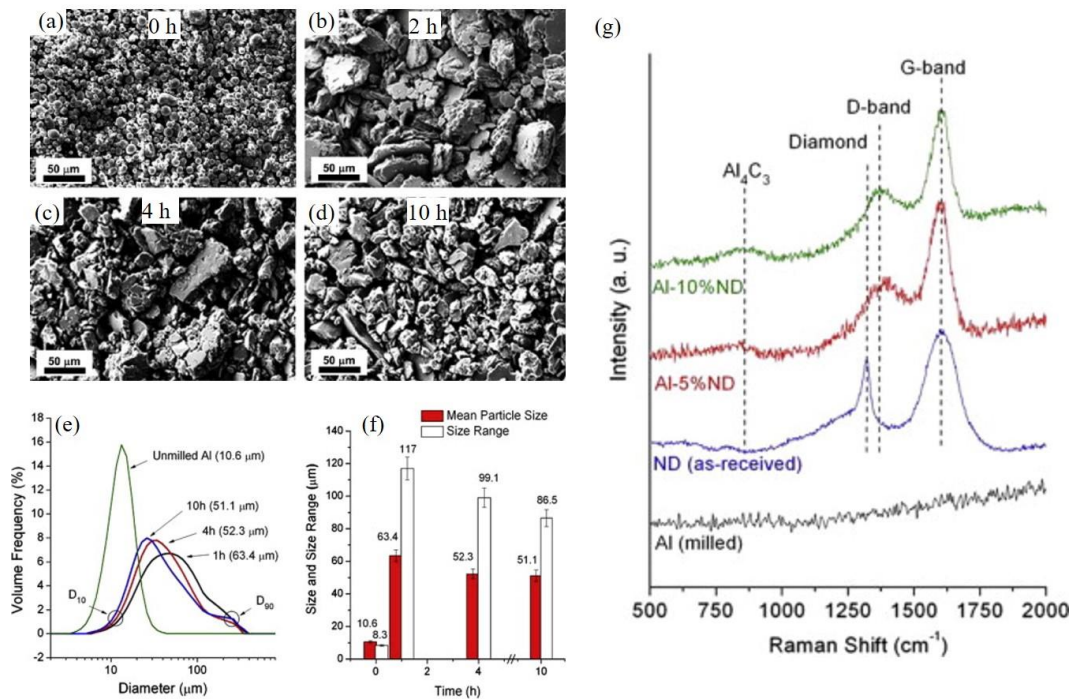


Fig. 10 SEM images showing the (a) as-received Al and nanodiamond/Al composite powders (5 wt.% ND) after ball-milling for (b) 1 h, (c) 4 h, and (d) 10 h. (e) and (f) Particle size distribution evolution. (f) Raman spectra of the ball-milled ND/Al composite powder[98].

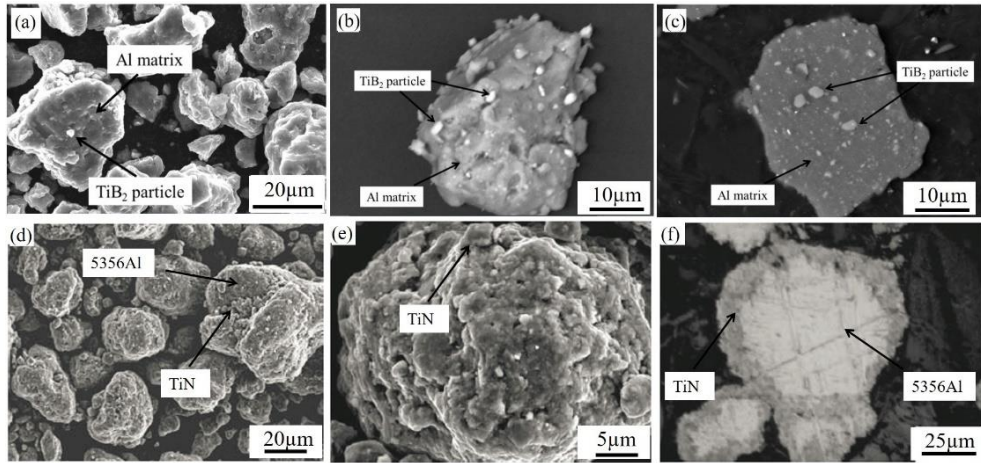


Fig. 11 Surface morphologies and cross-sectional views of the composite powders using high energy ball milling (a-c)  $\text{TiB}_2/\text{Al}$  [113] and low energy ball milling (d-f)  $\text{TiN}/5356\text{Al}$  [114].

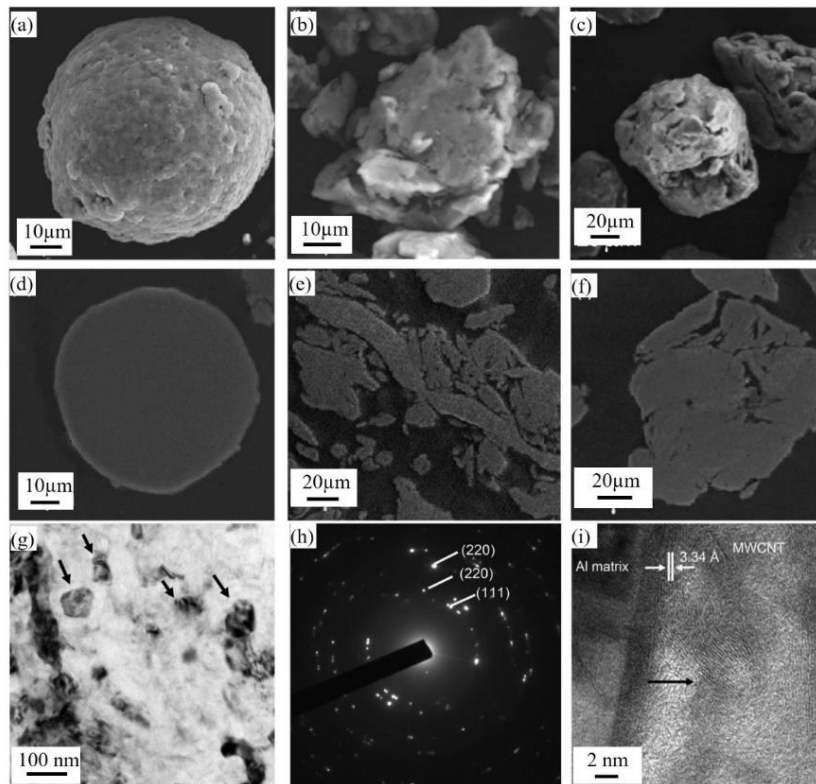
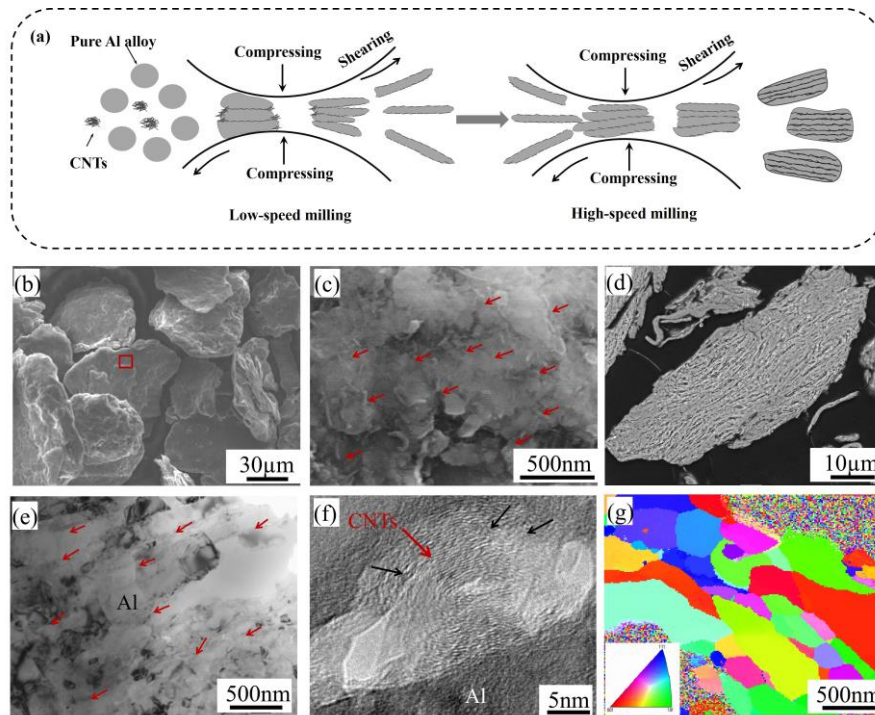


Fig. 12 Particle morphology evolution of the ball-milled CNTs/Al composite powder with different content of CNTs: (a, d) pure Al, (b, e) 1.0 vol.% CNTs, and (c, f) 3.0 vol.% CNTs. (g-h) Transmission Electron Microscope (TEM) characterization of the 3.0 vol.% CNTs/Al composite powder showing the nanocrystalline structure and the embedded CNTs in the Al matrix [112].



*Fig. 13 (a) Schematic illustration of the shift-speed ball milling process for the synthesis of the CNT/AlSi composite powder for CS deposition; (b) Particle morphology and (d) cross-sectional view of the CNT/AlSi composite particle; (c) observation of CNTs on the particle surface at high magnification; (e) and (f) TEM images showing the dispersed CNTs within the Al matrix; (g) TEM/electron backscattered diffraction (EBSD) orientation map [96].*

## 2.4 Spray drying

The spray drying involves a full mixing of the fine powders in a slurry, gas spraying/atomization, and followed by drying using hot gas. This approach allows for producing composite powders with a near-spherical shape and homogeneous structure. Due to its feasibility in the dispersion of CNTs into metallic particles and no structural damage of CNTs, this approach was employed to synthesize CNT/Al composite powders for CS deposition [95]. After drying water from the mixture slurry, CNTs were uniformly dispersed on the surface of the fine AlSi particles (Fig. 14), which agglomerated to form large composite particles with high-level porosities. Composite deposits having a content of 1 wt.% CNTs were successfully fabricated by using the mixtures of the pure Al powder and the spray-dried composite powder [95]. CNTs were found to distribute not only at the inter-splat boundaries but also inside the particles. However, the severe plastic deformation and shearing effect induced by high-velocity impact resulted in structural damages of CNTs [115]. For this reason, this method is not widely used to prepare composite powder for CS in addition to its low production efficiency and high cost.

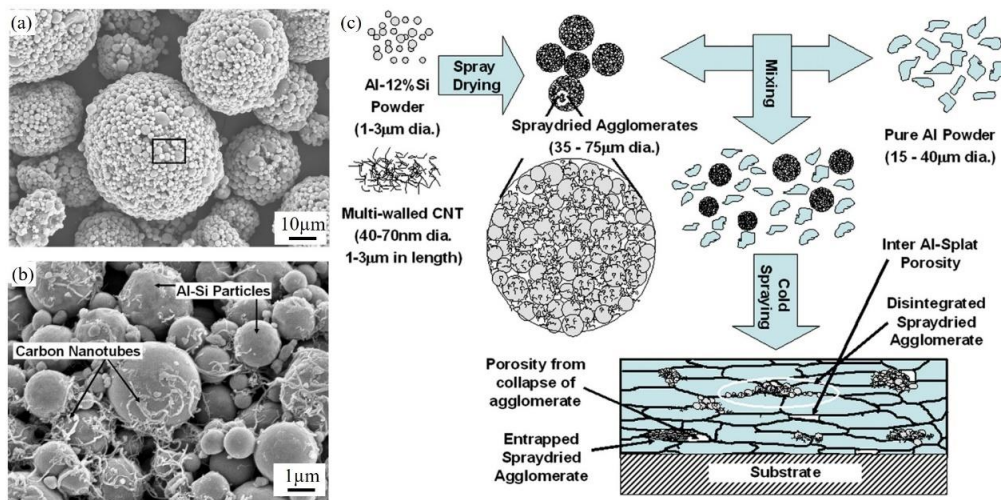


Fig. 14 SEM images showing (a) spray-dried Al-Si agglomerates and (b) magnified region in (a) to highlight agglomerated CNTs. (c) Schematic diagram of the composite powder preparation and CS deposition processes [95].

## 2.5 Gas atomization

This powder preparation method is completely different from the above-mentioned methods. Recently, Xie et al. [76] used a new feedstock material for CS, a gas-atomized Al matrix composite powder reinforced with in-situ  $TiB_2$  nanoparticles. The  $TiB_2$  nanoparticles were in-situ formed in the Al matrix by chemical reaction of mixed salts ( $K_2TiF_6$  and  $KBF_4$ ) inside the liquid phase before atomization. The gas-atomized composite powder displayed a near-spherical shape. The in-situ formed  $TiB_2$  reinforcement particles with a size range of tens of nanometres up to a few microns enabled ununiform distribution in the composite particles with a preferential distribution along the grain boundaries (see Fig. 15). The addition of  $TiB_2$  particles can provide nucleating sites during gas atomization, and thereby effectively refine the Al grains [116, 117]. The use of this composite powder for CS deposition solved the problems of uneven distribution of the reinforcement particles, poor reinforcement/matrix interfacial bonding, as well as low DE which are encountered in other methods. A possible disadvantage of this method is that the amount of reinforcement cannot be too high. Otherwise, agglomeration could occur, and metal liquid will become viscous and affect the subsequent gas-atomization process. Nevertheless, it offers a new route for producing nanocomposite powders suitable for CS deposition.

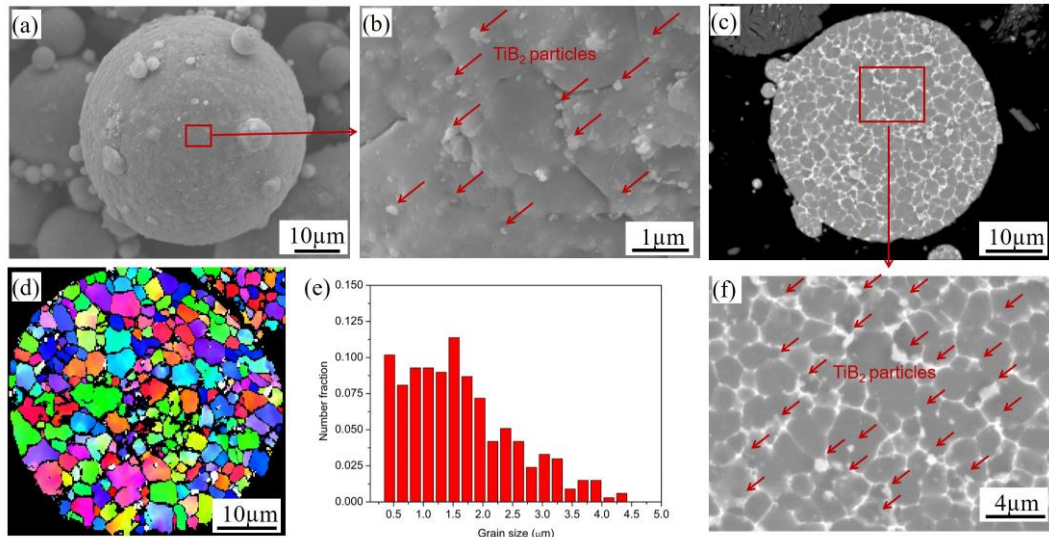


Fig. 15 The morphology of gas-atomized  $\text{TiB}_2/7075\text{Al}$  composite powder with uniformly distributed  $\text{TiB}_2$  nanoparticles [76]: (a) Particle surface morphology; (b) Magnified view showing uniformly distributed  $\text{TiB}_2$  nanoparticles on the particle surface; (c) Cross-sectional view of the composite particle; (d) EBSD orientation mapping; (e) Grain size distribution; (f) Magnified view of the region marked in (c).

Table 2 Summary of the CS-processed AMCs using mixed/blended composite powders.

Composites	Main processing parameters	Substrate material	Ceramic particle size	Ceramic particle content in powders, vol. %	Ceramic particle content in deposits, vol. %	Composite deposit hardness, HV	Adhesion strength (MPa)	Reference
SiC/Al12Si	He, P <sub>g</sub> =3.0 MPa T <sub>g</sub> =500 °C	Al6061-T6	5-45	0	0	110 ± 25 (HV <sub>0.3</sub> )	21.7 ± 3.8	[118] [87]
				20.0	10.0	145 ± 14	20.9 ± 4.3	
				30.0	14.0	163 ± 16	--	
				40.0	17.0	175 ± 19	16.7 ± 3.6	
				60.0	20.0	205 ± 25	--	
Al <sub>2</sub> O <sub>3</sub> /Al	N <sub>2</sub> , P <sub>g</sub> =0.62 MPa T <sub>g</sub> =500 °C	7075Al	25.5	0	0	52 ± 2 (HV <sub>0.3</sub> )	40 ± 5	[88] [119]
				7.1	7.2	60 ± 2.3	53 ± 4	
				24.1	11.7	62 ± 2.3	60 ± 1	
				40.6	16.5	75 ± 4.5	>60	
				67.2	19.2	94 ± 10.2	>60	
Al <sub>2</sub> O <sub>3</sub> /6061Al	He, P <sub>g</sub> =0.62 MPa T <sub>g</sub> =125 °C	Cast AZ91E alloy	20	0	0	112 ± 10 (HV <sub>0.2</sub> )	36.2 ± 2.9	[89]
				25	11	160 ± 10	40.4 ± 3.1	
				50	19	168 ± 15	--	
				75	29	190 ± 20	42.0 ± 0.2	
α-Al <sub>2</sub> O <sub>3</sub> /Al	Compressed air P <sub>g</sub> =1.6 MPa T <sub>g</sub> =230 °C	AZ91 Mg alloy	1-30	0	0	53 ± 3 (HV <sub>0.025</sub> )	18	[120]
				18.6	15.1	65 ± 5	25	
				40.6	29.3	--	32	
TiN/5356Al	Compressed air P <sub>g</sub> =2.7 MPa T <sub>g</sub> =510 °C	Pure Al	10-45	0	0	53 ± 2 (HV <sub>0.2</sub> )	32 ± 4	[90]
				13.9	17	146 ± 10	--	
				32.7	26	175 ± 10	>50	
TiN/2319	Compressed air, P <sub>g</sub> =2.6 MPa T <sub>g</sub> =490 °C	Al	10-45	0	0	106 ± 7.8 (HV <sub>0.2</sub> )	--	[121]
				32.7	38.7	154 ± 18.9	--	
Al <sub>2</sub> O <sub>3</sub> /Al	He, P <sub>g</sub> =0.62 MPa T <sub>g</sub> =200 °C	AZ91 Mg alloy	25	0	0	0.96 GPa	--	[122]
				40.3	15	1.1	--	
SiC/5056Al	Compressed air, P <sub>g</sub> =2.5-2.6 MPa T <sub>g</sub> =600 °C	Pure Al	66.9	0	0	110.4 (HV <sub>0.3</sub> )	--	[91]
				15	21.2	135 ± 20	--	
				30	26.4	156 ± 15	--	
				45	33.6	170 ± 30	--	

				60	41.4	$213.8 \pm 25$	--	
SiC/7075Al	He, $P_g=0.98$ MPa $T_g=300$ °C	Al6061-T6	7	0	0	$136 \pm 10.5$ (HV <sub>0.3</sub> )	--	[94]
				10	8	$179 \pm 8$	--	
				20	16	$190 \pm 8$	--	
B <sub>4</sub> C/7075Al			15	10	$167 \pm 8$	--		
				20	12	$178 \pm 8$	--	
Al <sub>2</sub> O <sub>3</sub> /A380	Compressed air, $P_g$ $=2.5$ MPa $T_g=450$ °C	AZ31	48.3	0	0	$105 \pm 6$ (HV <sub>0.3</sub> )	--	[106]
				7.4	1.2	$135 \pm 3$	--	
				15	2.5	$130 \pm 5$	--	
				26	4.8	$136 \pm 4$	--	
				33	5.3	$124 \pm 8$	--	
Al <sub>2</sub> O <sub>3</sub> /Al	He, $P_g=0.62$ MPa $T_g=125$ °C	AZ91D Mg alloy	20	0	0	$62.0 \pm 4$ (HV <sub>2.5</sub> )	$20 \pm 3$	[104]
				15	8.9	$76 \pm 2$	$28 \pm 6$	
				25	13.9	$74 \pm 2$	$39 \pm 6$	
				35	19.8	$83 \pm 3$	$38 \pm 7$	
				50	26.4	$88 \pm 4$	$43 \pm 8$	
				75	39.8	$120 \pm 6$	$32 \pm 4$	
Al <sub>2</sub> O <sub>3</sub> /Al	N <sub>2</sub> , $P_g=3.0$ MPa $T_g=400$ °C	6061Al	25.5 (angular)	0	0	$43 \pm 3$ (HV <sub>0.2</sub> )	--	[123]
				7.1	7.0	$58 \pm 5$	--	
				40.6	16.1	$75 \pm 6$	--	
				24.26 (spherical)	7.1	2.7	$47 \pm 5$	
				40.6	8.5	$59 \pm 4$	--	
Al <sub>2</sub> O <sub>3</sub> /Al	N <sub>2</sub> , $P_g=1.65$ MPa $T_g=250$ °C	6061Al	22	0	0	$45.0 \pm 8.9$ (HV <sub>0.3</sub> )	$19 \pm 2$	[124]
				7	6.3	$52.3 \pm 1.3$	$30 \pm 2$	
				15	10.8	$64.4 \pm 1.6$	$30 \pm 2$	
				23	16.1	$68.5 \pm 2.8$	$32 \pm 2$	
				31	21.0	$72.3 \pm 7.1$	$40 \pm 2$	
				41	22.7	$78.1 \pm 5.7$	$43 \pm 4$	
				51	25.2	$79.9 \pm 4.3$	$43 \pm 2$	
				61	30.4	$86.1 \pm 8.1$	$62 \pm 7$	
				73	34.0	$89.5 \pm 3.9$	$>70$	
86	41.6	$114.2 \pm 12.1$	$>70$					
SiC/Al	Compressed air, $P_g$ $=1.5$ MPa $T_g=300$ °C	-	11-34	0	0	$50 \pm 3$ (HV <sub>0.3</sub> )	--	[125]
				23	23	$62 \pm 4$	--	
				46	47	$75 \pm 8$	--	
				71	52	$88 \pm 4$	--	

B <sub>4</sub> C/Al	Compressed air, P <sub>g</sub> =2.2 MPa T <sub>g</sub> =300~350 °C	Al6061-T6	5	42	23	58 ± 2.8	—	[126]
---------------------	--	-----------	---	----	----	----------	---	-------

Table 3 Summary of the CS-processed AMCs using ball-milled composite powders.

Materials	Main processing parameters	Substrate material	Ceramic particle size	Ceramic particles content in powders, vol.%	Ceramic particles content in deposits, vol.%	Composite deposit hardness	Reference
B <sub>4</sub> C/5356Al	He, P <sub>g</sub> = 3.0 MPa T <sub>g</sub> = 500 °C Preheating powder (150 °C)	Al6061-T6	3-14	0	0	133.1 ± 6.5 (HV <sub>0.3</sub> )	[127]
				20	17.5 ± 1.8	251.4 ± 7.8	
Diamond/Al	N <sub>2</sub> , P <sub>g</sub> = 1.73 MPa T <sub>g</sub> = 450 °C	1018 steel substrate	nanosized	0 10	0 ~10	1.10 GPa 3.02	[97]
TiB <sub>2</sub> /Al	He, P <sub>g</sub> = 2.9 MPa	Al6061	5-100 nm	20 wt.%	~20 wt.%	132 ± 22 (HV)	[93]
TiN/Al5356	Compressed air, P <sub>g</sub> = 2.7 MPa T <sub>g</sub> = 510 °C	Al	-	0 60.8 ± 7.7	0 53.2 ± 10.8	68.7 ± 11.6 (HV <sub>0.2</sub> ) 250 ± 33.8	[114]
Al <sub>2</sub> O <sub>3</sub> /Al	He, P <sub>g</sub> = 0.78 MPa T <sub>g</sub> = 500 °C annealed at 450 °C for 15min	Mild steel	4 nm	0	0	0.96 ± 0.09 GPa	[128]
				5	5	1.3 ± 0.3	
SiC/5056Al	N <sub>2</sub> , P <sub>g</sub> = 2.8 MPa T <sub>g</sub> = 500 °C	SiC/2009Al T4	26.5 μm	0 20	0 18	125 ± 6 (HV <sub>0.01</sub> ) 143 ± 16	[110]
			2.1 μm	20	20	148 (HV <sub>0.1</sub> )	
CNT/Al	He, P <sub>g</sub> = 2.4 MPa T <sub>g</sub> = 300 °C	Al 1050	20–50 nm	0	0	58.6 (HV <sub>0.1</sub> )	[111]
				0.5 wt.% 1.0 wt.%	0.5 wt.% 1.0 wt.%	131.2 172.1	

P<sub>g</sub> and T<sub>g</sub> represent the propelling gas pressure and temperature, respectively

Table 4 Summary of the wear behavior of the CS AMC deposits.

Materials	Substrate material	Test method	Testing conditions	Main finding	Reference
Al <sub>2</sub> O <sub>3</sub> /Al	7075Al	Dry abrasive test	A load of 45 N for 10 min.	Abrasion resistance was independent of the alumina mass fraction in the deposits. The poor cohesion between Al and Al <sub>2</sub> O <sub>3</sub> limits the improvement of the abrasion resistance.	[88]
Al <sub>2</sub> O <sub>3</sub> /6061Al	Cast AZ91E alloy	Ball-on-disc	A load of 3 N, the linear speed of 20 cm s <sup>-1</sup> ; a sliding length of 500 m and 6 mm ball-bearing steel.	Significant reduction of the wear rate of the composite deposit. Increasing Al <sub>2</sub> O <sub>3</sub> addition gradually changes the wear mode from adhesive to abrasive.	[89]
TiN/Al5356	Pure Al	Ball-on-disc	A load of 2 N and 0.2 m/s, a sliding distance of 50 m, 6 mm diameter steel ball.	Wear rates of the ball-milled composites is lower than the blend mixed composite.	[90]
SiC/5056Al	Pure Al	Ball-on-disc	Loads of 2 N and 10 N, A peed of 20 cm/s, sliding distance of 500 m, 6 mm diameter WC/Co ball.	The SiC particle and its content in the deposit influence the tribological behavior of the composite deposit.	[91]
SiC/7075Al	6061Al-T6	Reciprocating wear test	A normal load of 1 N, sliding stroke, total sliding distance, and sliding velocity were 0.002 m, 10 m, and 0.002 m/s, 6 mm Al <sub>2</sub> O <sub>3</sub> ball.	B <sub>4</sub> C reinforced composite deposits exhibited higher wear resistance when compared to SiC reinforced ones.	[94]
B <sub>4</sub> C/7075Al					
Al <sub>2</sub> O <sub>3</sub> /A380	AZ31	Ball-on-disc	A load of 3 N, a speed of 180 rpm wear length was 37.7 m, 6 mm diameter Al <sub>2</sub> O <sub>3</sub> ball.	With an increase of Al <sub>2</sub> O <sub>3</sub> content in the composite deposits, the wear mechanism of the deposit is changed from adhesive wear to a combination of delamination and abrasive wear.	[106]
Al <sub>2</sub> O <sub>3</sub> /Al	6061Al	Sliding wear tests	A normal load of 1 N, sliding speed of 3 mm/s, a track length of 10 mm, α-Al <sub>2</sub> O <sub>3</sub> ball of 6.35 mm diameter.	The spherical Al <sub>2</sub> O <sub>3</sub> morphology was associated with improved tribological behavior compared to the angular morphology.	[123]
Al <sub>2</sub> O <sub>3</sub> /Al	6061Al	Sliding wear test	A load of 25 N, three different travel lengths: 25, 50, and 100 m. Al <sub>2</sub> O <sub>3</sub> ball.	Deposit with higher alumina content did not show an increment in wear resistance.	[124]
SiC/Al	--	Sliding wear test	Different sliding velocities (0.5, 1, and 2 m/s) and loads (1, 5, and 10 kg). sliding time was 15 min. WC-Co discs.	Increasing SiC particulate volume greatly enhances the wear performance of the deposits.	[125]

B <sub>4</sub> C/5356Al	6061Al-T6	Reciprocating sliding wear test	The normal load of 16.25 N, a linear 10 mm/s velocity, a sliding distance of 500 m.	The presence of homogeneously distributed fine B <sub>4</sub> C reinforcement particles within the matrix could significantly improve the dry sliding wear resistance.	[127]
MWCNT/Al	1050Al	Pin-on-disc tests	A load of 100 N duration of 300 s. The rotating diameter of the pin was 20 mm under 100 rpm. cylindrical bearing steel of 3 mm diameter.	The wear loss decreased, and COF decreased with an increase in CNT fractions.	[111]
TiC/6061Al	6082Al	Ball-on-flat reciprocating dry-sliding wear tests	A normal load of 5N, a linear displacement of 5mm, and 1 Hz frequency for 10 min.	Using a satellite feedstock is more efficient in reducing the deposit wear rate in comparison to deposits made using blended mixtures.	[109]

Table 5 Summary of the corrosion behavior of the CS AMC deposits [129].

Materials	Main processing parameters	Substrate material	Ceramic particle size, $\mu\text{m}$	Ceramic particles content in powders, vol. %	Corrosion test conditions	Corrosion behavior	Reference
$\alpha\text{Al}_2\text{O}_3/\text{Al}$	Air, $P_g = 1.6 \text{ MPa}$ $T_g = 230 \text{ }^\circ\text{C}$	AZ91D Mg alloy	1-30	25, 50	3.5 wt.% NaCl solution	The addition of $\alpha\text{-Al}_2\text{O}_3$ has no passive effect on the anti-corrosion ability of the composite deposits.	[120]
$\text{Al}_2\text{O}_3/\text{Al}$	$\text{N}_2$ , $P_g = 0.62 \text{ MPa}$ $T_g = 500 \text{ }^\circ\text{C}$	mild steel and Al7075	25.5	10, 30, 50, 75	3.5 wt.% NaCl solution	Composite deposits were as efficient as pure Al deposits in providing corrosion protection against alternated immersion in saltwater and salt spray environment.	[88]
$\text{Al}_2\text{O}_3/\text{Al}$ $\text{Al}_2\text{O}_3/6061 \text{ Al}$	He, $P_g = 0.62 \text{ MPa}$ $T_g = 125 \text{ }^\circ\text{C}$	AZ91E Mg alloy	20	25, 50, 75	5 wt % NaCl solution	Neither the $\text{Al}_2\text{O}_3$ content nor a post-spray heat treatment had any significant effect on the polarization behavior of the deposits.	[89]
SiC/5056Al	Air, $P_g = 2.6 \text{ MPa}$ $T_g = 600 \text{ }^\circ\text{C}$	Al	48-92.6	15, 30, 60	0.1M $\text{Na}_2\text{SO}_4$ solution	Composite deposits showed better corrosion resistance than the 5056Al deposit, but the SiC content make no sense on anodic polarization behavior.	[92, 130]
SiC/7075Al $\text{B}_4\text{C}/7075\text{Al}$	He, $P_g = 0.98 \text{ MPa}$ $T_g = 300 \text{ }^\circ\text{C}$	T6 6061 Al alloy	28 7	20	3.5 wt.% NaCl solution	The addition of ceramic particles increased corrosion current densities.	[94]
$\text{Mg}_{17}\text{Al}_{12}/\text{Al}$	He, $P_g = 0.98 \text{ MPa}$ $T_g = 300 \text{ }^\circ\text{C}$	AZ91D Mg alloy	48.5	50, 70	3.5 wt.% NaCl solution	The anti-corrosion performance was degraded by adding the hard particles to the Al matrix.	[131]

Al <sub>2</sub> O <sub>3</sub> /Al	N <sub>2</sub> , P <sub>g</sub> =2.5 MPa T <sub>g</sub> =350 °C	Low carbon steel	63	25	5 wt % NaCl solution	The reinforced deposit showed a slightly higher corrosion resistance compared to the pure Al deposits.	[132]
Al <sub>2</sub> O <sub>3</sub> /Al	He, P <sub>g</sub> =0.62 MPa T <sub>g</sub> =125 °C	AZ91 Mg alloy	20	25, 50, 75	3.5 wt% NaCl solution	Corrosion potentials were lower than the bulk Al.	[133]
Al <sub>2</sub> O <sub>3</sub> /2024 Al	Air, P <sub>g</sub> =0.9 MPa T <sub>g</sub> =600 °C	2024Al-T3	15-45	20, 40, 60	3.5 wt% NaCl solution	Al <sub>2</sub> O <sub>3</sub> /Al2024 deposit displayed the lowest corrosion current density and highest corrosion resistance.	[134]
Al <sub>2</sub> O <sub>3</sub> /5083 Al	He, P <sub>g</sub> =1.0 MPa T <sub>g</sub> =400 °C	ZM 5 magnesium alloy	40	20, 40, 60	3.5 wt% NaCl solution	Better corrosion resistance was obtained for the 20 vol.% Al <sub>2</sub> O <sub>3</sub> /5083Al.	[135]
TiB <sub>2</sub> /7075Al	Compressed air, P <sub>g</sub> =3.0MPa, T <sub>g</sub> =500 °C He, P <sub>g</sub> =1.8MPa, T <sub>g</sub> =320 °C	7075Al-T6	Nano-sized	4.2	0.1M & 0.6M NaCl solution	The addition of TiB <sub>2</sub> nanoparticles reduces the corrosion resistance of CS 7075Al coatings. Greater plastic deformation and precipitation lead to lower corrosion resistance. A low-temperature annealing treatment improves the corrosion resistance of CS coatings.	[129]

### 3 Cold spray processing of Al matrix composites: deposition behavior and features

#### 3.1 Deposition behavior

The deposition behavior of CS AMCs is dependent on the powder preparation method. For the composites produced using mechanically blended powders, the Al phase (soft metal) deforms significantly, while the ceramic particle (hard phase) rather embeds into the Al matrix. The addition of ceramic particles into the ductile powder feedstocks can increase DE (see Fig. 16) through the following two possible mechanisms [124]. Firstly, the grit blasting effect induced by ceramic particles can increase the roughness of the substrate. The formation of asperities can promote particle deposition through improved mechanical anchoring and thus increase the DE. Secondly, the oxide cleaning effect of ceramic particles may also contribute to DE improvement. The native oxide films on the surface of the metallic particles and the substrate can be removed by the ceramic particles during impact, creating oxide-free surfaces that are favorable for metallurgical bonding.

The increase of DE with the ceramic contents was also true when the satellited TiC/6061Al composite powders were used (Fig. 8). Using this composite powder gained 20% higher momentum than non-satellite Al particles for similar particle size. Thus, the satellite particle powders produced higher plastic deformation in the deposit, and thus improve the particle deposition. Fig. 17 illustrates two schematics to compare the deposition mechanisms of the mechanical blended and satellited powders. For the mechanically blended feedstock, most of the ceramic particles rebounded from the substrate surface after impact. Comparatively, much more ceramic particles were successfully deposited using the satellited powders due to the pre-bond between the ceramic particle and the metal particle prior to impact.

However, the deposition behavior of the ball-milled composite powders is quite different from the blended mixtures and satellited powders, where the ceramic reinforcement particles are primarily dispersed at the interfaces of Al splats. In this case, the ceramic particles are pre-milled into composite particles, which will then be deposited as a whole. The reinforcement of ceramic particles and the work hardening effect produced during the ball milling process can significantly increase the hardness of the particle. This effectively results in a lower DE because a higher critical velocity is required during deposition. Besides, the size and morphology change of the particle during ball milling can influence the particle impact velocity which in turn affects the DE of the composite powder. Fig. 18 shows the deposition behavior of the ball-milled ND/Al composite powder. It was found that the increase of milling time decreased the DE, probably due to the grain size refinement and the increased work hardening effect produced

during the ball-milling process. It should be noticed that annealing has been proved as an effective method for improving the DE of the composite powders (see Fig. 18).

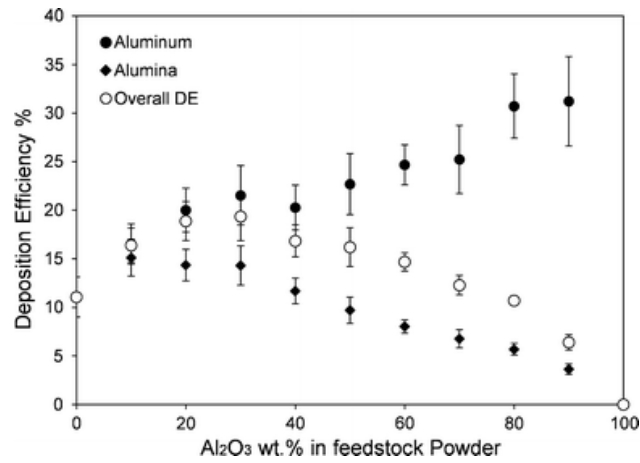


Fig. 16 DE evolution during the deposition of Al<sub>2</sub>O<sub>3</sub>/Al composite feedstock powders [124].

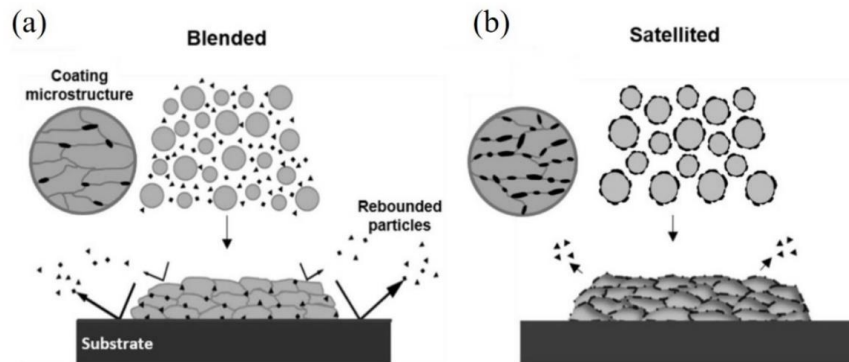


Fig. 17 Schematic diagrams of two deposition mechanisms using: (a) mechanically blended mixtures, (b) satellited particles [108].

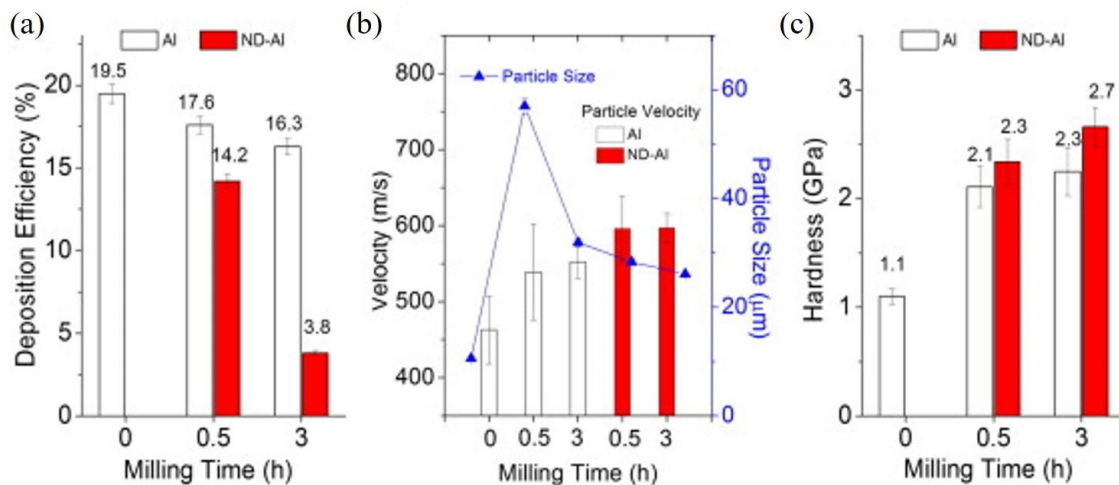


Fig. 18 The CS deposition behavior of the ball-milled ND/Al composite powder: (a) DE, (b)

*particle impact velocity, and (c) microhardness of pure Al and composite powders as a function of milling time [97].*

### **3.2 Reinforcement volume fraction and porosity evolution**

Fig. 19 summarizes the volume fraction of the ceramic particles in the final composites as a function of the ceramic content in the mechanically blended feedstocks. It is clearly shown that the ceramic contents in the composites are generally lower than those in the initial feedstocks due to their relatively low DEs. The four dotted lines shown in Fig. 19 refer to the fraction of the ceramic phase in the composite deposits and the feedstocks. Based on these values, it can be seen that the DE of the ceramic particles in most of the composite systems ranges between 30 % and 70 %. It should be noticed that several composite systems (SiC/Al, SiC/5056Al, and TiN/5356Al) possess very high DE of ceramic particles within the composite deposits. Moreover, it can be found in Fig. 20 that the DE depends on both size and morphology of the ceramic particles. Generally, angularly shaped ceramics are better deposited onto the Al matrix compared to the spherical ones. According to the study in [91], a larger ceramic particle was beneficial for deposition and the highest DE was obtained when the ceramic particle sizes were about 20  $\mu\text{m}$ . However, a further increase of ceramic particle size can hardly affect the DE.

Gojon et al. [110] studied the influence of composite powder preparation methods (mechanical blending and ball milling) on the evolution of the SiC content within the 5056Al matrix after CS depositions. It was confirmed that the SiC content of the composite deposit produced from mechanical blending was lower than its initial content, especially when the SiC particles had the smallest size, as shown in Fig. 21. Comparatively, a higher SiC content was obtained in the final composite deposit using the ball-milled composite powders and their content increased with the milling time. It was also found that the DE of the reinforcement ceramic particles using the ball milling method was independent of the initial SiC particle size [110]. Therefore, using ball-milled composite powders can improve the rentability of reinforcement in the composite deposits compared to the mechanical blending method. However, the enhanced work hardening effect produced during the ball milling process can increase the strength of the composite powder and decrease the overall DE. It should be pointed out that when the composite powder is prepared by ball milling, the content of the reinforcement cannot be too high, and the ball milling processing parameters must be well controlled. Otherwise, it can be difficult to have thick deposits even though using high CS processing parameters.

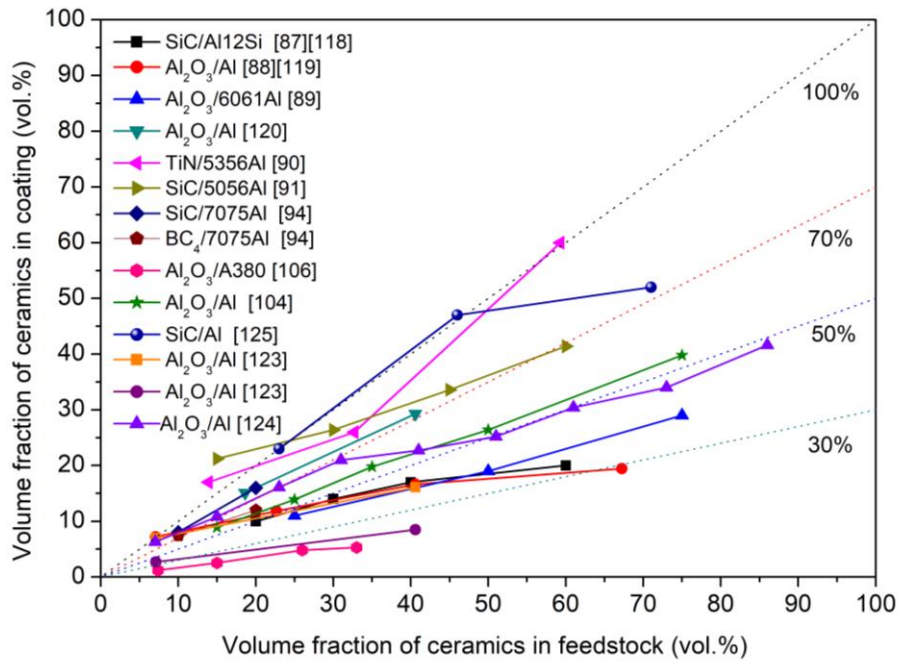


Fig. 19 The volume fraction of ceramic particles within the composite deposits as a function of the initial powder mixtures.

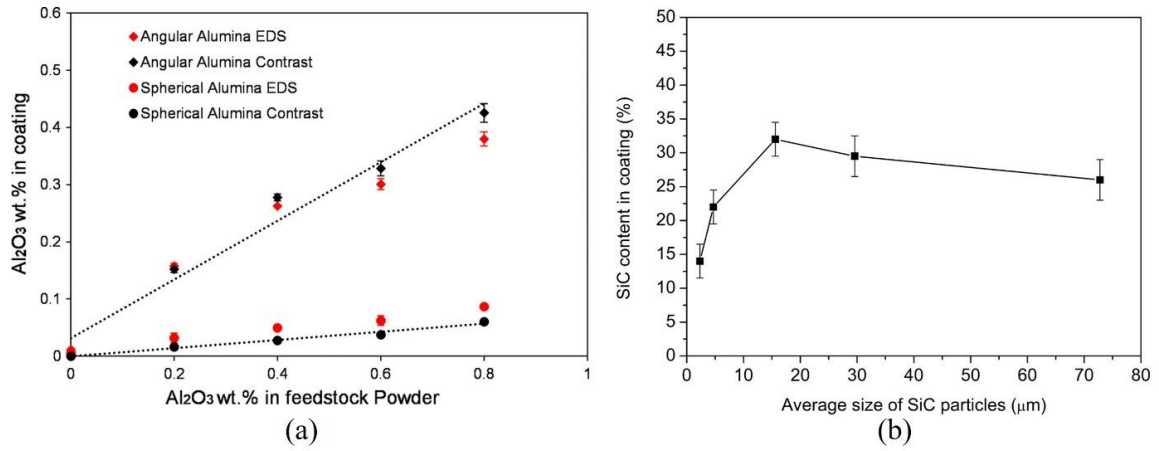


Fig. 20 (a)  $Al_2O_3$  content in deposits versus  $Al_2O_3$  content in feedstock powder with different morphologies (spherical and angular) [136]. (b) SiC content in deposits as a function of SiC particle size using the same content of SiC particles (30 vol.%) in the feedstocks [92].

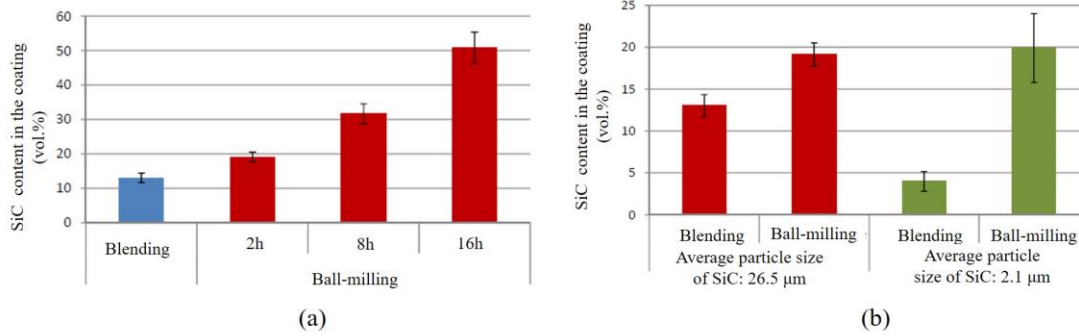


Fig. 21 Evolution of the SiC content within the 5056Al matrix as a function of powder preparation methods (mechanical blending and ball milling) using the same initial volume fraction of SiC (20 vol.%) in the composite powders [110].

Generally, the addition of ceramic particles in the feedstock reduces the porosity of the deposit due to enhanced peening effects generated by the particles. As shown in Fig. 22a, the porosity of the deposit decreases with the increase of ceramic content and finally keeps at a very low level, demonstrating a fully dense structure of the composite deposit. The reduced porosities are likely caused by the enhanced plastic deformation of the Al particles when more ceramic particles were added and acted as peening particles. In addition to the ceramic content, the size and morphology of the mixed ceramic particles also play an important role in reducing the porosity. As displayed in Fig. 22, the porosity of the SiC/5056Al composite deposit decreased slightly with the increase of ceramic particle size. According to Qiu et al. [106], the spherical ceramic particles were more efficient for reducing the porosity compared to irregularly shaped particles due to the enhanced in-situ peening effect of the spherical powders.

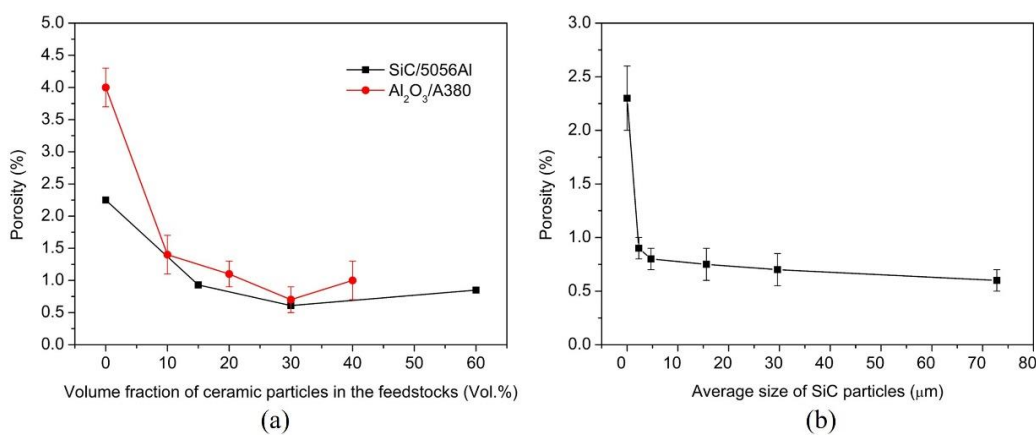


Fig. 22 Porosity evolution as a function of (a) volume fraction of ceramic particles in the feedstocks and (b) average SiC particle size [92, 106].

### 3.3 Characterization of deposit microstructure and its formation mechanisms

Typical cross-sectional morphologies of the CS AMC deposits produced using mechanically blended powders are shown in Fig. 23. The composite deposits exhibited a very dense structure with severely deformed Al particles and the embedded ceramic particles. These ceramic particles were primarily located at the particle-particle boundaries with some large ones fractured into small fragments during the deposition. According to EBSD analysis of the composite (Fig. 23e and Fig. 24), the Al matrix next to the  $\text{Al}_2\text{O}_3$  particles (independent of shapes) were highly deformed and the grains were significantly refined due to the enhanced peening effect [122]. Detailed TEM investigation (Fig. 23f) revealed an intimate interfacial bonding at Al/ $\text{Al}_2\text{O}_3$  particles. However, the reason for such a chemical bonding between the ceramic particle and the Al matrix is still unclear yet.

Fig. 25 shows the cross-sectional morphologies of SiC/5056Al composites produced using the mechanically blended composite powder and the ball-milled composite powders using different ball-milling time [110]. It was found that the angular SiC particles with larger sizes were primarily located at the inter-splat boundaries in the composite deposit produced using the mechanical blending method. Comparatively, the composite deposits produced using the ball milling method showed a more uniform distribution of small SiC particles within the 5056Al matrix. Increasing the ball milling time further refined the SiC particles and improved the uniformity of their distribution. However, it could significantly reduce the deposit thickness due to lowered DE.

The CS CNT/Al composites showed a dense structure with intimate inter-splat bonding (Fig. 26 and Fig. 27). The TEM images revealed ultrafine grains inside the particles, which were created by ball-milling and well retained after CS deposition. Accordingly, the inter-splat regions were characterized by elongated grains and uniformly distributed CNTs with the direction parallel to the shear stress propagation (Fig. 26e and Fig. 27c).

The microstructure of the CS  $\text{TiB}_2$ /7075Al composite deposit produced using the gas-atomized composite powder is shown in Fig. 28. Nano-sized  $\text{TiB}_2$  particles were uniformly dispersed across the 7075Al matrix, which was different from the composites produced using other powder preparation methods. The SEM/EBSD and TEM images of the composite sample revealed a heterogenous structure with ultrafine grains formed at the inter-splat boundary regions where particles were highly deformed. Moreover, the great plastic deformation during the CS deposition resulted in dislocation networks and precipitation formation. TEM images in Fig. 28c and d revealed that the nanosized  $\text{TiB}_2$  particles primarily dispersed along the grain

boundaries of the Al matrix. However, the interfacial features of this nanosized TiB<sub>2</sub>/Al are still unknown and need further investigation.

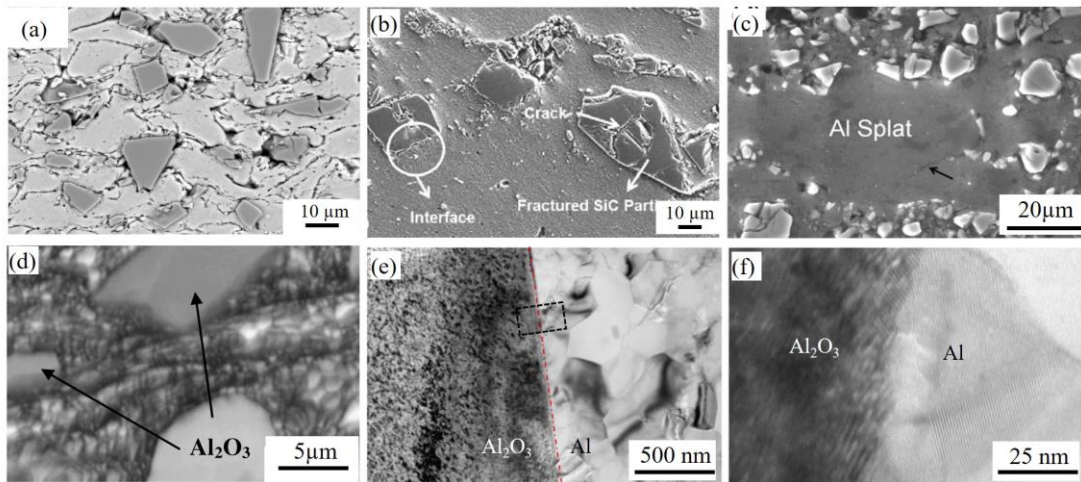


Fig. 23 Typical microstructures of the CS composites using mechanical blending method: (a) Al<sub>2</sub>O<sub>3</sub>/Al [137]; (b) SiC/5056Al [130]; (c) SiC/Al [122]; (d) EBSD pattern quality map of the cross-section of Al<sub>2</sub>O<sub>3</sub>/Al composite. (e) TEM and (f) high resolution images showing the Al/Al<sub>2</sub>O<sub>3</sub> interface [122].

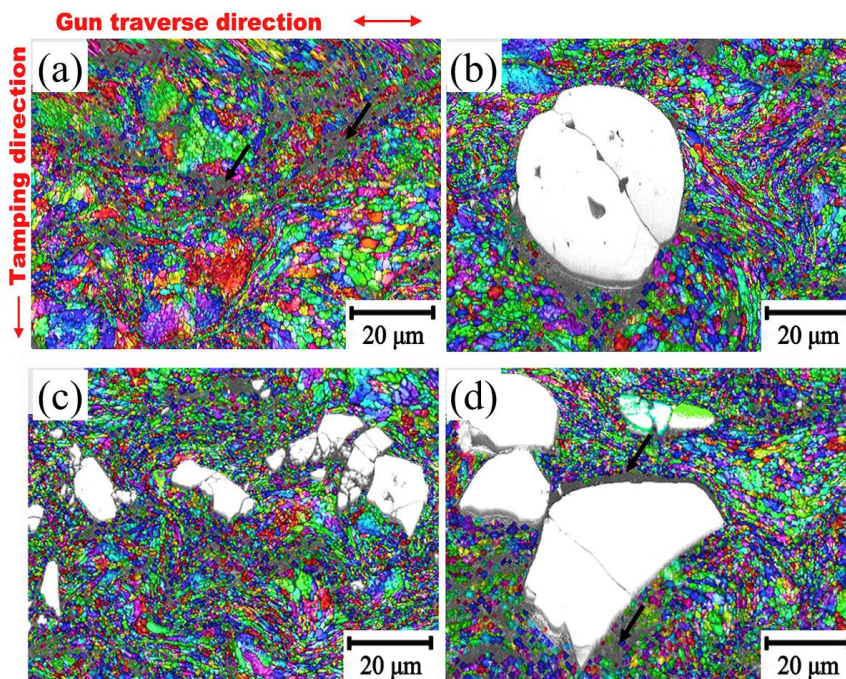


Fig. 24 SEM/EBSD orientation maps of the (a) CS pure A380 deposit and Al<sub>2</sub>O<sub>3</sub>/A380 composites with the addition of (b) spherical and (c) irregular or (d) both spherical and irregular Al<sub>2</sub>O<sub>3</sub> particles (white particles) [138].

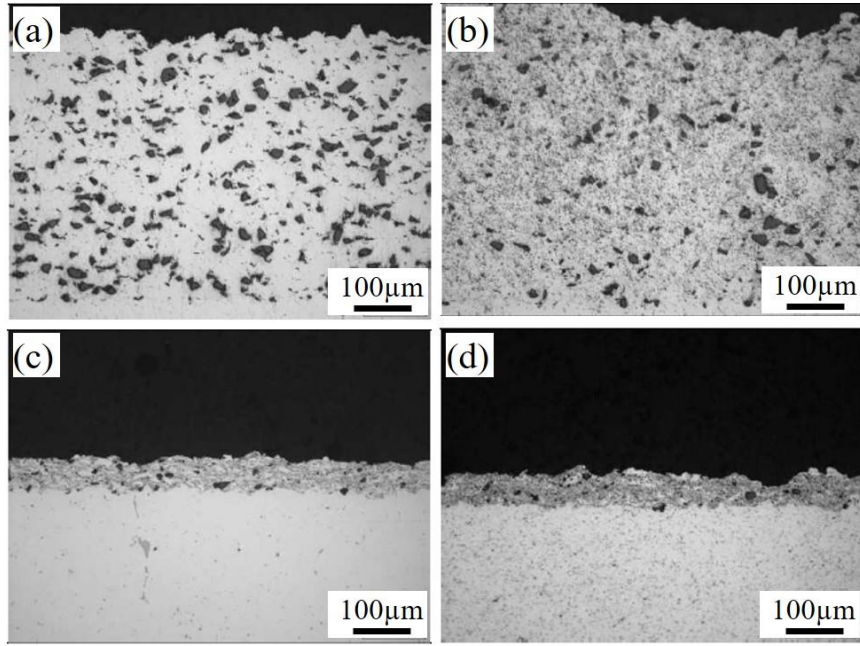


Fig. 25 Microstructure comparison of the 20 vol.% SiC/5056Al composites produced using (a) mechanical blended powders and ball-milled composite powders with different ball milling duration: (b) 2h (c) 8h; (d) 16h [110].

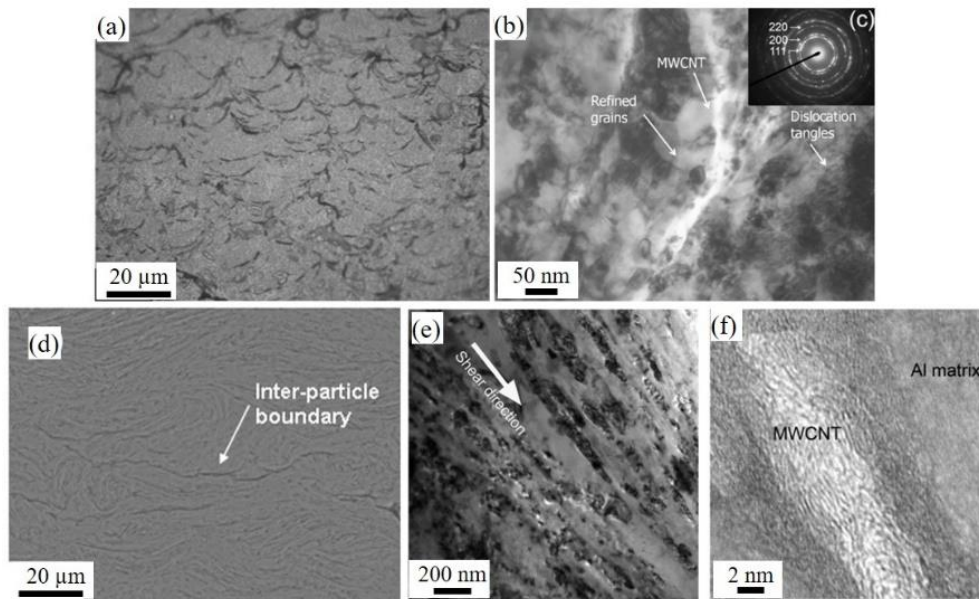


Fig. 26 (a, d) SEM and (b, e) TEM images showing the microstructure of the CS CNT/Al composite. (c) SAED pattern of the Al matrix in (b). (f) High resolution TEM image showing the embedded CNTs in the Al matrix [111, 112].

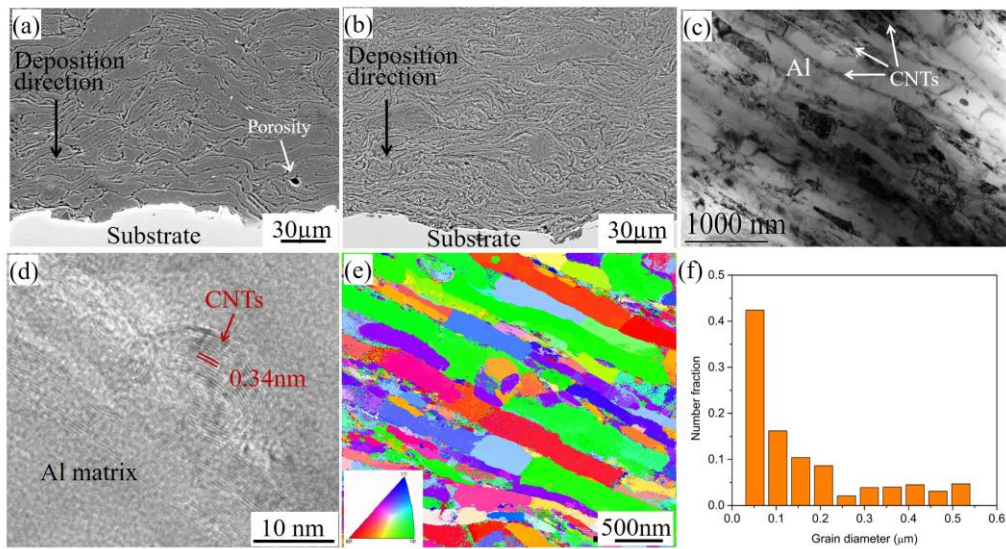


Fig. 27 (a, b) SEM and (c, d) TEM images showing the CS (a) pure AlSi and (b) CNT/AlSi composites. (e) TEM/EBSD orientation map; (f) grain size distribution of Al matrix [96].

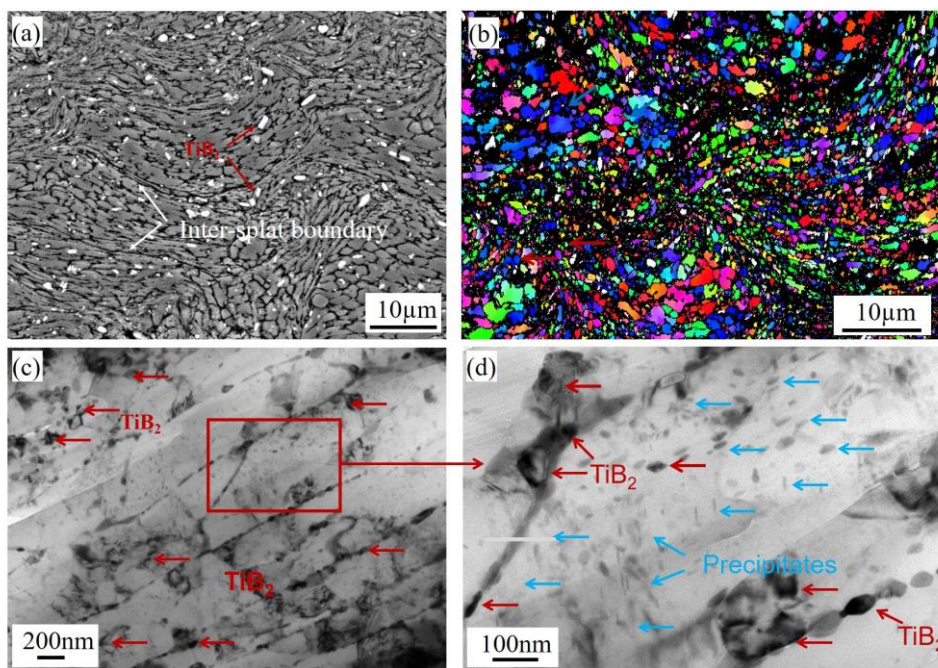


Fig. 28 (a) SEM image showing the microstructure of the CS TiB<sub>2</sub>/7075Al composite produced using gas-atomized composite powder. (b) SEM/EBSD orientation map of the Al matrix; (c) and (d) TEM images showing the uniformly distributed TiB<sub>2</sub> nanoparticles and precipitates [76].

## 4 Properties of Al matrix composites manufactured by cold spraying

### 4.1 Hardness and bonding strength

Fig. 29 summarizes the microhardness of the CS AMCs produced using mechanical blended mixtures. The microhardness of the Al matrix can be largely improved by incorporating micro-sized hard particles due to a high degree of plastic deformation of the Al matrix and the hammering effect induced by the hard ceramics during the CS deposition. The hardness of the composite increases with the increase of ceramic content. The hardness can be also affected by the shape of reinforcement particles. Fernandez et al. [136] reported that a lower content of spherical  $\text{Al}_2\text{O}_3$  particles resulted in higher microhardness than the angular  $\text{Al}_2\text{O}_3$ . This was attributed to the greater deformation of Al particles, arising from the low DE using the spherical  $\text{Al}_2\text{O}_3$ .

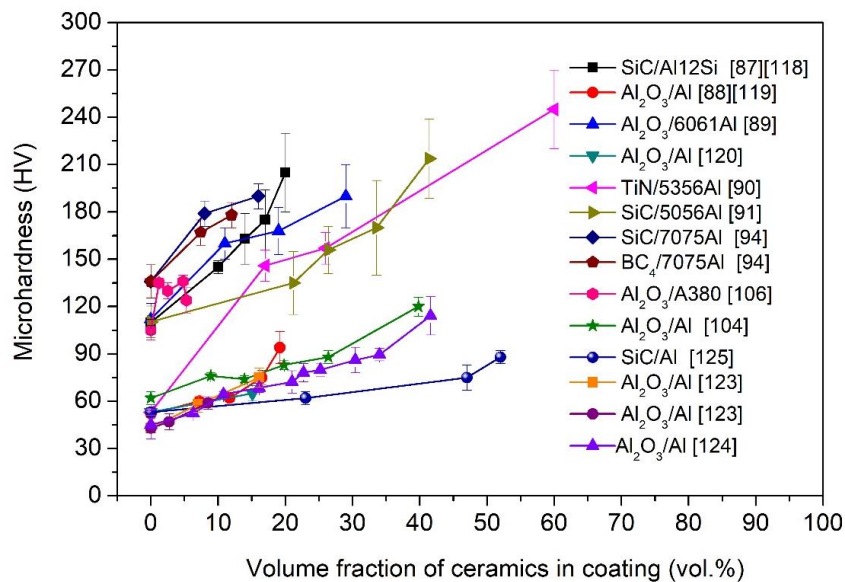


Fig. 29 Deposit microhardness as a function of ceramic content in the composite deposits produced from the mechanical blending method.

Generally, the composite produced using a ball-milled feedstock has higher microhardness due to an increased work hardening effect, grain refinement, and better strengthening effect of fine particles. As reported in [97], significant improvement in both hardness and Young modulus was achieved by adding homogenous nano-diamond particles in the Al deposit using ball-milled composite powder. It was also found that the microhardness of the CS CNT/Al composite was highly affected by the uniformly dispersed CNTs as they could inhibit plastic stress flow and dislocation movement. Ultrafine grains and high dislocation density within the composite deposit also contributed to the strengthening effect.

The deposit bonding strength against the ceramic particle content in the deposit is shown in Fig. 30. In most cases, the addition of ceramic particles increases the bonding strength of the deposit. However, this relation becomes no more true if the volume fraction exceeds a certain value. The addition of ceramic particles has two major effects on the bonding behavior of the composite deposit. On the one hand, the presence of ceramic particles promotes the plastic deformation of Al particles which produces stronger interfacial bonding between the Al particles, and also between the Al particles and the substrate. On the other hand, with a further increase in the content of ceramic particles, these gains will be offset by an increased proportion of weak Al/ceramic particles and substrate/ceramic interfaces. Therefore, it is plausible to consider that the maximum bonding strength closely depends on the ceramic content [87].

It was also reported that the bonding strength of the composite deposit was related to the morphology of ceramic particles [106, 139]. Generally, spherical ceramic particles were more efficient in enhancing the deposit bonding strength than angular ceramic particles [136]. This difference was attributed to a prominent peening effect of the spherical particles that can lead to a high deformation of the Al particles, and thus strengthening the bonding of the deposit/substrate interface.

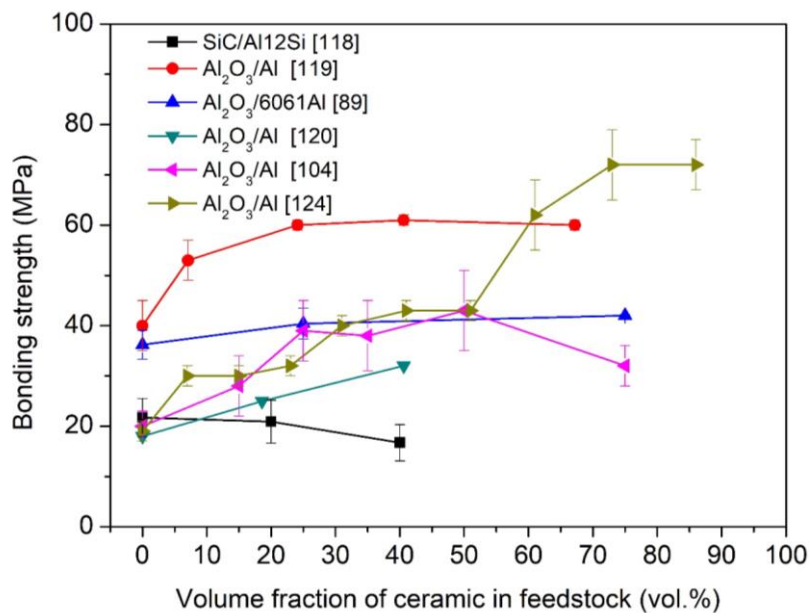


Fig. 30 Bonding strength as a function of ceramic particle content in the powder mixture.

Furthermore, the adhesion strength also depends on the composite powder preparation method. Gojon et al. [110] reported that compared to the mechanical blending method, the SiC/5056Al composite deposits produced using the ball milling method exhibited lower

adhesion strength especially when longer ball milling time was used (see Fig. 31). This could be explained by the reduced plastic deformation of the ball-milled composite particles upon the impact that resulted in reduced metallic bonding between the particles and the substrate. Moreover, the introduction of impurities such as oxides during the ball milling process could also have a negative effect on the metallic particle/particle and particle/substrate bonding.

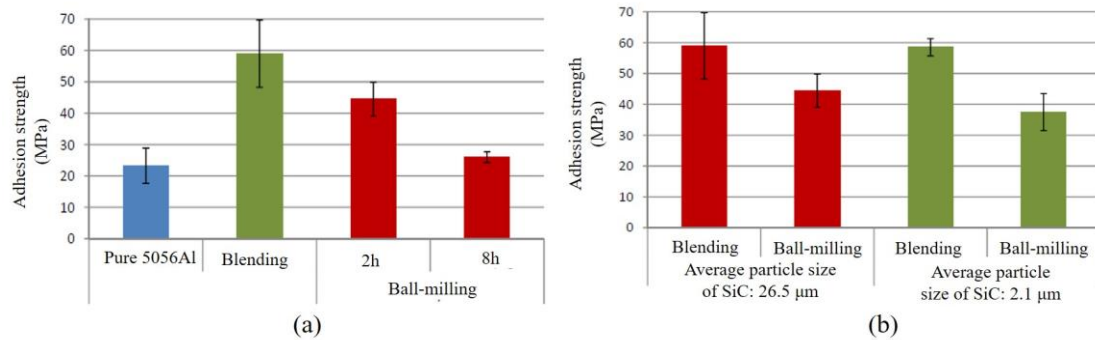


Fig. 31 Variation of adhesion strength of the 20 vol.% SiC/5056Al composite deposit as a function of the powder preparation method and the SiC particle size [110].

#### 4.2 Wear resistance

The wear performance of the CS AMCs is summarized in Table 4. It can be seen that the addition of ceramic particles or CNTs can significantly improve the wear performance of the Al or Al alloy deposits. Both the coefficient of friction (COF) and wear rates are largely reduced due to the increased deposit hardness and the effect of third-body abrasion created by the ceramic particles. Generally, increasing the ceramic content can enhance the microhardness and change the wear mode from adhesive to abrasive (Fig. 32). However, some studies showed that the wear resistance was independent of the ceramic mass fraction in the deposits. A poor cohesion between the Al matrix and the ceramic particles limited the improvement of the abrasion resistance of the composite deposits. It was also reported that adding spherical  $\text{Al}_2\text{O}_3$  particles into the Al matrix was more efficient in improving the tribological performance of the composites than adding angular  $\text{Al}_2\text{O}_3$  particles [140]. Tribological mechanisms investigated using in-situ tribometry and ex-situ analysis demonstrated that the formation of a thin but highly oxidized coherent layer with refined grains was of great importance to the wear resistance (Fig. 33). There was a ‘critical’  $\text{Al}_2\text{O}_3$  volume fraction that determines the formation of the coherent layer, and the critical value depended on the morphology of  $\text{Al}_2\text{O}_3$  particles. The spherical  $\text{Al}_2\text{O}_3$  was better in comparison with angular particles when comparing similar coating concentrations of  $\text{Al}_2\text{O}_3$  particles [140, 141]. This was explained by the reduced ductility and damage

accumulation at the sharp corners of angular particles, leading to material detachment during sliding, more readily generating wear debris, and higher overall wear rate [123].

Different ceramic powders and different synthesis methods can produce a different reinforcing effect on the wear resistance. It was reported that CS 7075Al composite reinforced by B<sub>4</sub>C particles exhibited better wear resistance than reinforced by SiC powders [94]. According to ref. [127], the CS B<sub>4</sub>C/5356Al composite produced using ball-milled composite powder showed higher dry sliding wear resistance compared to that prepared using mechanical blended composite powder under the same content of reinforcements. Additionally, using satellited feedstock was more efficient in reducing the deposit wear rate than using blended mixtures [109]. The previous study conducted by C. Chen et al. [99] demonstrated that the CS Al/diamond composites had superior wear-resistance properties that are comparable to SLM Inconel 625 and 17-4PH alloys. The highly improved wear performance of the diamond/Al composite was attributed to the high retainability and content of diamond particles in the composite coating by using the blending mixture of Al particle and Cu-Ni coated diamond particle.

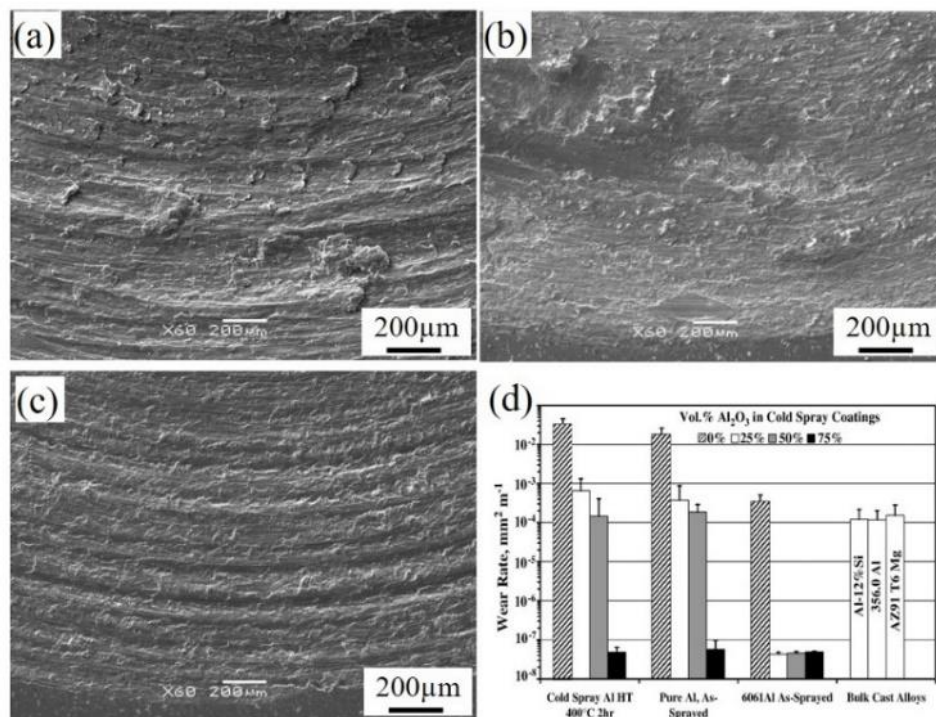
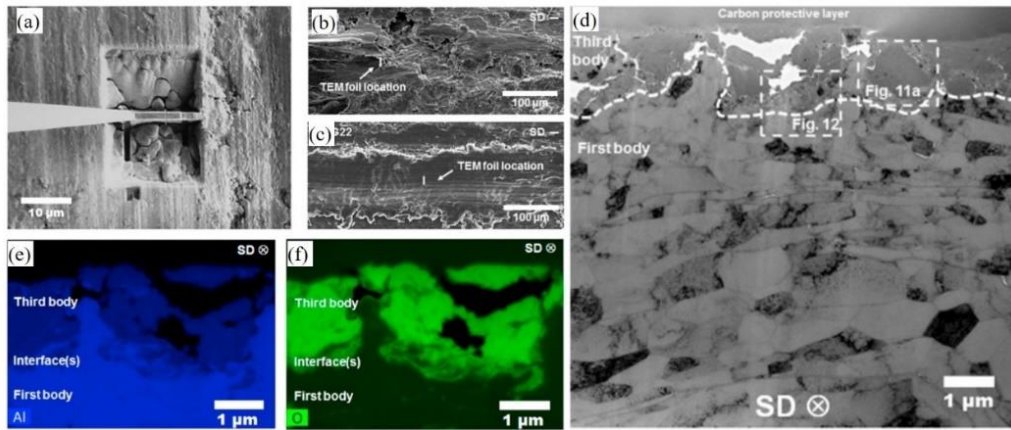


Fig. 32 SEM images showing the wear tracks of the CS pure Al deposit, (b) 50% Al<sub>2</sub>O<sub>3</sub>/Al composite, and (c) 75% Al<sub>2</sub>O<sub>3</sub>/Al composite. (d) Comparison of the wear rates of Al deposits and bulk alloys [140].



*Fig. 33 TEM investigation of the wear mechanisms of CS  $Al_2O_3/Al$  composite deposit: (a) technique of TEM foil preparation by focus ion beam; (b) and (c) wear track surfaces showing TEM foil locations; (d) TEM micrograph of the cross-sectional region near the wear track surface; (e) and (f) TEM/EDS mapping of Al and O elemental maps in the third body, the surrounding first body, and interfaces [141].*

### 4.3 Corrosion resistance

The corrosion property of the CS AMCs is also very important for the application of the repaired components in the corrosive environment such as in aerospace and marine areas. It is well known that the addition of hard ceramic particles into the Al matrix is an effective way to improve the mechanical properties without sacrificing corrosion resistance [139]. As summarized in Table 5, many studies have investigated the corrosion behavior of the CS AMCs deposits. Different kinds of AMCs have been deposited onto different substrates as corrosion protective coatings by CS [89, 94, 120, 130, 131, 134, 142, 143]. Generally, when AMC is sprayed onto the steel with lower potential, it can act as the anode in the saltwater [132]. Comparatively, when AMC is sprayed on Mg alloys with higher potential, it can act as the cathode. Previous studies have proved that CS of AMC deposits can effectively protect the substrate (i.e Mg alloys) from corrosion since the deposits show better anti-corrosion resistance [120] [135].

Metallurgical defects such as porosities, impurities, and poorly bonded boundaries in cold-sprayed coatings decrease the corrosion resistance since they promote a path for solution propagation to the substrate [130, 144]. Generally, the addition of ceramic particles can lead to slightly higher corrosion resistance in comparison with that of the pure Al deposits. The reason for this could be the enhanced density and reduced active regions within the composite deposit due to the substitution of some Al particles by ceramic particles on the electrode surface [92, 132]. For example, the experimental results conducted by Da Silva et al. [132] revealed that the

addition of  $\text{Al}_2\text{O}_3$  particles in pure Al coating resulted in slightly better corrosion resistance due to the decreased active area in the composite coating. However, some studies found out that the presence of ceramic particles in the composite coating increased the corrosion rate comparing with the pure Al deposit [94]. The increased corrosion rate of the CS AMCs was mainly caused by greater plastic deformation of the particles, which, in turn, created more active sites for corrosion compared to the unreinforced Al deposit [40, 94, 138]. Some other studies found that the corrosion resistance of the CS AMCs deposits was equivalent to that of pure Al deposits against the saltwater [88, 120, 145]. According to Tao et al. [120] and Spencer et al. [89], the addition of  $\alpha\text{-Al}_2\text{O}_3$  into the Al matrix has little effect on its protection ability.

Moreover, the influence of ceramic content on the corrosion property of CS AMCs was investigated by using different mechanically blended mixtures [92, 112, 130, 146]. Some of these studies pointed out that the anodic polarization behavior was scarcely affected by the content of ceramic particles [92, 130]. However, some studies found that adding 20 vol.% of  $\text{Al}_2\text{O}_3$  into the 2024Al matrix resulted in the highest corrosion resistance due to its lowest porosity and fewer fractured  $\text{Al}_2\text{O}_3$  particles [134]. It can also be learned from the literature that the type of ceramic particles could affect the corrosion behavior of AMCs [94]. In general, SiC and  $\text{Al}_2\text{O}_3$  particles are the two most commonly used reinforcements for anti-corrosion AMC coatings due to their neutral property. Xie et al. [129] investigated the corrosion behavior of the cold sprayed  $\text{TiB}_2/7075\text{Al}$  composite coating. Electrochemical tests revealed that the  $\text{TiB}_2/7075\text{Al}$  composite coating exhibited a higher corrosion rate than the pure 7075Al coating due to a galvanic coupling between  $\text{TiB}_2$  nanoparticles and the more active Al matrix. Therefore, the corrosion property of the CS AMCs was found closely connected to the porosity, microstructures, interactions between the Al matrix and the reinforcement particles, and the type of reinforcement particles [129].

The corrosion evolution of CS SiC/5056Al composites into a  $\text{NaSO}_4$  solution was revealed by Wang et al. [130]. As shown in Fig. 34, the cross-sectional morphologies of the composite deposits after the immersion test demonstrated that dissolution initiated cracks in the matrix and around the SiC particles. Then, the cracks propagated and induced fragmentation with a partial dissolution of the deposit. Localized corrosion tended to take place at the inter-particle boundaries where there were a lower Gibbs' free energy and some tiny defects. When an aggressive solution entered into these regions, the promoted hydrogen evolution led to crack coalescence and removal of particles. As corrosion progressed, new cracks started to form on the fresh surface (see Fig. 35g).

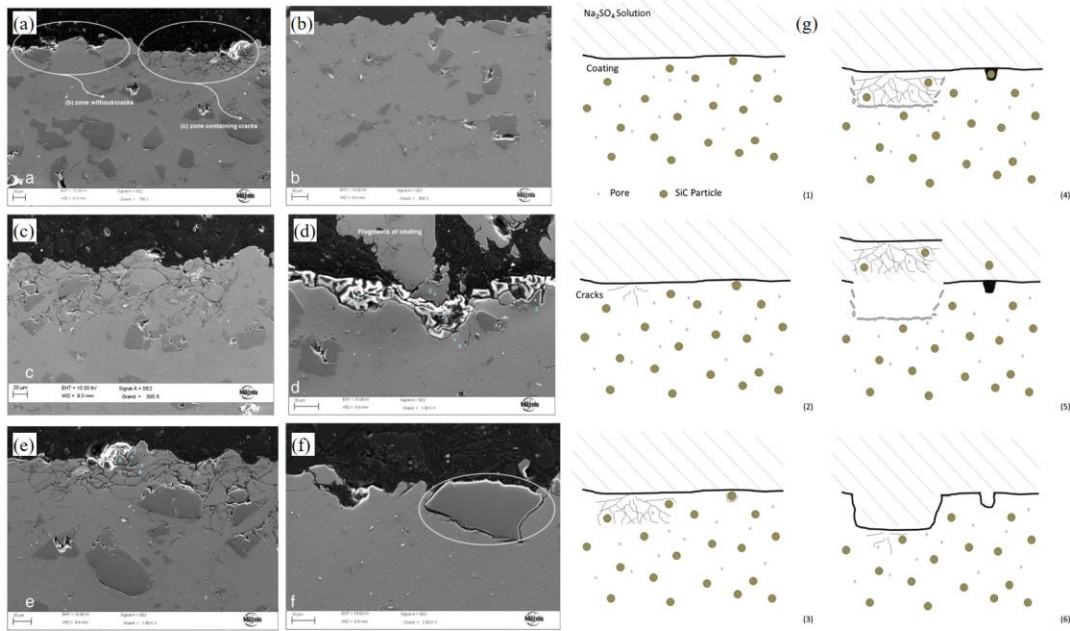


Fig. 34 (a-f) SEM images showing the corroded morphologies of the CS SiC/5056Al composite deposits after immersion in a Na<sub>2</sub>SO<sub>4</sub> solution. (g) Corrosion process of the CS SiC/Al 5056 composite deposit and release of SiC particle [130].

#### 4.4 Tensile properties

The bulk properties such as tensile properties of CS AMCs are important for structural load-bearing parts. Fig. 35 summarizes the tensile properties of the AMCs produced by CS. It can be clearly seen that the CS AMCs exhibited high tensile strength with little to no ductility in most cases. Such tensile performance could be mainly attributed to the following factors: work hardening effect produced by severe plastic deformation during the impact that largely increases the strength but reduces the ductility; poor interface bonding between Al/Al splats and the reinforcement/Al matrix. Since the metallic particles are bonded primarily through mechanical interlocking and very limited localized metallurgical bonding, the fracture is likely to take place through these poorly bonded inter-splat boundaries. The composites produced using mechanically blended composite powders could have a very poor interface between the reinforcing and Al matrix (without any metallurgical bonding), which can further reduce the tensile properties of the CS AMCs. An example of the tensile properties of CS SiC/Al composite is shown in Fig. 36. The fracture occurred at a very early stage, indicating a brittle feature of the as-sprayed composite. As shown in the fractured morphologies (Fig. 36c and d), the clear surface of the ceramic phase revealed the absence of chemical bonding between the Al splat and the SiC particles.

To solve the problems of poor interfacial bonding and uneven distribution of the reinforcement particles, a novel  $\text{TiB}_2/7075\text{Al}$  composite powder produced through in-situ reaction followed by gas-atomization was used as the feedstock for CS deposition [76]. The tensile properties of the CS  $\text{TiB}_2/7075\text{Al}$  composites are summarized in Fig. 37. The as-sprayed composite samples exhibited higher ultimate tensile strength (UTS) values compared to those of the pure 7075Al deposits. However, the as-sprayed composites exhibited typical brittle behavior, even though He was used as the propellant gas. This again due to the limited metallurgical bonding of the deformed particles within the as-sprayed state, as the fracture primarily occurred along the inter-splat boundaries (see Fig. 37 c-e). Some dimples were located at the highly deformed regions on the fracture surface of the air-processed sample, indicating the metallurgical bonding in these regions. This observation was explained by the higher particle impact temperature in this case which was beneficial for the occurrence of ASI at locally interparticle regions during the CS deposition [147, 148]. Therefore, the absence of defects and good inter-splat bonding are the most important factors that determine the final tensile properties of the CS samples.

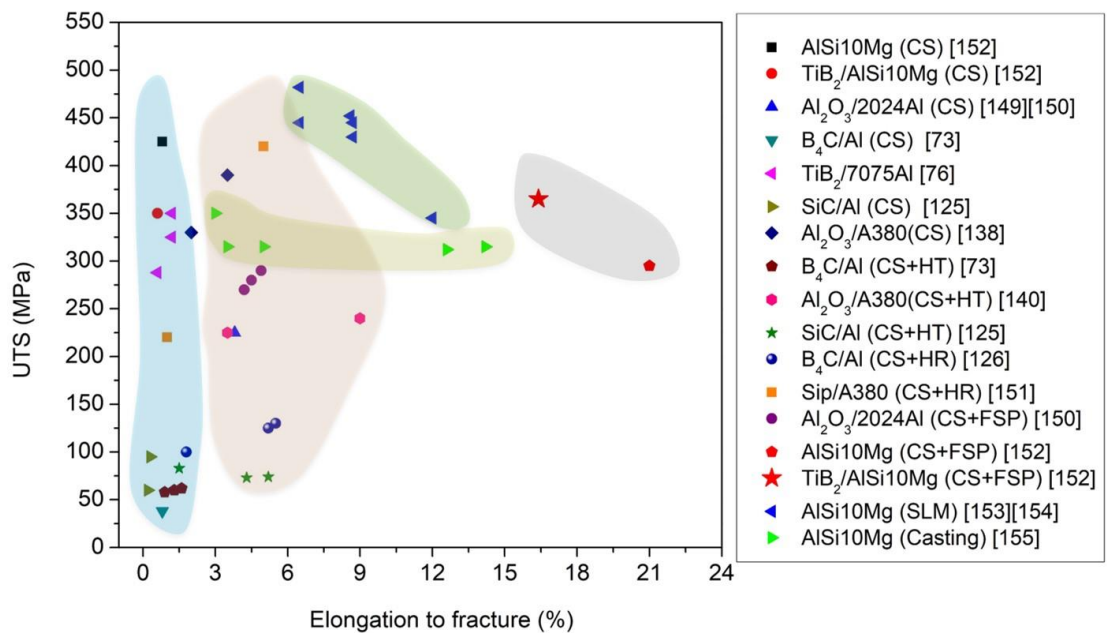


Fig. 35 Summary of the tensile properties of AMCs produced by CS and post-treatments including heat treatment, hot rolling (HR), and FSP, as well as the Al alloy parts produced by SLM and casting [73, 76, 125, 126, 138, 149-155].

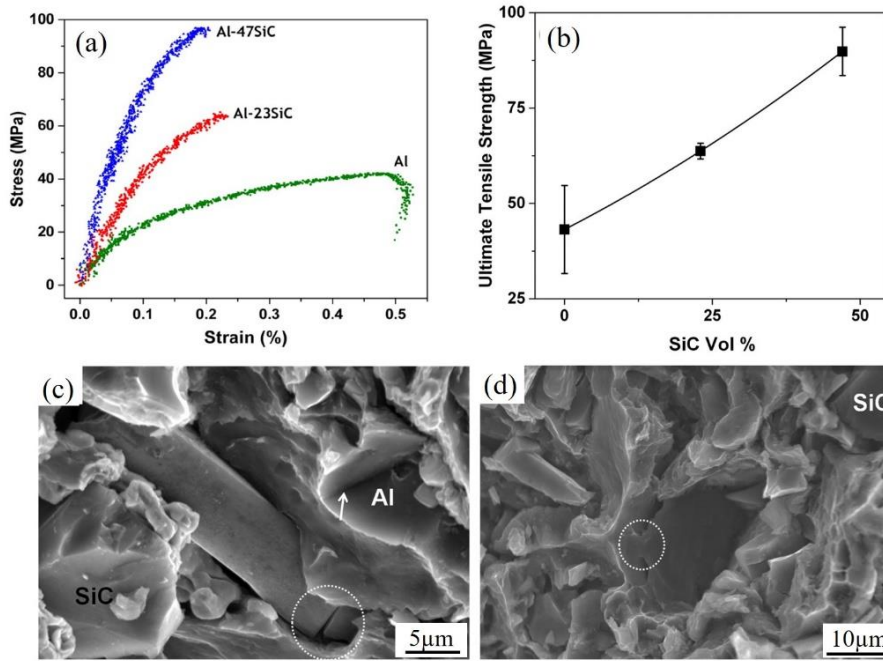


Fig. 36 Tensile properties of the CS SiC/Al composites:(a) stress-strain curves and (b) ultimate tensile strength as a function of SiC content; (C) and (d) Fractured morphologies of the as-sprayed Al-47SiC composite [125].

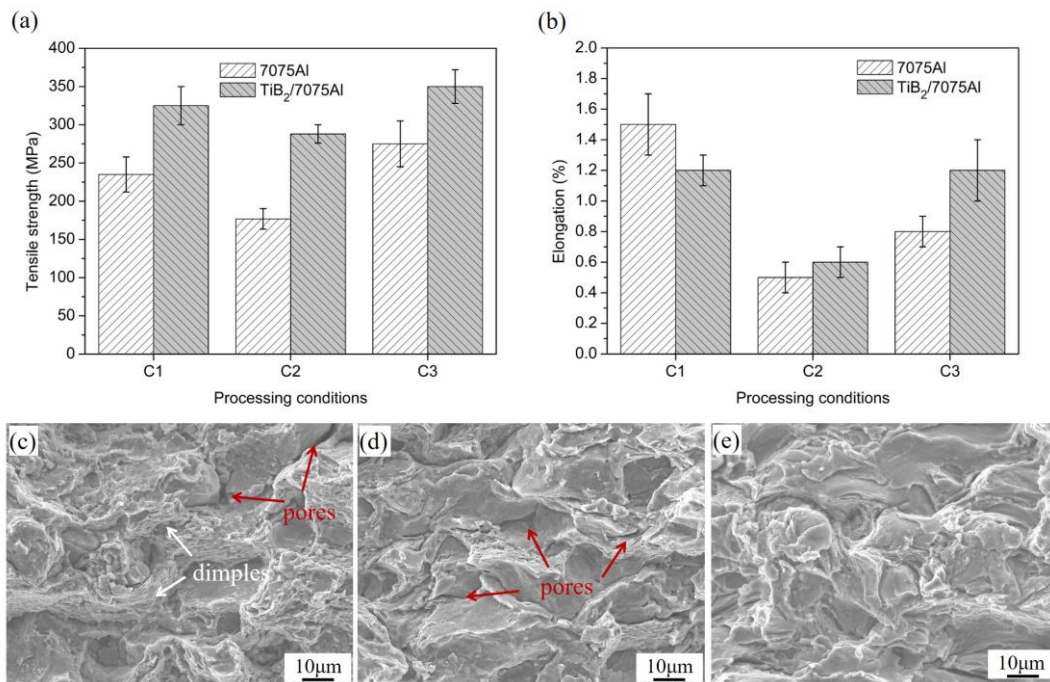


Fig. 37 Variation of (a) UTS and (b) elongation of the as-sprayed 7075Al and TiB<sub>2</sub>/7075Al composite samples fabricated using different CS parameters (C1: compressed air, 3.0MPa, 550 °C; C2: N<sub>2</sub>, 5.0 MPa, 500 °C; C3: He, 1.8MPa, 320 °C). SEM images showing the

*fracture morphologies of the as-sprayed TiB<sub>2</sub>/7075 Al composites fabricated using different CS parameters after tensile tests: (c) C1; (b) C2; C3 [76].*

## **5 Strengthening strategies for cold sprayed Al matrix composites**

### **5.1 Post-heat treatment**

Heat treatments are commonly used to relieve residual stress and to further improve the mechanical properties of the as-sprayed deposits or components. As indicated in Fig. 38, the observation of decreased microhardness in CS TiN/5356Al at the low annealing temperature was mainly due to the elimination of the work hardening effect. The strengthening effect by TiN particles, which played a key role in microhardness increment, was independent of the annealing temperatures. However, as for the CNT/Al composites produced using ball-milled powders (Fig. 38b), the microhardness of the composites increased slightly after annealing treatment, whereas that of pure Al decreased significantly due to grain growth and removal of dislocations. The increased microhardness of the CNTs/Al composite could be mainly explained by the preservation of the nanocrystalline structure by CNTs.

Annealing has been proved to be an effective approach for improving both the tensile strength and ductility of the CS metallic components due to the elimination of defects such as pores and inter-splat boundaries within the deposits. Unfortunately, when it comes to CS AMCs, the post-heat treatment seems to have a very limited improvement in their tensile properties because the interfacial bonding between the Al matrix and reinforcement ceramic particles can scarcely be enhanced through atomic diffusion during the heat treatment. As shown in Fig. 39, only a slight improvement in tensile strength and ductility of the heat-treated B<sub>4</sub>C/Al composite was obtained using a high annealing temperature. The fracture morphologies of heat-treated samples still showed very limited dimples, and the ceramic/matrix interfaces remained the weakest sites for crack or fracture initiation. Moreover, heat treatment does not affect the size and distribution of ceramic particles in the CS AMCs, which are also important factors for strengthening mechanical properties.

The influence of reinforcement particle morphology on the tensile properties of the CS AMCs was also investigated [138]. The Al<sub>2</sub>O<sub>3</sub>/A380 composites with different types of reinforcement particles were fabricated by CS using the mixtures of spherical, irregular, and spherical + irregular shaped Al<sub>2</sub>O<sub>3</sub> particles and A380 alloy powder. The results of tensile tests revealed that all the as-sprayed AMC samples exhibited a premature failure, while the ductility of the samples was remarkably improved after heat-treatment at 350 °C for 4h (Fig. 40 a and b). The composite samples reinforced with the spherical shaped Al<sub>2</sub>O<sub>3</sub> particles showed better tensile properties than those reinforced with irregular shaped Al<sub>2</sub>O<sub>3</sub> particles. The authors

attributed this difference to the larger amount of poor bonded  $\text{Al}_2\text{O}_3/\text{A380}$  interfaces within the composite which was caused by the fragmentation of irregular  $\text{Al}_2\text{O}_3$  particles during CS deposition. The enhanced inter-splat bonding and re-crystallization phenomena during heat treatment significantly improved the plasticity of CS AMCs, and therefore more dimples were observed on the fracture surface of the heat-treated composite sample (Fig. 40 e and f).

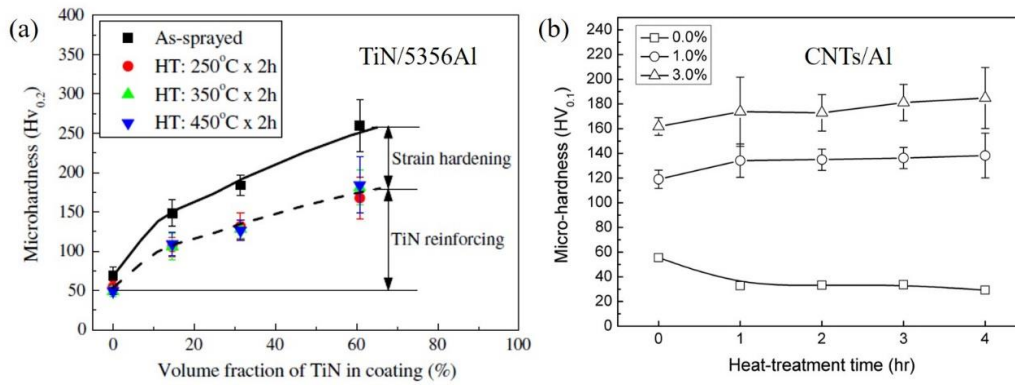


Fig. 38 Microhardness evolution of the annealed (a) TiN/5356Al [90] and (b) CNT/Al composite deposits [112].

However, for CS  $\text{TiB}_2/\text{AlSi10Mg}$  composites produced using the in-situ reaction and gas-atomized powder, the brittleness of the as-fabricated samples was notably improved by introducing annealing treatments. As shown in Fig. 41, in-situ formed nano/micro-sized  $\text{TiB}_2$  particles were uniformly distributed in the AlSi10Mg matrix. In the as-sprayed state, some poorly bonded inter-splat boundaries together with some small pores were observed at inter-splat boundaries. Increasing the annealing temperature significantly improved the inter-splat bonding via atoms diffusion and increased grain size. Both pure AlSi10Mg and  $\text{TiB}_2/\text{AlSi10Mg}$  composite deposits exhibited high UTS values and no elongations in the as-sprayed state, which characterized the typical brittle behavior of the CS deposits. As the annealing temperature increased, the ductility increased significantly (Fig. 42a and b). However, the elimination of the work hardening effect and grain growth resulted in a significant decrease in tensile strength. As revealed from the fracture morphologies in Fig. 42c-f, the as-sprayed samples showed a brittle feature, while the dominant dimples structure was observed on the fracture surface of annealed samples, indicating a significant improvement of ductility.

Based on the above discussions, we can conclude that the as-sprayed composite samples generally have low tensile properties and particularly very poor ductility due to the weak interface bonding and enhanced work hardening effect generated during high-velocity particle impact. Generally, heat treatment is not effective for improving the tensile properties of the AMCs produced from mechanical blending composite powders or ball-milled composite



composite sample reinforced with irregular  $Al_2O_3$  particles, and (S+I) composite indicates the composite sample reinforced with both spherical and irregular  $Al_2O_3$  particles [138].

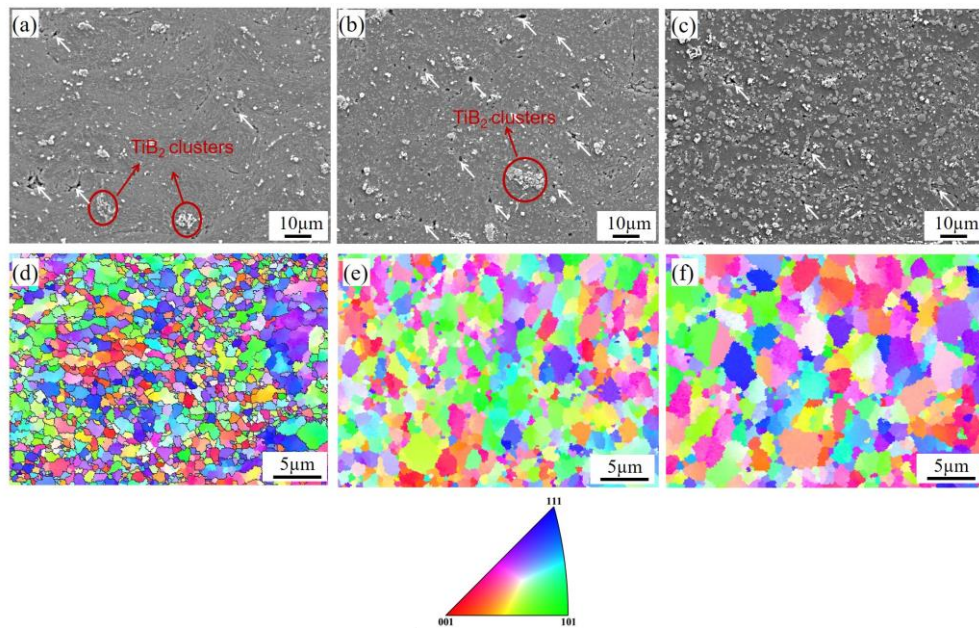


Fig. 41 (a-c) SEM images and (d-f) EBSD orientation maps showing the etched microstructure of the (a, d) as-sprayed and annealed  $TiB_2/AlSi10Mg$  composite samples at (b, e)  $400\text{ }^\circ\text{C}$  and (c, f)  $500\text{ }^\circ\text{C}$  for 4h [156].

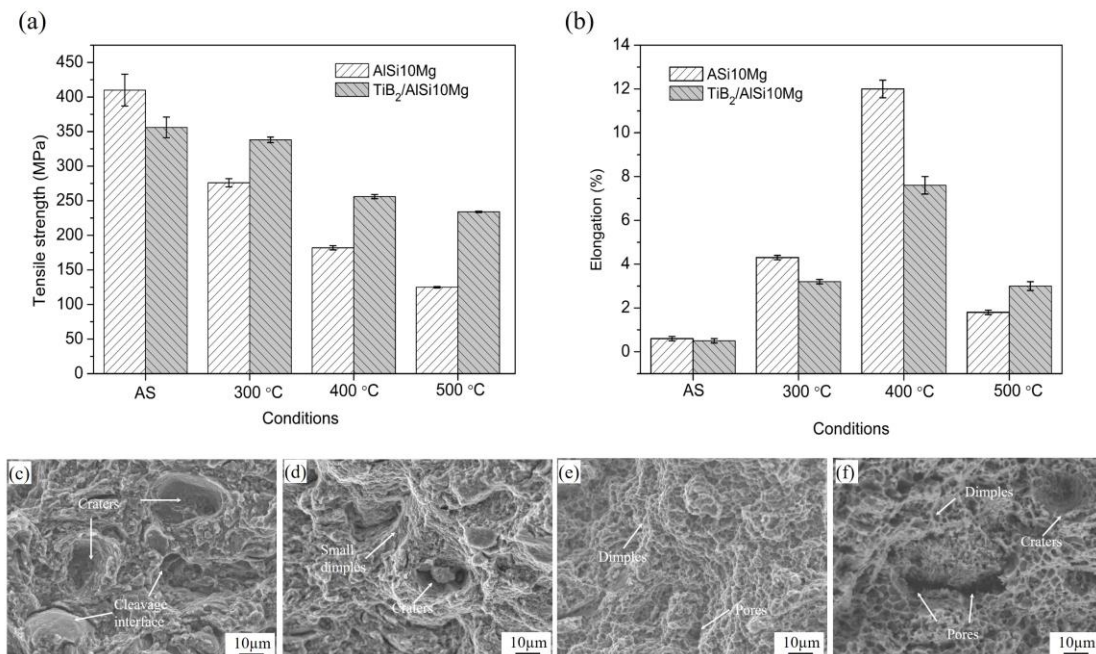


Fig. 42 (a) UTS and (b) elongation values of the as-sprayed and annealed pure  $AlSi10Mg$  and  $TiB_2/AlSi10Mg$  composites. Fracture morphologies of the (c) as-sprayed and annealed  $TiB_2/AlSi10Mg$  composite samples at (d)  $300\text{ }^\circ\text{C}$ , (e)  $400\text{ }^\circ\text{C}$ , and (f)  $500\text{ }^\circ\text{C}$  [156].

## 5.2 Post hot rolling treatment

Recently, HR treatment has been employed to efficiently remove defects and improve the mechanical properties of the CS coatings through modifications in their microstructure [74, 126, 151, 157]. For example, a crack-free Ni-Al sheet with large deformation was achieved by Zhao et al. [158] using CS deposition followed by cold-pack rolling. Qiu et al. [151] reported that the mechanical properties of cold sprayed A380 aluminum alloy can be largely improved by post-HR treatment mainly attributed to the progressive elimination/reduction of inter-splat defects together with in-situ composite microstructure formation. The well bonded Ti/steel clad plates were obtained by CS deposition of Ti powder on steel substrate followed by hot-rolling and annealing operations [157, 159]. In addition to the pure metallic materials, post HR also exhibits high potential in applications of CS AMCs [74, 126].

The schematic diagram of the CS-HR hybrid manufacturing of AMCs is illustrated in Fig. 43. The feedstock powders were blended in a long roll jar mill with the aid of ZrO<sub>2</sub> balls. Then, the mixed powders were sprayed on a rotating cylindrical substrate to fabricate thick B<sub>4</sub>C/Al composite components (>5 mm), which have potential applications in the nuclear area for neutron absorbing [126]. After removing the substrate, the composite specimens were hot rolled to achieve a different reduction in thickness. After HR, the porosity of the composite was reduced, and Al grains were extensively refined through continuous dynamic recrystallization. More importantly, the interfacial bonding between Al/Al splats and B<sub>4</sub>C/Al was remarkably enhanced by inter-particle atomic diffusion (Fig. 44). The results of tensile tests revealed that the post HR resulted in much better mechanical properties than those of the as-sprayed composite samples, and the samples with a higher thickness reduction showed higher UTS and elongation values (Fig. 45 a and b). This was probably due to an efficient healing effect of the inter-splat boundaries and pores through diffusion during the HR treatment, as confirmed by the fracture morphologies (Fig. 45c-h). Nevertheless, this hybrid process itself has limitations in fabricating complex-shaped components.

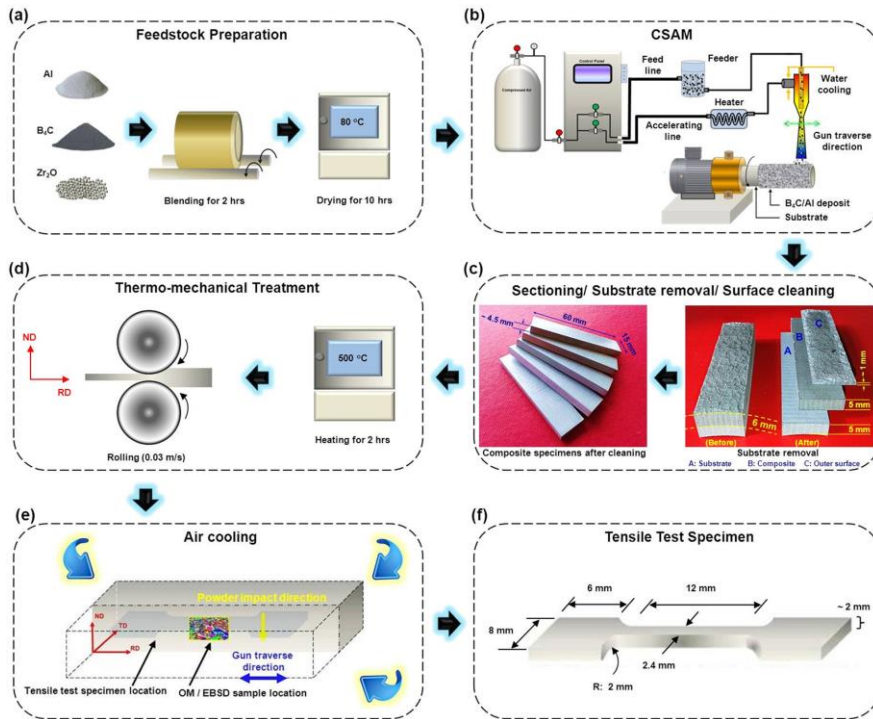


Fig. 43 Schematic diagram of the CS-HR hybrid CSAM process [126].

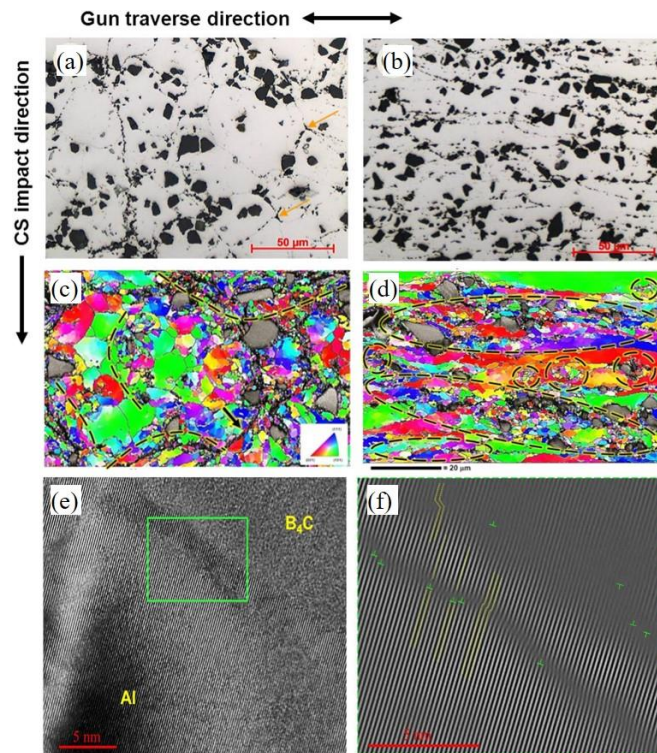


Fig. 44 Microstructure of the (a, c) as-sprayed and (b, d) hot rolled  $B_4C/Al$  composite samples (60% thickness reduction) [126]: (a) and (b) optical micrographs; (c) and (d) EBSD maps; (e) High resolution TEM image showing the interface feature. (f) shows the Fourier transform (IFFT) image of the region highlighted in panel (e).

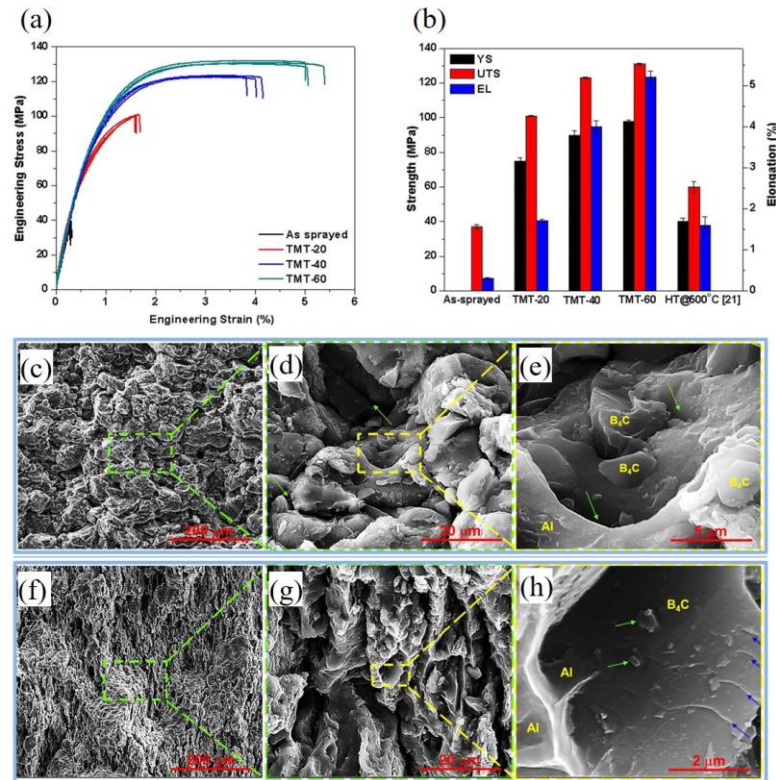
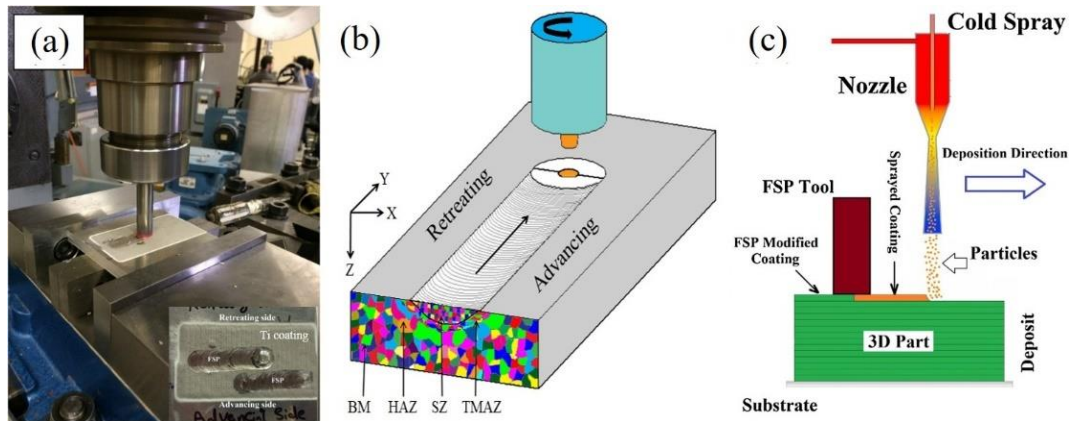


Fig. 45 (a) Tensile stress-strain curves of as-sprayed and hot-rolled  $B_4C/Al$  composite samples, (b) comparison between YS (yield strength), UTS, and elongation values of the as-sprayed, hot rolled, and heat-treated samples. SEM images showing the fractured morphologies of (c–e) as-sprayed and (f–h) hot rolled  $B_4C/Al$  composite samples (60% thickness reduction) after tensile tests [126]. TMT-20, TMT-40, and TMT-60 represent the hot-rolled samples with the thickness reduction of 20%, 40% and 60%, respectively. HT@600°C indicates the samples heat-treated at 600°C for 4h.

### 5.3 Post friction stir processing treatment

FSP has been widely used as an effective solid-state surface modification technique for post-treating deposits produced using the processes such as thermal spray, electro-deposition, surface adhesive binding, and CS. In this process, a non-consumable tool with a high rotating speed, consisting of a probe and shoulder, is plunged into a metal plate under a very high compressive force and then the tool is traversed in the desired direction (Fig. 46). During FSP, severe plastic deformation of the material can create a microstructure with fine, equiaxed grains, which is beneficial for mechanical properties. Nowadays, FSP has been employed on CS deposits to offer the following benefits: (i) elimination of defects such as pores and inter-splat boundaries to form a fully dense structure and strong metallurgical bonding, (ii) creating a refined structure and uniformly mixed phases through severe plastic deformation of the material,

(ii) generation of intermetallic phases or even chemical bonding at the interface via the thermal softening effect, and (iii) hot consolidation to form a fully dense solid deposit layer after CS. Owing to these advantages, many attempts have been made to modify CS deposits, such as Ti [160], CuZn alloy [161], 7075Al alloy [162], NiTi alloy, and MMCs [149, 150, 163, 164]. A hybrid AM technique combined with CS and FSP post-processing has been developed for component manufacturing and repairing (Fig. 46c).



*Fig. 46 (a) FSP modification of CS Ti deposits onto Al substrate. (b) Schematic of FSP process; (c) Schematic representation of FSP as a modifying post-processing technique during CSAM [165].*

In recent years, FSP has been used for CS AMCs to refine the distribution of reinforcement particles and to improve bonding between deposited particles. For example, Hodder et al. [166] investigated the effects of FSP on a CS deposited  $\text{Al}_2\text{O}_3/\text{Al}$  composite. It was found that re-distributed and refined  $\text{Al}_2\text{O}_3$  particles by FSP improve the microhardness of the CS AMCs. Huang et al. [163] investigated the effect of FSP on CS  $\text{SiC}/5056\text{Al}$  composite showing improved microhardness and tribological performance. Moreover, Yang et al. [149] investigated the influence of rotation speeds of the tool during the FSP process on microstructure evolution, ceramic particle distribution, and mechanical properties of the CS  $\text{Al}_2\text{O}_3/2024\text{Al}$  composites. It was found that a higher rotation rate resulted in more significant  $\text{Al}_2\text{O}_3$  particle refinement and improved particle distribution. Fig. 47a-f show the microstructure evolution of the CS  $\text{Al}_2\text{O}_3/2024\text{Al}$  composite before and after FSP. It can be seen that compared to the as-sprayed state, some large  $\text{Al}_2\text{O}_3$  particles were fractured into small ones and the particle-particle interfaces were absent after FSP treatment. As a result, higher microhardness and tensile strength, and better wear resistance were acquired for the FSP processed composite samples (Fig. 47g and h). However, ductility showed a limited improvement, being still much less than that prepared by other traditional processes (e.g.PM). This was mainly because some large ceramic particles were still retained in the composite deposit and interfacial bonding

between the ceramic and Al matrix was not strong enough. Yang et al [164] also studied the effect of FSP passes on the corrosion behavior of the as-sprayed  $\text{Al}_2\text{O}_3/2024\text{Al}$  composites. The results demonstrated that FSP with a low pass number (typically 1 and 2 passes) was more efficient in improving the corrosion resistance of the CS  $\text{Al}_2\text{O}_3/2024\text{Al}$  composites, and the best corrosion property was obtained by repeating 2-passes FSP. These results show that the FSP has great potential in modifying the microstructure of CS AMCs to improve both mechanical and corrosion properties.

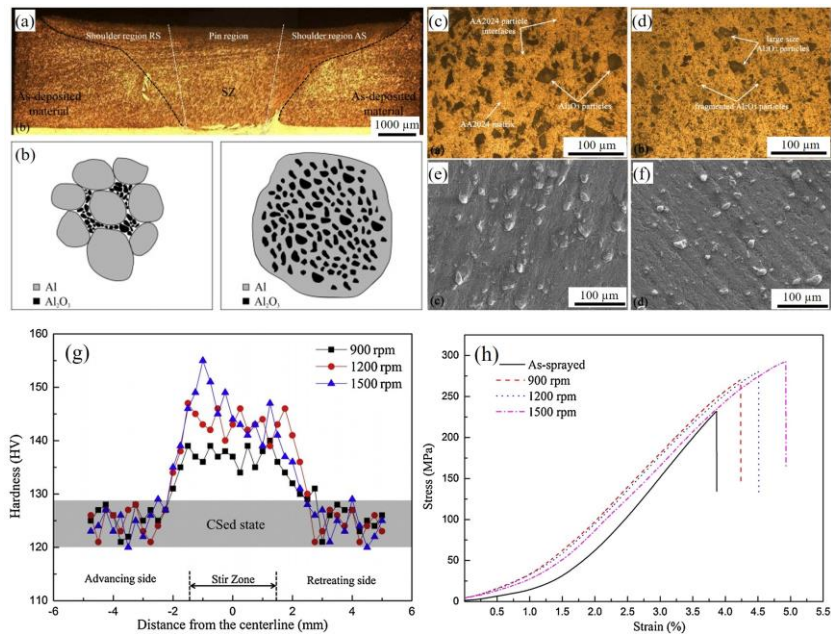


*Fig. 47 Microstructure modification of the CS AMCs conducted by FSP post-treatment: (a) macroscopic cross-section of the CS  $\text{Al}_2\text{O}_3/2024\text{Al}$  after FSP treatment [150]; (b) Schematic diagram showing the redistributed reinforcement particles in AMCs by FSP. [166]; Optical micrographs (c, d) and SEM (e, f) images showing the microstructure of as-sprayed (c, e) and FSP treated (d, f)  $\text{Al}_2\text{O}_3/2024\text{Al}$  composites [150]. (g) Microhardness evolution and (h) the tensile stress-strain curves of the FSP processed  $\text{Al}_2\text{O}_3/2024\text{Al}$  composites [150].*

The other successful application where post-FSP treatment was also performed to improve the mechanical performance in the CS  $\text{TiB}_2/\text{AlSi10Mg}$  composites [152]. As shown in Fig. 48a, evident inter-splat boundaries, small pores, and  $\text{TiB}_2$  clusters were observed in the as-sprayed  $\text{TiB}_2/\text{AlSi10Mg}$  composite. However, the stir zone was characterized by a dense structure with remarkably refined  $\text{TiB}_2$  particles uniformly dispersed in the  $\text{AlSi10Mg}$  matrix (Fig. 48d). As illustrated in Fig. 48c and f, it is interesting to note that FSP redistributed the  $\text{TiB}_2$  particles from intergranular distribution at as-sprayed state to intragranular distribution through the vigorous stirring action of the rotating tool that forced the  $\text{TiB}_2$  particles into the grains [167].

This indicated that a homogeneous and refined structure with uniformly distributed reinforcement particles can be successfully produced by FSP through severe plastic deformation of the deposited matrix (Fig. 48e). The  $\text{TiB}_2$  nanoparticles were tightly bonded with the Al matrix. (Fig. 48g-i). The overall semi-coherent  $\text{TiB}_2/\text{Al}$  interface due to the in-situ chemical reaction in the melt contributed to the formation of the high interfacial bonding [19]. Significant improvement in ductility while maintaining high strength was achieved in the  $\text{TiB}_2/\text{AlSi10Mg}$  composite samples after FSP treatment (Fig. 49). Fig. 35 summarizes the tensile properties of CS AMCs after post-treatments including heat treatment, HR, and FSP, as well as the tensile property of Al alloys produced by SLM and traditional casting. A breakthrough enhancement in tensile property especially the outstanding ductility was achieved for the FSP treated in-situ  $\text{TiB}_2/\text{AlSi10Mg}$  composite. A simultaneous enhancement in both strength and ductility was mainly attributed to the refined grain structure, uniformly distributed reinforcement nanoparticles, and the robust interfacial bonding between the in-situ  $\text{TiB}_2$  particles and the Al matrix.

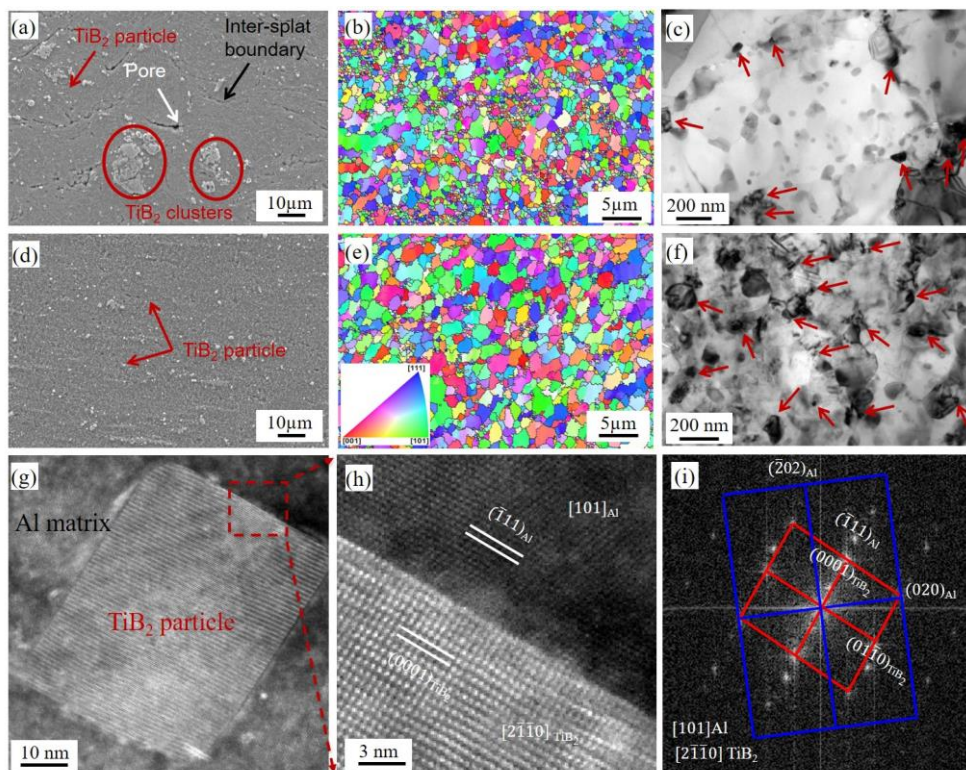


Fig. 48 Comparison of the microstructure of the as-sprayed  $\text{TiB}_2/\text{AlSi10Mg}$  composite (a-c) with the one after post-FSP treatment (d-f): (a) and (d) SEM images showing the cross-sectional morphologies; (b) and (e) SEM/EBSD orientation maps; (c) and (f) TEM images; (g) and (h) High resolution TEM images showing the  $\text{TiB}_2/\text{Al}$  interface, and (i) corresponding FFT pattern of (h) [152].

Table 6 compares the ability of post heat treatment, HR, and FSP on microstructure modification and property improvement of CS AMCs. It can be concluded that the heat treatment shows very limited improvement in porosity, inter-splat or interface bonding and no improvement in reinforcement particle redistribution, and thereby very limited improvement in tensile properties of the CS AMCs. HR is effective in reducing the porosities and enhancing the inter-splat bonding but fails to redistribute and refine the ceramic particles. As a result, limited improvement in tensile properties was obtained. Comparatively, most of these problems can be solved effectively by FSP treatment. FSP appears to be a very promising post-technique in improving the properties of CS AMCs. However, this technique may have the technical problems of geometry limitation for net-shape forming.

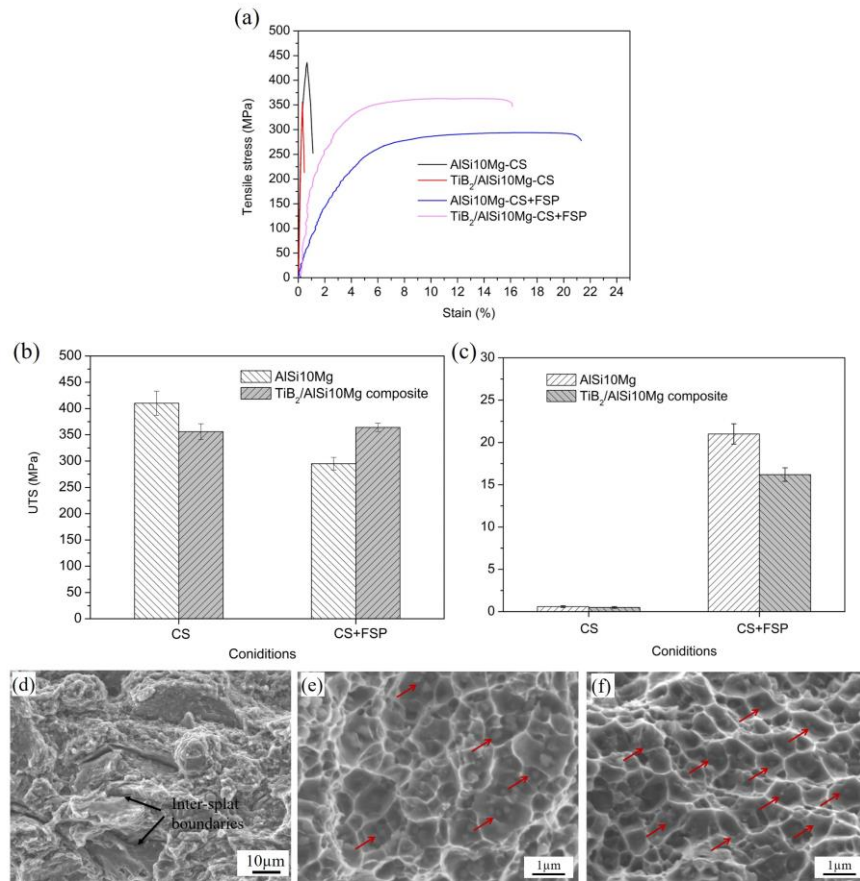


Fig. 49 (a) Tensile stress-strain curves for pure AlSi10Mg and TiB<sub>2</sub>/AlSi10Mg composites before and after FSP treatment. (b) and (c) Comparison of the UTS and elongation values of the tensile specimens, respectively. Fracture surface morphologies of the (d) CS TiB<sub>2</sub>/AlSi10Mg and post-FSP treated (e) AlSi10Mg and TiB<sub>2</sub>/AlSi10Mg composites samples [152].

*Table 6 Comparison of different post-treatment methods in microstructure modification and property improvement of the CS AMCs.*

Post-treatment methods	Heat treatment	Hot-rolling	Friction stir processing
Porosity reduction	Limited	Good	Very good
Inter-splats bonding improvement	Limited	Good	Very good
Grain refinement	No (grain growth)	No	Good
Residual stress release	Good	Good	Good
Reinforcement particle redistribution	No	No	Good
Reinforcement particle size reduction	No	No	Good
Interface bonding of reinforcement particle/Al matrix	No	Limited	Good
Mechanical property improvement	Limited	Limited	Good

## **6 Conclusions and future perspectives**

Based on the literature investigations, various AMC deposits and components have been tentatively produced by CSAM using the different types of feedstock powders prepared by mechanical mixing/blending, ball milling, spray drying, satelliting, or gas atomization. Each preparation technique has its own advantages and shortcomings, determining the state of the initial powders including the size and distribution of the reinforcement particles and interfacial bonding. This plays an important role in the quality and performance of the CS samples as well as the effectiveness of the post-treatment including heat treatment, HR, and FSP.

Mechanical mixing/blending has been commonly used for composite powders preparation due to its low cost and easy operation. However, this method has the problems of non-uniform distribution of reinforcements and poor interfacial bonding between the reinforcement phase and the Al matrix. The ball milling process is effective in improving both distributions of reinforcement particles and reinforcement/matrix interfacial bonding. The hardening effect and grain refinement produced during the ball milling process effectively increase the hardness of the composite particle, which results, however, in a very low particle DE. The satelliting method allows for better aggregation of fine ceramic particles onto the Al alloy particles.

However, the presence of ceramic reinforcements around the Al alloy particle surface could affect the metallic bonding of the particles during the CS deposition or even hinder the bonding. Moreover, this method has the problems of ceramic reinforcement distribution and poor interface bonding. Comparatively, the in-situ reaction/gas-atomization process appears to be the most potential approach for composite powder production, which enables to disperse of the nanosized ceramic particles inside the composite particle and to produce a robust interfacial bonding of reinforcement/Al matrix due to in-situ reaction in liquid Al.

Further, it should be mentioned that the co-deposition behavior varies with the different composite powders preparation. As for the mechanical blended or satellited composite powders, the soft Al matrix particles deform severely and acts as a binder, while hard-ceramic particles are embedded in the matrix. In the case of mechanically blended composite powders, due to the difference in physical properties and particle morphology and size, the Al particles and ceramic particles could have different impact velocities, and loss of ceramic particles during deposition usually takes place. Comparatively, the satellited composite powder could be accelerated in the gas flow and impact upon the substrate as a whole but ceramic particles rebounding always occurs, that is also the case of mechanically blended powders. The ball-milled and gas-atomized composite powders could be deposited as a whole so that the content of the reinforcements in the composite deposit is basically the same as in the initial composite powders. However, the gas-atomized composite powder is easy to deform and could have higher DE since no work hardening effect was produced compared to the ball-milled composite powders.

By integrating ceramic particles or CNTs into an Al matrix, porosity, microhardness, adhesion strength, and tribological performance of the composite deposits were largely improved in comparison with the unreinforced counterparts due to enhanced hammering and strengthening effects of the reinforcement particles. However, when their volume fraction reaches a critically high level, the bonding strength starts to decrease because soft Al particles will be offset by an increased proportion of weak Al/ceramic particles and substrate/ceramic interfaces. Some experimental results also reveal that the particle morphology and powder preparation methods could have a great influence on the properties of the CS composite deposit. The CS composite deposits exhibited low tensile properties with very poor ductility, owing to the poor interface bonding (reinforcement/Al matrix and interparticle interfaces) and some defaults within the composite deposit. The addition of ceramic reinforcement particles could also affect the corrosion behavior of the composite deposit. However, it seems difficult to make a general conclusion on the corrosion behavior at this stage.

The as-sprayed composite samples generally exhibit poor tensile properties, especially very poor ductility due to the weak interface bonding and enhanced work hardening effect generated during high-velocity particle impact. Post-heat treatment is not effective for improving tensile properties of CS AMCs produced from mechanically blended composite powders or ball-milled composite powders as it fails to enhance the bonding between the reinforcement ceramic particles and the matrix and to homogeneously redistribute the reinforcement particles. However, significant improvement in ductility was achieved after annealing treatment for the CS AMCs produced from in-situ gas-atomized composite powders. This is because the in-situ formed fine  $TiB_2$  particles are already uniformly distributed inside the deformed particles and have a very strong interface bonding with the Al matrix.

Post-HR seems effective in improving the bonding between Al/Al splats and ceramic/Al interfaces through promoted inter-particle atomic diffusion with thermo-mechanical coupling mechanism. Nevertheless, this hybrid CSAM process has limitations in fabricating complex-shaped components. The post-FSP process leads to the improvement of tensile properties by refining and redistributing reinforcement particles and by improving the metallurgical bonding between the deposited particles through complete recrystallization of the matrix. It was found that the ductility didn't show significant improvement for the cold-sprayed AMCs produced from blending mixed composite powders. Despite this, significant improvement in ductility while maintaining high strength was only achieved in the CS AMCs using in-situ formed gas-atomized composite powders after FSP treatment.

To further improve the properties of the CS AMCs and extend their applications in industries, some general aspects should be considered:

Firstly, before a specific application of such CS AMCs, it is necessary to make a comprehensive and detailed evaluation of various performances, including bonding strength, wear resistance, corrosion performance, and tensile properties. This technique shows unique advantages in applications for damage repair using mechanically blended composite powders.

Secondly, more attention should be paid to the interfacial feature of the reinforcement/Al matrix since it basically plays an important role in determining the overall mechanical and physical properties of AMCs. Note that this feature is related to AMCs themselves being independent of production techniques.

Thirdly, the strength-ductility trade-off is pronounced in the CS AMCs at this stage which ruled out possible applications in structural load-bearing parts. Hybrid AM technique seems to be a good choice for improving the performance of the CS AMCs. More systematic work needs to be carried out from the aspects of powder design, process optimization, and microstructure

control. In addition to heat treatment, HR, and FSP, hot isostatic pressing is also a promising post-treatment approach that allows to reduce the defects (e.g. pores and poor interface bonding) and improve the properties of CS deposits. Unfortunately, to our best knowledge, there are few reports related to using HIP as a post-treatment method to improve the properties of CS AMCs.

At last, little attention has been focused on the spray strategy development on producing AMCs components with complex-shapes, which is very important for the applications in damage repair and net-shape forming. Therefore, this aspect also deserves more systemic investigations.

## **Acknowledgments**

Dr. Xinliang Xie is grateful for the financial support of the Chinese Scholarship Council (No. 201604490100), Université Bourgogne - Franche-Comté, and Centre National de la Recherche Scientifique (CNRS). The microscopy facilities in Lille (France) are supported by the Conseil Régional du Nord-Pas de Calais, and the European Regional Development Fund (ERDF). Dr. Wenya Li thanks the financial support from the National Natural Science Foundation of China (No. 51875471).

## **References**

- [1] Bala G Narasimha, Vamsi M Krishna, Anthony M Xavier, A review on processing of particulate metal matrix composites and its properties, *Int. J. Appl. Eng. Res.*, 8 (2013), 647-666.
- [2] M Jagannatham, Prathap Chandran, S Sankaran, Prathap Haridoss, Niraj Nayan, Srinivasa R Bakshi, Tensile properties of carbon nanotubes reinforced aluminum matrix composites: A review, *Carbon*, 160 (2020), 14-44.
- [3] IA Ibrahim, FA Mohamed, EJ Lavernia, Particulate reinforced metal matrix composites—a review, *J. Mater. Sci.*, 26 (1991), 1137-1156.
- [4] Yingbin Hu, Weilong Cong, A review on laser deposition-additive manufacturing of ceramics and ceramic reinforced metal matrix composites, *Ceram. Int.*, 44 (2018), 20599-20612.
- [5] RS Rana, Rajesh Purohit, S Das, Review of recent studies in Al matrix composites, *Int. J. Sci. Eng. Res*, 3 (2012), 1-16.
- [6] Suraj P Rawal, Metal-matrix composites for space applications, *JOM*, 53 (2001), 14-17.
- [7] Kazi Md Shorowordi, Tahar Laoui, ASMA Haseeb, Jean-Pierre Celis, Ludo Froyen, Microstructure and interface characteristics of B<sub>4</sub>C, SiC and Al<sub>2</sub>O<sub>3</sub> reinforced Al matrix composites: a comparative study, *J. Mater. Process. Technol.*, 142 (2003), 738-743.
- [8] MK Surappa, Aluminium matrix composites: Challenges and opportunities, *Sadhana*, 28 (2003), 319-334.
- [9] Toru Kuzumaki, K Miyazawa, Hideki Ichinose, Kunio Ito, Processing of carbon nanotube reinforced aluminum composite, *J. Mater. Res.*, 13 (1998), 2445-2449.

- [10] TW Clyne, PJ Withers, An introduction to metal matrix composites, Cambridge university press, 1995.
- [11] Riccardo Casati, Maurizio Vedani, Metal matrix composites reinforced by nano-particles—a review, *Metals*, 4 (2014), 65-83.
- [12] Dongshuai Zhou, Feng Qiu, Qichuan Jiang, The nano-sized TiC particle reinforced Al–Cu matrix composite with superior tensile ductility, *Mater. Sci. Eng., A*, 622 (2015), 189-193.
- [13] Mehdi Rahimian, Nader Parvin, Naser Ehsani, Investigation of particle size and amount of alumina on microstructure and mechanical properties of Al matrix composite made by powder metallurgy, *Mater. Sci. Eng., A*, 527 (2010), 1031-1038.
- [14] C Saravanan, K Subramanian, V Ananda Krishnan, R Sankara Narayanan, Effect of particulate reinforced aluminium metal matrix composite—a review, *Mech. Mech. Eng.*, 19 (2015), 23-30.
- [15] CN He, NQ Zhao, CS Shi, SZ Song, Mechanical properties and microstructures of carbon nanotube-reinforced Al matrix composite fabricated by in situ chemical vapor deposition, *J. Alloys Compd.*, 487 (2009), 258-262.
- [16] S Lakshmi, L Lu, M Gupta, In situ preparation of TiB<sub>2</sub> reinforced Al based composites, *J. Mater. Process. Technol.*, 73 (1998), 160-166.
- [17] TG Durai, Karabi Das, Siddhartha Das, Synthesis and characterization of Al matrix composites reinforced by in situ alumina particulates, *Mater. Sci. Eng., A*, 445 (2007), 100-105.
- [18] Namrata Gangil, Arshad Noor Siddiquee, Sachin Maheshwari, Aluminium based in-situ composite fabrication through friction stir processing: A review, *J. Alloys Compd.*, 715 (2017), 91-104.
- [19] I. S. Lee, C. J. Hsu, C. F. Chen, N. J. Ho, P. W. Kao, Particle-reinforced aluminum matrix composites produced from powder mixtures via friction stir processing, *Compos. Sci. Technol.*, 71 (2011), 693-698.
- [20] Hooyar Attar, Shima Ehtemam-Haghighi, Damon Kent, Matthew S Dargusch, Recent developments and opportunities in additive manufacturing of titanium-based matrix composites: A review, *Int. J. Mach. Tools Manuf.*, 133 (2018), 85-102.
- [21] Tarasankar DebRoy, HL Wei, JS Zuback, T Mukherjee, JW Elmer, JO Milewski, Allison Michelle Beese, A Wilson-Heid, A De, W Zhang, Additive manufacturing of metallic components—process, structure and properties, *Prog. Mater. Sci.*, 92 (2018), 112-224.
- [22] AP Alkhimov, A method of cold gas-dynamic deposition, *Sov. Phys. Dokl.*, 1990, pp. 1047-1049.
- [23] V Champagne, D Helfrich, The unique abilities of cold spray deposition, *Int. Mater. Rev.*, 61 (2016), 437-455.
- [24] R Lupoi, W O'Neill, Deposition of metallic coatings on polymer surfaces using cold spray, *Surf. Coat. Technol.*, 205 (2010), 2167-2173.
- [25] Christina Wüstefeld, David Rafaja, Mykhaylo Motylenko, Christiane Ullrich, Rico Drehmann, Thomas Grund, Thomas Lampke, Bernhard Wielage, Local heteroepitaxy as an adhesion mechanism in aluminium coatings cold gas sprayed on AlN substrates, *Acta Mater.*, 128 (2017), 418-427.
- [26] R Drehmann, T Grund, T Lampke, B Wielage, C Wüstefeld, M Motylenko, G Schreiber, D Rafaja, Investigation of the bonding mechanisms of Al coatings on ceramic substrates

deposited by cold gas spraying and magnetron sputtering, Proceedings International Thermal Spray Conference, 2015, pp. 544-552.

[27] Wenya Li, Congcong Cao, Shuo Yin, Solid-state cold spraying of Ti and its alloys: a literature review, *Prog. Mater. Sci.*, (2019), 100633.

[28] RN Raoelison, Ch Verdy, H Liao, Cold gas dynamic spray additive manufacturing today: Deposit possibilities, technological solutions and viable applications, *Mater. Des.*, 133 (2017), 266-287.

[29] H Assadi, H Kreye, F Gärtner, T Klassen, Cold spraying—A materials perspective, *Acta Mater.*, 116 (2016), 382-407.

[30] Atieh Moridi, SEYYED MOSTAFA Hassani-Gangaraj, Mario Guagliano, Ming Dao, Cold spray coating: review of material systems and future perspectives, *Surf. Eng.*, 30 (2014), 369-395.

[31] MR Rokni, SR Nutt, CA Widener, VK Champagne, RH Hrabe, Review of relationship between particle deformation, coating microstructure, and properties in high-pressure cold spray, *J. Therm. Spray Technol.*, 26 (2017), 1308-1355.

[32] Mostafa Hassani-Gangaraj, David Veysset, Keith A Nelson, Christopher A Schuh, In-situ observations of single micro-particle impact bonding, *Scripta Mater.*, 145 (2018), 9-13.

[33] Mostafa Hassani-Gangaraj, David Veysset, Victor K Champagne, Keith A Nelson, Christopher A Schuh, Adiabatic shear instability is not necessary for adhesion in cold spray, *Acta Mater.*, 158 (2018), 430-439.

[34] Anatolii Papyrin, Vladimir Kosarev, Sergey Klinkov, Anatolii Alkhimov, Vasily M Fomin, *Cold spray technology*, Elsevier, 2006.

[35] Hamid Assadi, Frank Gärtner, Thorsten Stoltenhoff, Heinrich Kreye, Bonding mechanism in cold gas spraying, *Acta Mater.*, 51 (2003), 4379-4394.

[36] Mica Grujicic, CL Zhao, WS DeRosset, Dennis Helfritch, Adiabatic shear instability based mechanism for particles/substrate bonding in the cold-gas dynamic-spray process, *Mater. Des.*, 25 (2004), 681-688.

[37] Michael Saleh, Vladimir Luzin, Kevin Spencer, Analysis of the residual stress and bonding mechanism in the cold spray technique using experimental and numerical methods, *Surf. Coat. Technol.*, 252 (2014), 15-28.

[38] DM Chun, MH Kim, JC Lee, SH Ahn, TiO<sub>2</sub> coating on metal and polymer substrates by nano-particle deposition system (NPDS), *CIRP annals*, 57 (2008), 551-554.

[39] Guan-Jun Yang, Chang-Jiu Li, Feng Han, Wen-Ya Li, Akira Ohmori, Low temperature deposition and characterization of TiO<sub>2</sub> photocatalytic film through cold spray, *Appl. Surf. Sci.*, 254 (2008), 3979-3982.

[40] Shuo Yin, Yingchun Xie, Xinkun Suo, Hanlin Liao, Xiaofang Wang, Interfacial bonding features of Ni coating on Al substrate with different surface pretreatments in cold spray, *Mater. Lett.*, 138 (2015), 143-147.

[41] Yingchun Xie, Shuo Yin, Chaoyue Chen, Marie-Pierre Planche, Hanlin Liao, Rocco Lupoi, New insights into the coating/substrate interfacial bonding mechanism in cold spray, *Scripta Mater.*, 125 (2016), 1-4.

[42] Chaoyue Chen, Yingchun Xie, Renzhong Huang, Sihao Deng, Zhongming Ren, Hanlin Liao, On the role of oxide film's cleaning effect into the metallurgical bonding during cold spray, *Mater. Lett.*, 210 (2018), 199-202.

- [43] Wen-Ya Li, Chang-Jiu Li, Hanlin Liao, Significant influence of particle surface oxidation on deposition efficiency, interface microstructure and adhesive strength of cold-sprayed copper coatings, *Appl. Surf. Sci.*, 256 (2010), 4953-4958.
- [44] Xiao-Tao Luo, Cheng-Xin Li, Fu-Lin Shang, Guan-Jun Yang, Yu-Yue Wang, Chang-Jiu Li, High velocity impact induced microstructure evolution during deposition of cold spray coatings: a review, *Surf. Coat. Technol.*, 254 (2014), 11-20.
- [45] Atanu Chaudhuri, Y Raghupathy, Dheepa Srinivasan, Satyam Suwas, Chandan Srivastava, Microstructural evolution of cold-sprayed Inconel 625 superalloy coatings on low alloy steel substrate, *Acta Mater.*, 129 (2017), 11-25.
- [46] Tian Liu, Jeremy D Leazer, Luke N Brewer, Particle deformation and microstructure evolution during cold spray of individual Al-Cu alloy powder particles, *Acta Mater.*, 168 (2019), 13-23.
- [47] Tobias Schmidt, Frank Gärtner, Hamid Assadi, Heinrich Kreye, Development of a generalized parameter window for cold spray deposition, *Acta Mater.*, 54 (2006), 729-742.
- [48] Dominik Hanft, Jörg Exner, Michael Schubert, Thomas Stöcker, Paul Fuierer, Ralf Moos, An overview of the aerosol deposition method: Process fundamentals and new trends in materials applications, *J. Ceram. Sci. Technol.*, 6 (2015), 147-182.
- [49] Xuemei Wang, Feng Feng, Michael A Klecka, Matthew D Mordasky, Jacquelynn K Garofano, Tahany El-Wardany, Aaron Nardi, Victor K Champagne, Characterization and modeling of the bonding process in cold spray additive manufacturing, *Addit. Manuf.*, 8 (2015), 149-162.
- [50] Peter C King, Gyuyeol Bae, Saden H Zahiri, Mahnaz Jahedi, Changhee Lee, An experimental and finite element study of cold spray copper impact onto two aluminum substrates, *J. Therm. Spray Technol.*, 19 (2010), 620-634.
- [51] T Hussain, DG McCartney, Philip H Shipway, D Zhang, Bonding mechanisms in cold spraying: the contributions of metallurgical and mechanical components, *J. Therm. Spray Technol.*, 18 (2009), 364-379.
- [52] Mica Grujicic, CL Zhao, Chenning Tong, WS DeRosset, D Helfrich, Analysis of the impact velocity of powder particles in the cold-gas dynamic-spray process, *Mater. Sci. Eng., A*, 368 (2004), 222-230.
- [53] Mica Grujicic, John R Saylor, Donald E Beasley, WS DeRosset, D Helfrich, Computational analysis of the interfacial bonding between feed-powder particles and the substrate in the cold-gas dynamic-spray process, *Appl. Surf. Sci.*, 219 (2003), 211-227.
- [54] Tian Liu, Jeremy D Leazer, Luke N Brewer, Particle deformation and microstructure evolution during cold spray of individual Al-Cu alloy powder particles, *Acta Mater.*, (2019), 13-23.
- [55] Mostafa Hassani-Gangaraj, David Veysset, Victor K Champagne, Keith A Nelson, Christopher A Schuh, Response to Comment on “Adiabatic shear instability is not necessary for adhesion in cold spray”, *Scripta Mater.*, 162 (2019), 515-519.
- [56] H Assadi, F Gärtner, T Klassen, H Kreye, Comment on ‘Adiabatic shear instability is not necessary for adhesion in cold spray’, *Scripta Mater.*, 162 (2019), 512-514.
- [57] MR Rokni, CA Widener, GA Crawford, MK West, An investigation into microstructure and mechanical properties of cold sprayed 7075 Al deposition, *Mater. Sci. Eng., A*, 625 (2015), 19-27.

- [58] MR Rokni, CA Widener, VK Champagne, GA Crawford, SR Nutt, The effects of heat treatment on 7075 Al cold spray deposits, *Surf. Coat. Technol.*, 310 (2017), 278-285.
- [59] Ying-Kang Wei, Xiao-Tao Luo, Xin Chu, Guo-Sheng Huang, Chang-Jiu Li, Solid-state additive manufacturing high performance aluminum alloy 6061 enabled by an in-situ micro-forging assisted cold spray, *Mater. Sci. Eng., A*, 776 (2020), 139024.
- [60] Barry Aldwell, Elaine Kelly, Ronan Wall, Andrea Amaldi, Garret E O'Donnell, Rocco Lupoi, Machinability of Al 6061 deposited with cold spray additive manufacturing, *J. Therm. Spray Technol.*, 26 (2017), 1573-1584.
- [61] Shuo Yin, Richard Jenkins, Xingchen Yan, Rocco Lupoi, Microstructure and mechanical anisotropy of additively manufactured cold spray copper deposits, *Mater. Sci. Eng., A*, 734 (2018), 67-76.
- [62] Pierre Coddet, Christophe Verdy, Christian Coddet, François Debray, On the mechanical and electrical properties of copper-silver and copper-silver-zirconium alloys deposits manufactured by cold spray, *Mater. Sci. Eng., A*, 662 (2016), 72-79.
- [63] Jin-Hyeon Cho, Young-Min Jin, Dong-Yong Park, Hyung-Jun Kim, Ik-Hyun Oh, Kee-Ahn Lee, Manufacture and properties of cold spray deposited large thickness Cu coating material for sputtering target, *Met. Mater. Int.*, 17 (2011), 157-166.
- [64] Chaoyue Chen, Yingchun Xie, Xingchen Yan, Shuo Yin, Hirotaka Fukanuma, Renzhong Huang, Ruixin Zhao, Jiang Wang, Zhongming Ren, Min Liu, Effect of hot isostatic pressing (HIP) on microstructure and mechanical properties of Ti6Al4V alloy fabricated by cold spray additive manufacturing, *Addit. Manuf.*, 27 (2019), 595-605.
- [65] Venkata Satish Bhattiprolu, Kyle W Johnson, Ozan C Ozdemir, Grant A Crawford, Influence of feedstock powder and cold spray processing parameters on microstructure and mechanical properties of Ti-6Al-4V cold spray depositions, *Surf. Coat. Technol.*, 335 (2018), 1-12.
- [66] Sara Bagherifard, Asghar Heydari Astaraee, Matteo Locati, Ali Nawaz, Stefano Monti, Ján Kondás, Reeti Singh, Mario Guagliano, Design and analysis of additive manufactured bimodal structures obtained by cold spray deposition, *Addit. Manuf.*, 33 (2020), 101131.
- [67] Xiao-Tao Luo, Meng-Lin Yao, Ninshu Ma, Makoto Takahashi, Chang-Jiu Li, Deposition behavior, microstructure and mechanical properties of an in-situ micro-forging assisted cold spray enabled additively manufactured Inconel 718 alloy, *Mater. Des.*, 155 (2018), 384-395.
- [68] Wenhua Ma, Yingchun Xie, Chaoyue Chen, Hirotaka Fukanuma, Jiang Wang, Zhongming Ren, Renzhong Huang, Microstructural and mechanical properties of high-performance Inconel 718 alloy by cold spraying, *J. Alloys Compd.*, 792 (2019), 456-467.
- [69] Pierre Coddet, Christophe Verdy, Christian Coddet, François Debray, Florence Lecouturier, Mechanical properties of thick 304L stainless steel deposits processed by He cold spray, *Surf. Coat. Technol.*, 277 (2015), 74-80.
- [70] AL-Mangour Bandar, Phuong Vo, Rosaire Mongrain, Eric Irissou, Stephen Yue, Effect of heat treatment on the microstructure and mechanical properties of stainless steel 316L coatings produced by cold spray for biomedical applications, *J. Therm. Spray Technol.*, 23 (2014), 641-652.
- [71] Shuo Yin, Jan Cizek, Xingchen Yan, Rocco Lupoi, Annealing strategies for enhancing mechanical properties of additively manufactured 316L stainless steel deposited by cold spray, *Surf. Coat. Technol.*, 370 (2019), 353-361.

- [72] CJ Huang, HJ Wu, YC Xie, WY Li, C Verdy, M-P Planche, HL Liao, G Montavon, Advanced brass-based composites via cold-spray additive-manufacturing and its potential in component repairing, *Surf. Coat. Technol.*, 371 (2019), 211-223.
- [73] NH Tariq, L Gyansah, JQ Wang, X Qiu, B Feng, MT Siddique, TY Xiong, Cold spray additive manufacturing: A viable strategy to fabricate thick B4C/Al composite coatings for neutron shielding applications, *Surf. Coat. Technol.*, 339 (2018), 224-236.
- [74] Lawrence Gyansah, Xiang Qiu, Chunni Jia, Hasan Bin Awais, Chengwu Zheng, Hao Du, Jiqiang Wang, Tianying Xiong, Achieving strength-ductility synergy in cold spray additively manufactured Al/B4C composites through a hybrid post-deposition treatment, *J. Mater. Sci. Technol.*, 35 (2019), 1053-1063.
- [75] Xinliang Xie, Chaoyue Chen, Yingchun Xie, Zhongming Ren, Eric Aubry, Gang Ji, Hanlin Liao, A novel approach for fabricating Ni-coated FeSiAl soft magnetic composite via cold spraying, *J. Alloys Compd.*, 749 (2018), 523-533.
- [76] Xinliang Xie, Yu Ma, Chaoyue Chen, Gang Ji, Christophe Verdy, Hongjian Wu, Zhe Chen, Sheng Yuan, Bernard Normand, Shuo Yin, Cold spray additive manufacturing of metal matrix composites (MMCs) using a novel nano-TiB<sub>2</sub>-reinforced 7075Al powder, *J. Alloys Compd.*, 819 (2020), 152962.
- [77] Chaoyue Chen, Yingchun Xie, Xincheng Yan, Renzhong Huang, Min Kuang, Wenyuan Ma, Ruixin Zhao, Jiang Wang, Min Liu, Zhongming Ren, Cold sprayed WC reinforced maraging steel 300 composites: Microstructure characterization and mechanical properties, *J. Alloys Compd.*, 785 (2019), 499-511.
- [78] Shuo Yin, Pasquale Cavaliere, Barry Aldwell, Richard Jenkins, Hanlin Liao, Wenya Li, Rocco Lupoi, Cold spray additive manufacturing and repair: Fundamentals and applications, *Addit. Manuf.*, 21 (2018), 628-650.
- [79] A Sova, S Grigoriev, A Okunkova, I Smurov, Potential of cold gas dynamic spray as additive manufacturing technology, *Int. J. Adv. Manuf. Technol.*, 69 (2013), 2269-2278.
- [80] J Pattison, S Celotto, R Morgan, M Bray, W O'neill, Cold gas dynamic manufacturing: A non-thermal approach to freeform fabrication, *Int. J. Mach. Tools Manuf.*, 47 (2007), 627-634.
- [81] Wenya Li, Kang Yang, Shuo Yin, Xiawei Yang, Yaxin Xu, Rocco Lupoi, Solid-state additive manufacturing and repairing by cold spraying: A review, *J. Mater. Sci. Technol.*, 34 (2018), 440-457.
- [82] Wenyuan Chen, Yuan Yu, Anh Kiet Tieu, Junying Hao, Long Wang, Shengyu Zhu, Jun Yang, Microstructure, mechanical properties and tribological behavior of the low-pressure cold sprayed tin bronze-alumina coating in artificial seawater, *Tribol. Int.*, 142 (2020), 105992.
- [83] Sima A Alidokht, Stephen Yue, Richard R Chromik, Effect of WC morphology on dry sliding wear behavior of cold-sprayed Ni-WC composite coatings, *Surf. Coat. Technol.*, 357 (2019), 849-863.
- [84] HX Hu, SL Jiang, YS Tao, TY Xiong, YG Zheng, Cavitation erosion and jet impingement erosion mechanism of cold sprayed Ni-Al<sub>2</sub>O<sub>3</sub> coating, *Nucl. Eng. Des.*, 241 (2011), 4929-4937.
- [85] NM Melendez, VV Narulkar, GA Fisher, AG McDonald, Effect of reinforcing particles on the wear rate of low-pressure cold-sprayed WC-based MMC coatings, *Wear*, 306 (2013), 185-195.

- [86] Yik Tung Roy Lee, Hossein Ashrafizadeh, Gary Fisher, Andre McDonald, Effect of type of reinforcing particles on the deposition efficiency and wear resistance of low-pressure cold-sprayed metal matrix composite coatings, *Surf. Coat. Technol.*, 324 (2017), 190-200.
- [87] M Yandouzi, P Richer, B Jodoin, SiC particulate reinforced Al–12Si alloy composite coatings produced by the pulsed gas dynamic spray process: Microstructure and properties, *Surf. Coat. Technol.*, 203 (2009), 3260-3270.
- [88] Eric Irissou, Jean-Gabriel Legoux, Bernard Arsenault, Christian Moreau, Investigation of Al–Al<sub>2</sub>O<sub>3</sub> cold spray coating formation and properties, *J. Therm. Spray Technol.*, 16 (2007), 661-668.
- [89] K Spencer, DM Fabijanic, M-X Zhang, The use of Al–Al<sub>2</sub>O<sub>3</sub> cold spray coatings to improve the surface properties of magnesium alloys, *Surf. Coat. Technol.*, 204 (2009), 336-344.
- [90] Wen-Ya Li, Changlin Yang, Hanlin Liao, Effect of vacuum heat treatment on microstructure and microhardness of cold-sprayed TiN particle-reinforced Al alloy-based composites, *Mater. Des.*, 32 (2011), 388-394.
- [91] M Yu, XK Suo, WY Li, YY Wang, HL Liao, Microstructure, mechanical property and wear performance of cold sprayed Al5056/SiCp composite coatings: effect of reinforcement content, *Appl. Surf. Sci.*, 289 (2014), 188-196.
- [92] Yingying Wang, Bernard Normand, Nicolas Mary, Min Yu, Hanlin Liao, Effects of ceramic particle size on microstructure and the corrosion behavior of cold sprayed SiCp/Al 5056 composite coatings, *Surf. Coat. Technol.*, 315 (2017), 314-325.
- [93] H Chen, Z Pala, T Hussain, DG McCartney, Fabrication and microstrain evolution of Al–TiB<sub>2</sub> composite coating by cold spray deposition, *Proc. Inst. Mech. Eng. L*, (2017), 1044-1052.
- [94] Onur Meydanoglu, Bertrand Jodoin, E Sabri Kayali, Microstructure, mechanical properties and corrosion performance of 7075 Al matrix ceramic particle reinforced composite coatings produced by the cold gas dynamic spraying process, *Surf. Coat. Technol.*, 235 (2013), 108-116.
- [95] Srinivasa R Bakshi, Virendra Singh, Kantesh Balani, D Graham McCartney, Sudipta Seal, Arvind Agarwal, Carbon nanotube reinforced aluminum composite coating via cold spraying, *Surf. Coat. Technol.*, 202 (2008), 5162-5169.
- [96] Xinliang Xie, Chaoyue Chen, Gang Ji, Run Xu, Zhanqiu Tan, Yingchun Xie, Zhiqiang Li, Hanlin Liao, A novel approach for fabricating a CNT/AlSi composite with the self-aligned nacre-like architecture by cold spraying, *Nano Materials Science*, 1 (2019), 137-141.
- [97] DJ Woo, FC Heer, LN Brewer, JP Hooper, S Osswald, Synthesis of nanodiamond-reinforced aluminum metal matrix composites using cold-spray deposition, *Carbon*, 86 (2015), 15-25.
- [98] DJ Woo, B Sneed, F Peerally, FC Heer, LN Brewer, JP Hooper, S Osswald, Synthesis of nanodiamond-reinforced aluminum metal composite powders and coatings using high-energy ball milling and cold spray, *Carbon*, 63 (2013), 404-415.
- [99] Chaoyue Chen, Yingchun Xie, Xingchen Yan, Mansur Ahmed, Rocco Lupoi, Jiang Wang, Zhongming Ren, Hanlin Liao, Shuo Yin, Tribological properties of Al/diamond composites produced by cold spray additive manufacturing, *Addit. Manuf.*, 36 (2020), 101434.
- [100] RE Blöse, BH Walker, RM Walker, SH Froes, New opportunities to use cold spray process for applying additive features to titanium alloys, *Metal Powder Report*, 61 (2006), 30-37.

- [101] J Schell, Cold spray aerospace applications, CSAT Workshop, Worcester, USA, 2016.
- [102] G Kilchenstein, Cold spray technologies used for repair, JTEG Monthly Teleconference, 9 (2016).
- [103] Wenya Li, Hamid Assadi, Frank Gaertner, Shuo Yin, A review of advanced composite and nanostructured coatings by solid-state cold spraying process, *Crit. Rev. Solid State Mater. Sci.*, 44 (2019), 109-156.
- [104] Qiang Wang, Kevin Spencer, Nick Birbilis, Ming-Xing Zhang, The influence of ceramic particles on bond strength of cold spray composite coatings on AZ91 alloy substrate, *Surf. Coat. Technol.*, 205 (2010), 50-56.
- [105] Hansang Kwon, Seungchan Cho, Akira Kawasaki, Diamond-Reinforced Metal Matrix Bulk Materials Fabricated by a Low-Pressure Cold-Spray Process, *Mater. Trans.*, 56 (2015), 108-112.
- [106] Xiang Qiu, Ji-qiang Wang, Jun-rong Tang, Lawrence Gyansah, Zhi-po Zhao, Tian-ying Xiong, Microstructure, microhardness and tribological behavior of Al<sub>2</sub>O<sub>3</sub> reinforced A380 aluminum alloy composite coatings prepared by cold spray technique, *Surf. Coat. Technol.*, 350 (2018), 391-400.
- [107] Veronica De Simone, Diego Caccavo, Gaetano Lamberti, Matteo d'Amore, Anna Angela Barba, Wet-granulation process: Phenomenological analysis and process parameters optimization, *Powder Technol.*, 340 (2018), 411-419.
- [108] KS Al-Hamdani, JW Murray, T Hussain, A Kennedy, AT Clare, Cold sprayed metal-ceramic coatings using satellited powders, *Mater. Lett.*, 198 (2017), 184-187.
- [109] Kamaal S Al-Hamdani, James W Murray, Tanvir Hussain, Adam T Clare, Heat-treatment and mechanical properties of cold-sprayed high strength Al alloys from satellited feedstocks, *Surf. Coat. Technol.*, 374 (2019), 21-31.
- [110] Sébastien Gojon, Etude sur l'élaboration et la caractérisation de revêtements en alliages d'aluminium et de magnésium par projection dynamique à froid pour la réparation de pièces aéronautiques, PhD thesis, Université de Technologie de Belfort-Montbéliard, 2015, French.
- [111] Kicheol Kang, Gyuyeol Bae, Juyeon Won, Changhee Lee, Mechanical property enhancement of kinetic sprayed Al coatings reinforced by multi-walled carbon nanotubes, *Acta Mater.*, 60 (2012), 5031-5039.
- [112] Kicheol Kang, Jaeick Kim, Hyungkwon Park, Changhee Lee, Formation and heat treatment of kinetic sprayed nanocrystalline Al coatings reinforced with multi-walled carbon nanotubes: The relationship between microstructural features and physical properties, *Surf. Coat. Technol.*, 289 (2016), 124-135.
- [113] H Chen, Z Pala, T Hussain, DG McCartney, Fabrication and microstrain evolution of Al-TiB<sub>2</sub> composite coating by cold spray deposition, *Proc. Inst. Mech. Eng. L*, 233 (2019), 1044-1052.
- [114] W-Y Li, G Zhang, C Zhang, O Elkedim, H Liao, C Coddet, Effect of ball milling of feedstock powder on microstructure and properties of TiN particle-reinforced Al alloy-based composites fabricated by cold spraying, *J. Therm. Spray Technol.*, 17 (2008), 316-322.
- [115] Srinivasa R Bakshi, Virendra Singh, D Graham McCartney, Sudipta Seal, Arvind Agarwal, Deformation and damage mechanisms of multiwalled carbon nanotubes under high-velocity impact, *Scripta Mater.*, 59 (2008), 499-502.

- [116] Z Fan, Y Wang, Y Zhang, T Qin, XR Zhou, GE Thompson, T Pennycook, T Hashimoto, Grain refining mechanism in the Al/Al–Ti–B system, *Acta Mater.*, 84 (2015), 292-304.
- [117] Mengxing Chen, Xiaopeng Li, Gang Ji, Yi Wu, Zhe Chen, Wouter Baekelant, Kim Vanmeensel, Haowei Wang, Jean-Pierre Kruth, Novel composite powders with uniform TiB<sub>2</sub> nano-particle distribution for 3D printing, *Applied Sciences*, 7 (2017), 250.
- [118] E Sansoucy, P Marcoux, L Ajdelsztajn, B Jodoin, Properties of SiC-reinforced aluminum alloy coatings produced by the cold gas dynamic spraying process, *Surf. Coat. Technol.*, 202 (2008), 3988-3996.
- [119] JM Shockley, HW Strauss, RR Chromik, N Brodusch, R Gauvin, E Irissou, J-G Legoux, In situ tribometry of cold-sprayed Al–Al<sub>2</sub>O<sub>3</sub> composite coatings, *Surf. Coat. Technol.*, 215 (2013), 350-356.
- [120] Yongshan Tao, Tianying Xiong, Chao Sun, Huazi Jin, Hao Du, Tiefan Li, Effect of  $\alpha$ -Al<sub>2</sub>O<sub>3</sub> on the properties of cold sprayed Al/ $\alpha$ -Al<sub>2</sub>O<sub>3</sub> composite coatings on AZ91D magnesium alloy, *Appl. Surf. Sci.*, 256 (2009), 261-266.
- [121] W-Y Li, G Zhang, HL Liao, C Coddet, Characterizations of cold sprayed TiN particle reinforced Al<sub>2</sub>319 composite coating, *J. Mater. Process. Technol.*, 202 (2008), 508-513.
- [122] Qiang Wang, Nick Birbilis, Han Huang, Ming-Xing Zhang, Microstructure characterization and nanomechanics of cold-sprayed pure Al and Al–Al<sub>2</sub>O<sub>3</sub> composite coatings, *Surf. Coat. Technol.*, 232 (2013), 216-223.
- [123] JM Shockley, Sylvie Descartes, P Vo, Eric Irissou, RR Chromik, The influence of Al<sub>2</sub>O<sub>3</sub> particle morphology on the coating formation and dry sliding wear behavior of cold sprayed Al–Al<sub>2</sub>O<sub>3</sub> composites, *Surf. Coat. Technol.*, 270 (2015), 324-333.
- [124] Ruben Fernandez, Bertrand Jodoin, Cold spray aluminum–alumina cermet coatings: effect of alumina content, *J. Therm. Spray Technol.*, 27 (2018), 603-623.
- [125] S Kumar, Sai Kiran Reddy, Shrikant V Joshi, Microstructure and performance of cold sprayed Al–SiC composite coatings with high fraction of particulates, *Surface and Coatings Technology*, 318 (2017), 62-71.
- [126] NH Tariq, L Gyansah, X Qiu, H Du, JQ Wang, B Feng, DS Yan, TY Xiong, Thermo-mechanical post-treatment: A strategic approach to improve microstructure and mechanical properties of cold spray additively manufactured composites, *Mater. Des.*, 156 (2018), 287-299.
- [127] M Yandouzi, H Bu, M Brochu, B Jodoin, Nanostructured Al-based metal matrix composite coating production by pulsed gas dynamic spraying process, *J. Therm. Spray Technol.*, 21 (2012), 609-619.
- [128] Dominique Poirier, Jean-Gabriel Legoux, Robin AL Drew, Raynald Gauvin, Consolidation of Al<sub>2</sub>O<sub>3</sub>/Al nanocomposite powder by cold spray, *J. Therm. Spray Technol.*, 20 (2011), 275-284.
- [129] Xinliang Xie, Bilel Hosni, Chaoyue Chen, Hongjian Wu, Yuelin Li, Zhe Chen, Christophe Verdy, Omar El Kedim, Qingdong Zhong, Ahmed Addad, Corrosion behavior of cold sprayed 7075Al composite coating reinforced with TiB<sub>2</sub> nanoparticles, *Surf. Coat. Technol.*, 404 (2020), 126460.
- [130] Yingying Wang, Bernard Normand, Nicolas Mary, Min Yu, Hanlin Liao, Microstructure and corrosion behavior of cold sprayed SiCp/Al 5056 composite coatings, *Surf. Coat. Technol.*, 251 (2014), 264-275.

- [131] Hengyong Bu, Mohammed Yandouzi, Chen Lu, Daniel MacDonald, Bertrand Jodoin, Cold spray blended Al+ Mg17Al12 coating for corrosion protection of AZ91D magnesium alloy, *Surf. Coat. Technol.*, 207 (2012), 155-162.
- [132] FS Da Silva, J Bedoya, S Dosta, N Cinca, IG Cano, JM Guilemany, AV Benedetti, Corrosion characteristics of cold gas spray coatings of reinforced aluminum deposited onto carbon steel, *Corros. Sci.*, 114 (2017), 57-71.
- [133] Qiang Wang, Qi Sun, Ming-Xing Zhang, Wen-Juan Niu, Chang-Bin Tang, Kuai-She Wang, Xing Rui, Le Zhai, Lu Wang, The influence of cold and detonation thermal spraying processes on the microstructure and properties of Al-based composite coatings on Mg alloy, *Surf. Coat. Technol.*, 352 (2018), 627-633.
- [134] Zhichao Zhang, Fuchun Liu, En-Hou Han, Long Xu, Paul C Uzoma, Effects of Al<sub>2</sub>O<sub>3</sub> on the microstructures and corrosion behavior of low-pressure cold gas sprayed Al 2024-Al<sub>2</sub>O<sub>3</sub> composite coatings on AA 2024-T3 substrate, *Surf. Coat. Technol.*, 370 (2019), 53-68.
- [135] Xiawei Yang, Wenya Li, Siqi Yu, Yaxin Xu, Kaiwei Hu, Yaobang Zhao, Electrochemical characterization and microstructure of cold sprayed AA5083/Al<sub>2</sub>O<sub>3</sub> composite coatings, *J. Mater. Sci. Technol.*, 59 (2020), 117-128.
- [136] Ruben Fernandez, Bertrand Jodoin, Cold Spray Aluminum–Alumina Cermet Coatings: Effect of Alumina Morphology, *J. Therm. Spray Technol.*, 1-19.
- [137] Dalong Cong, Zhongsheng Li, Qingbing He, Hanbin Chen, Zipeng Zhao, Longping Zhang, Hulin Wu, Wear behavior of corroded Al-Al<sub>2</sub>O<sub>3</sub> composite coatings prepared by cold spray, *Surf. Coat. Technol.*, 326 (2017), 247-254.
- [138] Xiang Qiu, Lu Qi, Ji-Qiang Wang, Tian-Ying Xiong, A hybrid approach to improve microstructure and mechanical properties of cold spray additively manufactured A380 aluminum composites, *Mater. Sci. Eng., A*, 772 (2020), 138828.
- [139] HR Lashgari, AR Sufizadeh, M Emamy, The effect of strontium on the microstructure and wear properties of A356–10% B4C cast composites, *Mater. Des.*, 31 (2010), 2187-2195.
- [140] K. Spencer, D. M. Fabijanic, M. X. Zhang, The use of Al–Al<sub>2</sub>O<sub>3</sub> cold spray coatings to improve the surface properties of magnesium alloys, *Surf. Coat. Technol.*, 204 (2009), 336-344.
- [141] J Michael Shockley, EF Rauch, RR Chromik, Sylvie Descartes, TEM microanalysis of interfacial structures after dry sliding of cold sprayed Al-Al<sub>2</sub>O<sub>3</sub>, *Wear*, 376 (2017), 1411-1417.
- [142] Dmitry Dzhurinskiy, E Maeva, Ev Leshchinsky, R Gr Maev, Corrosion protection of light alloys using low pressure cold spray, *J. Therm. Spray Technol.*, 21 (2012), 304-313.
- [143] Ying-Kang Wei, Xiao-Tao Luo, Yi Ge, Xin Chu, Guo-Sheng Huang, Chang-Jiu Li, Deposition of fully dense Al-based coatings via in-situ micro-forging assisted cold spray for excellent corrosion protection of AZ31B magnesium alloy, *J. Alloys Compd.*, 806 (2019), 1116-1126.
- [144] E Lapushkina, S Yuan, N Mary, J Adrien, K Ogawa, B Normand, Contribution in optimization of Zn Cold-sprayed coating dedicated to corrosion applications, *Surf. Coat. Technol.*, 400 (2020), 126193.
- [145] P Wang, C Gammer, F Brenne, T Niendorf, J Eckert, S Scudino, A heat treatable TiB<sub>2</sub>/Al-3.5 Cu-1.5 Mg-1Si composite fabricated by selective laser melting: Microstructure, heat treatment and mechanical properties, *Composites Part B*, 147 (2018), 162-168.

- [146] Jiang Xu, Wenjin Liu, Wear characteristic of in situ synthetic TiB<sub>2</sub> particulate-reinforced Al matrix composite formed by laser cladding, *Wear*, 260 (2006), 486-492.
- [147] Shuo Yin, Xiaofang Wang, Xinkun Suo, Hanlin Liao, Zhiwei Guo, Wenya Li, Christian Coddet, Deposition behavior of thermally softened copper particles in cold spraying, *Acta Mater.*, 61 (2013), 5105-5118.
- [148] Yingchun Xie, Marie-Pierre Planche, Rija Raelison, Philippe Hervé, Xinkun Suo, Pengjiang He, Hanlin Liao, Investigation on the influence of particle preheating temperature on bonding of cold-sprayed nickel coatings, *Surf. Coat. Technol.*, 318 (2017), 99-105.
- [149] Kang Yang, Wenya Li, Chunjie Huang, Xiawei Yang, Yaxin Xu, Optimization of cold-sprayed AA2024/Al<sub>2</sub>O<sub>3</sub> metal matrix composites via friction stir processing: Effect of rotation speeds, *Journal of materials science & technology*, 34 (2018), 2167-2177.
- [150] Kang Yang, Wenya Li, Pengliang Niu, Xiawei Yang, Yaxin Xu, Cold sprayed AA2024/Al<sub>2</sub>O<sub>3</sub> metal matrix composites improved by friction stir processing: Microstructure characterization, mechanical performance and strengthening mechanisms, *J. Alloys Compd.*, 736 (2018), 115-123.
- [151] Xiang Qiu, Lu Qi, Yu-ning Zan, Yu-jiang Wang, Ji-qiang Wang, Hao Du, Tian-ying Xiong, In-situ Si/A380 alloy nano/micro composite formation through cold spray additive manufacturing and subsequent hot rolling treatment: Microstructure and mechanical properties, *J. Alloys Compd.*, 780 (2019), 597-606.
- [152] Xinliang Xie, Chaoyue Chen, Zhe Chen, Wen Wang, Shuo Yin, Gang Ji, Hanlin Liao, Achieving simultaneously improved tensile strength and ductility of a nano-TiB<sub>2</sub>/AlSi10Mg composite produced by cold spray additive manufacturing, *Composites Part B*, 202 (2020), 108404.
- [153] Ming Tang, P Chris Pistorius, Oxides, porosity and fatigue performance of AlSi10Mg parts produced by selective laser melting, *Int. J. Fatigue*, 94 (2017), 192-201.
- [154] Luca Girelli, Marialaura Tocci, Marcello Gelfi, Annalisa Pola, Study of heat treatment parameters for additively manufactured AlSi10Mg in comparison with corresponding cast alloy, *Mater. Sci. Eng., A*, 739 (2019), 317-328.
- [155] Qian Yan, Bo Song, Yusheng Shi, Comparative study of performance comparison of AlSi10Mg alloy prepared by selective laser melting and casting, *J. Mater. Sci. Technol.*, 41 (2020), 199-208.
- [156] Chaoyue Chen Xinliang Xie, Zhe Chen, Hongjian Wu, Christophe Verdy, Zhongming Ren, Gang Ji, Hanlin Liao, Microstructure and mechanical properties of in-situ TiB<sub>2</sub> particle reinforced AlSi10Mg composite components produced by cold spray additive manufacturing, Unpublished Data (2020).
- [157] Zhipo Zhao, Junrong Tang, Cunlei Jia, Xiang Qiu, Yupeng Ren, Hanhui Liu, Yanfang Shen, Hao Du, Xinyu Cui, Jiqiang Wang, Microstructural evolutions and mechanical characteristics of Ti/steel clad plates fabricated through cold spray additive manufacturing followed by hot-rolling and annealing, *Mater. Des.*, 185 (2020), 108249.
- [158] Huilin Zhao, Chengwen Tan, Xiaodong Yu, Xianjin Ning, Zhihua Nie, Hongnian Cai, Fuchi Wang, Yan Cui, Enhanced reactivity of Ni-Al reactive material formed by cold spraying combined with cold-pack rolling, *J. Alloys Compd.*, 741 (2018), 883-894.
- [159] Zhipo Zhao, Junrong Tang, Yupeng Ren, Hanhui Liu, Min Tong, Lisong Yin, Hao Du, Jiqiang Wang, Tianying Xiong, Influence of annealing on the microstructure and mechanical

properties of Ti/steel clad plates fabricated via cold spray additive manufacturing and hot-rolling, *Mater. Sci. Eng., A*, 775 (2020), 138968.

[160] Farzad Khodabakhshi, Bahareh Marzbanrad, Hamid Jahed, Adrian P Gerlich, Interfacial bonding mechanisms between aluminum and titanium during cold gas spraying followed by friction-stir modification, *Appl. Surf. Sci.*, 462 (2018), 739-752.

[161] CJ Huang, XC Yan, WY Li, WB Wang, C Verdy, MP Planche, HL Liao, G Montavon, Post-spray modification of cold-sprayed Ni-Ti coatings by high-temperature vacuum annealing and friction stir processing, *Appl. Surf. Sci.*, 451 (2018), 56-66.

[162] F Khodabakhshi, B Marzbanrad, LH Shah, H Jahed, AP Gerlich, Friction-stir processing of a cold sprayed AA7075 coating layer on the AZ31B substrate: structural homogeneity, microstructures and hardness, *Surf. Coat. Technol.*, 331 (2017), 116-128.

[163] Chunjie Huang, Wenya Li, Zhihan Zhang, Maosen Fu, Marie-pierre Planche, Hanlin Liao, Ghislain Montavon, Modification of a cold sprayed SiCp/Al5056 composite coating by friction stir processing, *Surf. Coat. Technol.*, 296 (2016), 69-75.

[164] Kang Yang, Wenya Li, Yaxin Xu, Xiawei Yang, Using friction stir processing to augment corrosion resistance of cold sprayed AA2024/Al<sub>2</sub>O<sub>3</sub> composite coatings, *J. Alloys Compd.*, 774 (2019), 1223-1232.

[165] F Khodabakhshi, AP Gerlich, Potentials and strategies of solid-state additive friction-stir manufacturing technology: a critical review, *J. Manuf. Process.*, 36 (2018), 77-92.

[166] KJ Hodder, H Izadi, AG McDonald, AP Gerlich, Fabrication of aluminum–alumina metal matrix composites via cold gas dynamic spraying at low pressure followed by friction stir processing, *Mater. Sci. Eng., A*, 556 (2012), 114-121.

[167] HB Michael Rajan, I Dinaharan, S Ramabalan, ET Akinlabi, Influence of friction stir processing on microstructure and properties of AA7075/TiB<sub>2</sub> in situ composite, *J. Alloys Compd.*, 657 (2016), 250-260.